PHD

Polarisation and spectral characteristics of spontaneous emission in active optical waveguides

Liddel, W. J.

Award date:
1986

Awarding institution:
University of Bath

Polarisation and Spectral Characteristics of Spontaneous Emission in Active Optical Waveguides

submitted by W.J.Liddell

for the degree of PhD of the University of Bath

1986

ProQuest LLC
789 East Eisenhower Parkway
P.O. Box 1346
Ann Arbor, MI 48106-1346

Summary of Thesis

A summary of the properties of a semiconductor laser structure which are necessary for the simultaneous confinement of charge and radiation within the active layer is presented. Current spreading above the active layer and charge diffusion within it are calculated.

Spontaneous and stimulated emission are considered as the emissions from atomic dipoles in a bulk material. The physics of band to band transitions is summarised and a simple computer model which allows transitions between semiconductor bands of arbitrary profile to be analysed is described. Results for band tails which are Gaussian or exponential well into the band gap are shown.

The confinement of radiation within the active layer is described in terms of electromagnetic theory. This is extended to a two dimensional gain guided stripe geometry structure by using the effective dielectric constant method. The field confinement parallel to the active layer is analysed and several approximate charge carrier profiles are considered. An inverse squared hyperbolic cosine profile is found to be most satisfactory for describing a gain guided waveguide.

The spontaneous emission from three orthogonal dipoles is related to the spontaneous emission per unit volume calculated from band to band transitions. The emitted dipole power is then related to the spontaneous emission coupled into the modes of an active gain guided optical waveguide. The calculation uses a Green's function method of analysis. The spontaneous power coupled per unit length to the fundamental gain guided TE and TM (LSE and LSM) modes is then calculated for a range of photon energies and for different drive currents and device geometries.

List of Symbols

a_m	Normalisation coefficient for the m^{th} mode.
$a(\rho)$	Normalisation coefficient for the continuous spectrum.
$a_k(t)$	Time varying amplitude coefficients for ϕ_k.
A_k	Amplitude coefficient for ϕ_k.
$A.A_{21}$	Spontaneous transition probability.
$A(r_0)$	Coefficient for TE modes in the expansion of $\bar{G}(r:r_0)$.
$B.B_{21}.B_{12}$	Stimulated transition probability.
$B(r_0)$	Coefficient for TM modes in the expansion of $\bar{G}(r:r_0)$.
C_{nx}^m	The x astigmatism factor for the n^{th} TE mode.
C_{ny}^m	The y astigmatism factor for the n^{th} TM mode.
$C_0^{(\mu)}.C_1^{(\mu)}etc.$	Gegenbauer polynomials.
d	The half thickness of a symmetric optical waveguide.
$d_1.d_2.d_3.d_4$	Thickness of heterostructure layers.
D	Diffusion coefficient.
D	Dipole moment in solution of Schroedinger's Equation.
E	Electric field vector.
$E_x.E_y.E_z$	Projections of the electric field onto x, y and z.
$E_1.E_2.E_k$	Photon energies.
E_c	Conduction band energy level.
E_v	Valence band energy level.
E_g	Band gap energy.
$f_c(E_c)$	Conduction band occupation factor.
$f_v(E_v)$	Valence band occupation factor.
F	Fermi level.
F_c	Conduction band quasi-Fermi level.
F_v	Valence band quasi-Fermi level.

g	Optical power gain.
$\bar{G}(r;r_0)$	Dyadic Green's function.
h	Planck's constant.
$h\nu$	Photon energy.
$\hbar$	Dirac's constant.
H	Magnetic field vector.
H_x, H_y, H_z	Projections of the magnetic field onto x, y and z.
$H_0, H_1 etc.$	Hermite polynomials.
I_A	Current into active layer.
I_S	Current through stripe contact.
I_X	Current parallel to active layer.
$I_0 l$	Electric dipole momemt.
$\bar{I}$	The unit dyadic, the idemfactor.
j	Square root of -1.
J_A	Current density into active layer, under stripe contact.
J_{sat}	Saturation current density of active layer p-n junction.
$J_Y(x)$	Current density entering the active layer.
J_S	Current density entering stripe contact.
J_Q	Normalisation current density.
J	Electric current density.
k	Boltzmann's constant.
k_0	Free space propagation constant.
k_s	Thomas-Fermi screening length for electrons.
K	Peterman's astigmatism factor.
l_0	Effective current spreading length.
l_S	Effective diffusion length.
L	The device length.

m	Electronic mass.
m_c	Effective electron mass.
m_v	Effective hole mass.
M	Stern's band to band matrix element.
n	Refractive index.
n_1, n_2, n_3	Refractive indices of device regions.
n_a	Average refractive index of active layer.
n_e	Effective refractive index for TE mode.
n_{ea}	Average of n_e.
n_f	Effective refractive index for TM mode.
n_{fa}	Average of n_f.
N	Electron density.
$N_{\max}$	Maximum electron density.
N_r	Electron density for region r.
N_{E1}, N_{E2}	Electron densities of energy levels E_1 and E_2.
p_0	Doping density.
P	Hole density.
$P(h\nu)$	Optical power density.
q	Electronic charge.
$q_{spon}(x)$	Variation of spontaneous emission with x.
r, r_0	General positional coordinate.
r_{spon}	Spontaneous transition coefficient.
r_{stim}	Stimulated transition coefficient.
R_S	Resistance of layers above the active layer.
R_{stim}	Rate of stimulated emission.
t	Time.

T	Temperature.
u	Normalised y propagation constant, inside active layer.
u_k	Spatial field function describing an electron.
v	Effective frequency of optical waveguide.
V	Potential energy, (in Shcroedinger's wave equation.)
V_{eff}	Peterman's effective volume.
V_j	Voltage drop at active layer p-n junction.
$V_X(x)$	Voltage drop parallel to active layer.
w	Width of stripe contact.
w	Normalised decay constant of field profile.
w_{eff}	Peterman's effective width.
w_{spon}	The spontaneous emission rate.
$X(x)$	General x directed field profile.
x	Cartesian coordinate.
$\hat{\mathbf{x}}$	The unit vector along x.
x_r	Coefficient in solution of diffusion equation.
Δx	A finite increment in x.
y	Cartesian coordinate perpendicular to active layer.
$\hat{\mathbf{y}}$	The unit vector along y.
y_r	Coefficient in solution of diffusion equation.
z	Cartesian coordinate, direction of propagation.
Z	Number of modes per unit volume.
$\hat{\mathbf{z}}$	The unit vector along z.
α	Imaginary part of dn/dN.
$\beta_{e(p)}$	z propagation constant for (the p^{th}) TE mode.
$\beta_{m(p)}$	z propagation constant for (the p^{th}) TM mode.

Γ	The y field confinement factor.
$\Gamma(z)$	The complex gamma function.
δ	Spontaneous power increase per unit length.
$\delta(r-r_0)$	Delta function.
Δ	Spin orbit splitting.
ϵ	Dielectric constant, ($\epsilon = n^2$, see n for subscripts).
ϵ_0	Dielectric constant of free space.
ϵ_r	Relative dielectric constant.
η	Band tail length.
η_1, η_2, η_3	Constants in refractive index profile approximations.
$\eta_{01}, \eta_{02}, \eta_{03}$	Constants in refractive index profile approximations.
λ_0	Free space wavelength
μ	Guiding parameter for Gegenbauer polynomial solutions.
μ_0	Permeability of free space.
ν	Frequency.
π	Ratio of circumference to diameter of circle.
$-\rho$	Real part of dn/N.
ρ_y	y propagation constant, outside active layer.
ρ_3, ρ_4	Sheet resistivities of layers above the active layer.
$\rho_c(E_c)$	Conduction band density of states function.
$\rho_v(E_v)$	Valence band density of states function.
σ_x	x propagation constant.
σ_y	y propagation constant, inside active layer.
τ_D	Diffusion lifetime.
τ_r	Spontaneous electron lifetime for region r.
τ_s	Spontaneous electron lifetime.
ϕ	Field function describing an electron.

χ_m	Field profile for the m^{th} TM mode.
$\chi(\rho)$	Continuous spectrum TM field profile.
ψ_m	Field profile for the m^{th} TE mode.
$\psi(\rho)$	Continuous spectrum TE field profile.
ω	Angular frequency.
ω_{bb}	Angular frequency of emitted photon.

Chapter 1

Chapter 2

Chapter 3

Chapter 4

Chapter 5

Chapter 6

Chapter 7

CHAPTER 1

1-1 Objective of Thesis

Light emitting diodes, LEDs, and semiconductor lasers rely on spontaneous emission to produce light. In a laser the spontaneous emission is amplified in a Fabry-Perot cavity and results in one or more lasing lines each with a line width of less than 0.1 nm. [1] In a laser the output spectrum is governed by the Fabry-Perot resonance but the spontaneous emission contribution to a lasing mode is the phenomenon which initiates lasing action, and controls laser line width. [2] In an LED the output is almost entirely due to spontaneous emission and amplification by stimulated emission is unimportant. An interesting half-way point is seen in the superluminescent LED, SLED, [3,4] where the spontaneous emission from well inside the device is of prime importance. This is amplified in a single pass through the medium to produce the output. SLEDs have potential as single pass optical amplifiers [5] but the spontaneous emission which accompanies the SLED action would act as noise in such an amplifier.

The thesis is a study of spontaneous emission in GaAs DH stripe geometry laser structures and its interaction with optical gain. In particular it is important to discover the variation of spontaneous emission and optical gain with photon energy in gain and index guided structures. The analysis of gain guiding structures is reviewed and the spontaneous emission coupled to a guided mode is calculated. No allowance is made for high light intensities and so the presence of light is not deemed to affect the material properties i.e. this analysis is only for devices operated below lasing threshold. An analysis of the spectral properties of gain and spontaneous emission is required in order to investigate the wavelength dependence of these phenomena.

1-2 Content of Thesis

To calculate the spectral characteristics of spontaneous emission with no reference to the stimulated gain would ignore the importance of the effects of gain guiding on the output spectrum of active waveguides. Whereas a knowledge of stimulated emission spectra without the corresponding spontaneous emission spectra will mean that no calculation of the spectral effect of noise would be possible. For this reason the guiding mechanism and the spontaneous emission are inextricably linked.

A summary of the physical reasons behind the choice of laser structures is given in Chapter 2. The basic idea of a D-H semiconductor material as an optical waveguide providing simultaneously a real refractive index step and a method of confining a region of population inversion is presented. The problems of current spreading and out diffusion are reviewed and some of the steps that have been reported to try to avoid these problems in laser diodes are outlined.

The calculations required in this study start with the solution of the current spreading properties of stripe geometry heterostructure devices and diffusion in the active layer. This allows the x variation of injected carrier density to be calculated. The current spreading is calculated from a simple analytic treatment which assumes that injection current density is a constant under the stripe contact. The analysis (based on Ref.6 & 7) calculates a $\frac{1}{1+x^2}$ type decay of current density beyond the stripe edge. A convenient normalisation for current density has been introduced to generalise the analysis. The calculation of the carrier density in the active layer has been performed numerically for a large number of discrete regions of width, Δx. This avoids the problems of using three or five layer models for carrier profiles

which are shown in Chpater 2 to be unsatisfactory. Should a slab model be desirable for calculation of the electromagnetic fields it would be reasonable to calculate the carrier profile first and then decide where to place the slab boundaries. The values used for the carrier density could then be calculated as an average value of the calculated profile over the appropriate region.

The quantum mechanics of spontaneous and stimulated emission are considered, and the basic equations required to calculate the emission spectra are derived. The properties of band to band transitions in semiconductors are analysed as it is necessary to find corresponding spontaneous and stimulated emission profiles before the aim of the thesis can be realised. Band to band transitions are calculated for parabolic bands both numerically and theoretically. The theoretical solutions are only valid near the band edge and are only based on parabolic bands. This analysis extends that of Marinelli [8] to include expressions for spontaneous emission. The main advantage of this kind of solution is that further calculations involving waveguiding properties can easily be made. By approximating the quasi-Fermi levels, F_c and F_v, in terms of the inversion populations, N and P, [9] the spontaneous and stimulated emission are expressed in terms of N and P . For low levels of inversion population it is the low energy end of the spectrum that is important. For this reason the effect of band tails on the semiconductor band shapes are considered and a computer model has been developed which includes these effects. Numerical calculations of the effect of changing parabolic bands for band shapes with a fixed band tail have shown that this produces stimulated and spontaneous emission profiles which no longer cut off so sharply near the band edge.

The guiding and the modal properties of dielectric slabs are outlined as a necessary part of the understanding of electromagnetic field confinement.

The gain guided laser structure analysed in this thesis is a relatively wide guiding structure with a width of over 5μm and thickness less than 0.3μm, this will always be the case when there is diffusion in the active layer. In this case it is appropriate to use an effective dielectric constant method to calculate the modal properties of the guide. This has been done for waveguides which are created when current is injected into 5,7 and 10 μm stripe contacts. The gain spectrum from previous calculations [10] has been used corresponding to Kane band tails [11] with band tail lengths of $0.6kT \approx 15$meV. The resulting values of waveguide gain for different wavelengths and injection currents for a Gegenbauer polynomial [1,12] modal solution have been presented. From the analysis of parabolic bands an expression for the guiding parameter μ has been formulated explaining its behaviour with photon energy and carrier concentration.

The spontaneous emission spectum is calculated from the band to band transitions assuming that the emissions are those of an atomic electric dipole and represented as a power per unit volume. It is therefore reasonable to continue to use an electric dipole to represent these emissions in a waveguide. Over a small volume an assumption is made that the power emitted by the dipoles within this volume can be represented by three orthogonal dipoles of equal strengths. The power from an infinitesimal dipole coupled to waveguide modes is then calculated for a spectrum of wavelengths using a dyadic Green's function method of analysis. This is then integrated over the guide cross-section to give the increase, δ, in the power, $P(h\nu)$, per unit length in z due to spontaneous emission. In the presence of optical gain, g, the rate of increase of power with length is

$$\frac{dP(h\nu)}{dz} = gP(h\nu) + \delta \qquad (1\text{-}2.1)$$

Calculation of the variation of δ with the inversion population, N, and photon energy, $h\nu$, is the final result of this thesis and is described in Chapter 6. The results show a complete spectrum of wavelengths for a gain guided waveguide. The power coupled from each of three orthogonal dipoles, $\hat{\mathbf{x}}$,$\hat{\mathbf{y}}$ and $\hat{\mathbf{z}}$-oriented, into both LSE and LSM, (TE and TM), modes. By using a dyadic Green's function to find each of the contributions it has been shown that the TE mode couples mainly from the x directed dipole but also from the z directed dipole. The TM mode couples power mainly from the y dipole but also from both other dipoles. The results of the analysis are compared to previous analyses, principally that of Peterman [12], to show how, for the peak wavelength, there is good agreement, but over the whole wavelength range of operation of a travelling wave optical amplifier the the wavelength dependent effects must be considered.

1-3 State of the Art Analysis

The problem of spontaneous emission in semiconductor light emitting devices, primarily in GaAs, has received much attention in recent years. In particular papers by Peterman [12] and Suematsu [13]. Both these authors calculate the spontaneous emission factor for laser diodes. Where the spontaneous emission factor is defined as

$$\frac{\text{rate of spontaneous emission into one oscillating mode}}{\text{total rate of spontaneous emission}} \qquad (1\text{-}3.1)$$

Both authors assume that the contribution to an oscillating mode with a dominant E_x field couples power excusively from x oriented dipoles in the active layer of the device. This is the TE mode of the structure and the mode which is dominant in laser diodes. It is also assumed that the TM mode, with a dominant E_y field, couples from the y oriented dipole.

Peterman [12] calculates the spontaneous emission factor and shows that it is proportional to $\frac{K}{V_{eff}}$ where

$$K = \frac{(\int |\psi(x)|^2 \, dx)^2}{|\int \psi^2(x) \, dx|^2} \qquad (1\text{-}3.2)$$

$$V_{eff} = \frac{L d w_{eff}}{\Gamma} \qquad (1\text{-}3.3)$$

and K is the astigmatism factor, $\psi(x)$ is the variation of the field profile parallel to the heterojunction for the mode in question, L is the device length, d the active layer halfthickness, Γ the confinement factor for the mode perpendicular to the heterojunction and w_{eff} is the effective width. The effective width is given by

$$w_{eff} = \frac{\int |\psi(x)|^2 \, dx \int q_{spon}(x) \, dx}{\int |\psi(x)|^2 \, q_{spon}(x) \, dx} \qquad (1\text{-}3.4)$$

where $q_{spon}(x)$ represents the variation of spontaneous emission with x.

Streifer [1] uses this value of K to show that with astigmatic modes, derived from a $\cosh^{-2}$ profile for the carrier density in the active layer, the astigmatism factor can be very large. Sommers [14] showed that the ratio between spontaneous and stimulated transition rates can be used to develop an expression for the fraction of the total spontaneous emission that appears in the mode of a laser cavity with the highest gain. However he did not compare this with K or consider the explicit form of the modes in the cavity. Following this, Patzak [15] pointed out that, according to quantum theory, the probability of photon emission into any mode is proportional to $(N+1)$, where N is the number of photons in the mode, regardless of the structure of the device. In this case K must be equal to one. This discrepancy was resolved by Marcuse [16] who showed that, for modes which are not power orthogonal, the astigmatism factor can be regarded as the number of power orthogonal modes required to express the field of a gainguided mode.

Several other approaches to the problem have been published. These include a heuristic approach [17] which agrees with Peterman's K factor for Gaussian profiles and analyses which show that very thin active layers also lead to astigmatism [18,19].

The calculation of the emission spectra obtained from a consideration of band to band transitions has a long history. Kane, [20], shows how parabolic bands [21] of a semiconductor are altered when the semiconductor is heavily doped. More rigorous treatment by Halperin and Lax [22] does not provide workable approximations for simple band to band transition models. Stern [16] has produced a band to band transition matrix element which has the correct behaviour to provide an altogether more acceptable gain profile than any other previous work. Generally spontaneous emission profiles which correspond to

these gain profiles are not known. In any case for detailed calculations the available data from graphs in papers is not sufficient. Previous calculations of approximate emission spectra have given results in terms of quasi-Fermi levels [23]. This is unfortunate since the refractive index is generally considered to vary with the inversion population and so calculations of gain and spontaneous emission spectra are incompatible with models of gain guiding.

1-4 Results Achieved

The thesis contains several features which are not present in published work, some of which are simple extensions of previous work and some which are new. This section highlights the results achieved and outlines some of the approximations made to achieve them.

In the category of extensions to previous work is the calculation of band to band transitions with exponential and Kane band tails [14]. The model produced by this is very simple but contains some features which are not contained in models which rely on parabolic bands. Importantly, the behaviour of the gain and spontaneous emission near the band edge no longer shows a sharp cut off which is shown by parabolic band shape models. The computer program which calculates these results has been arranged to store the band shapes in an array and interpolate from these points. In principle this allows an arbitrary band shape to be used to suit any required band tail shapes. The results of this model are encouragingly realistic and have been used to model real devices [10]. This is extendable to any III-V direct band gap semiconductor if different effective masses are given.

The ideas of Marinelli [8] and Joyce and Dixon [9] have been combined to produce not only gain spectra as Marinelli calculated but also expressions for spontaneous emission spectra. These calculations give both functions in terms of quasi-Fermi levels or carrier density. This is particularly important since the waveguiding properties are generally found assuming that the change in refractive index of the active layer is dependent on carrier density. These approximations have been used to explain the spectral behaviour of spontaneous emission coupled to waveguide modes.

In laser diode structures the transverse guiding properties of the laser are analysed for the case of gain guided modes. The calculation of active

waveguides takes the form af LSE and LSM modes. Spontaneous emission is represented by dipole radiation from infinitesimal dipoles within the active layer. The inclusion of all five fields and the use of a dyadic Green's function shows that the $\hat{y}$ dipole only couples to the TM (LSM) modes but both other dipoles couple to both LSE and LSM modes.

The calculation of the spectral properties of the gain allows a comprehensive formulation of the wavelength dependence of the modal gain for the fundamental mode to be computed. This shows that the same waveguide behaves differently at different wavelengths. In a laser diode this is not of great significance but in a travelling wave amplifier it is important. Not only is the gain dependent on the wavelength but also on the polarisation of the mode. The modal gain is calculated by using the effective dielectric constant method and this is used for both polarisations. The results do not show significant variations in the gain between the two polarisations. The use of the Green's dyadic allows the spontaneous emission into either polarisation to be calculated from each of the three orthogonal dipoles considered. In addition to the optical gain the spontaneous emission has been calculated for the bulk material. This allows the wavelength dependence of the coupling of spontaneous emission to be analysed for corresponding gain and spontaneous emission profiles. The spontaneous emission in the waveguide is calculated assuming that it is radiated by three orthogonal elementary dipoles. The coupling of the y dipole to TM modes and the x dipole to TE modes is most significant. The z dipole couples to both modes but the power coupled is only a few percent of that from the main contributors. The x dipole contributes to the TM modes but the power coupled is much less than the other two contributions.

The results show that the spontaneous emission at the peak gain can be approximated as being proportional to Peterman's astigmatism factor but

when the mode is near cut off the approximation breaks down. This can be explained in two ways. First, as a modification of Peterman's analysis to take account of the variation of the effective width with wavelength, which is expected as the field is near cut off and so spreads out anyway. Second, the idea of effective width itself can be disregarded and the full expression derived for spontaneous emission can be considered. This leads to the spontaneous emission being proportional to $C_0 = \sqrt{K}$ and another parameter

$$\frac{\int |\psi(x)|^2 q_{spon}\, dx}{\int \psi^2(x) dx \int q_{spon}\, dx} = \frac{K}{w_{eff}} \qquad (1\text{-}4.1)$$

Whichever explanation is used the result is that for a gain guided waveguide the spontaneous emission at any wavelength is increased by a factor which is between K and C_0 over a comparable index guided waveguide. However, for the wavelength at the peak gain, without reference to what the wavelength is, the spontaneous emission is increased by approximately K. It should be noted that no waveguide is entirely index guided if it has optical gain so that the astigmatism factor is never actually one. It is only one for lossless waveguides. If the structure is such that the guiding mechanism is totally dominated by the difference in the real part of the refractive index of the confining layers then the astigmatism will be approximately one.

References for Chapter 1

1/ W.Streifer, D.R.Scrifes, R.D.Burnham, " Spontaneous emission factor of narrow-stripe gain-guided diode lasers ", Electron. Let., 17 , (24), pp933-934, 1981.

2/ W.Streifer, D.R.Scrifes, R.D.Burnham, " Analysis of spontaneous emission effects on spectra and L vs. I characteristics of diode lasers ", Jap. J. Appl. Phys., 21 , (5), pp282-284, 1982.

3/ J.Boeck, M-C.Amann, " AlGaAs/GaAs double-heterostructure superluminescent diodes for optical transmission systems ", Frequenz, 33 , (10), pp278-283, 1979.

4/ M-C.Amann, J.Boeck, " High-efficiency superluminescent diodes for optical-fibre transmission ", Electron. Lett., 15 , (2), pp41-42, 1979.

5/ J.C.Simon, "Semiconductor laser amplifier for single mode optical fibre communications", J.Opt.Comm., 4 , (2), pp51-62, 1983.

6/ H.Yonezu, I.Sakuma, K.Kobayashi, T.Kamejima, M.Ueno, Y.Nannichi, " A GaAs-AlGaAs double heterostructure planar stripe laser ", Jap. J. Appl. Phys., 12 , (10), pp1585-1592, 1973.

7/ W.T.Tsang, " The effects of lateral current spreading carrier out-diffusion, and optical mode losses on the threshold current density of GaAs-GaAlAs stripe geometry D.H. lasers ", J.Appl. Phys., 51 , (3), pp1031-1044, 1978.

8/ F.Marinelli, "Approximate calculation of the spectral function for the stimulated recombination radiation in semiconductors", S.S.Electron, 8 , pp939-942, 1965.

9/ W.B.Joyce, R.W.Dixon, "Analytic approximations for the Fermi energy in an ideal Fermi gas", Appl.Phys.Lett., 32 , pp354-356, 1977.

10/ I.Middlemast, J.Sarma, T.Kambayashi, "A comprehensive study and characterisation of superluminescent light emitting diodes", IEEE TELD 82 , Ottawa, Canada, 1982.

11/ W.Steifer, R.D.Burnham, D.R.Scrifes, "Symmetrical and asymmetrical waveguiding in very narrow conducting stripe lasers", IEEE J.Q.Electron, QE-15 , (3), pp136-141, 1979.

12/ K.Peterman, "Calculated spontaneous emission factor for double-heterostructure injection lasers with gain induced waveguiding", IEEE J.Q.Electron., QE-15 , (7), pp566-570, 1979.

13/ Y.Suematsu, K.Furuya, "Theoretical spontaneous emission factor of injection lasers", Trans.IECE Jap., E60 , (9), pp61-66, 1977.

14/ H.S.Sommers, "Spontaneous emission factor β for injection lasers", J.Appl.Phys, 52 , (12), ppp7439, 1981.

14/ E.Patzak, "Spontaneous emission factor of narrow-stripe gain-guided diode lasers", Electron.Lett., 18 , (6), pp278-279, 1982.

16/ D.Marcuse, "Quantum mechanical explanation of spontaneous emission K-factor", Electron.Lett., 18 , (21), pp920-922, 1982.

17/ G.P.Agrawal, "Heuristic approach to spontaneous emission factor of gain-guided lasers', J.Opt.Soc.Am. B, 1 , (3), pp406-408, 1984.

18/ F.Coste, J.Fesquet, J.Arnaud, "Noise enhancement in laser amplifiers caused by gain nonuniformity", Electron.Lett., 20 , (18), pp719-720, 1984.

19/ J.Arnaud, "Role of Peterman's K-factor in semiconductor laser oscillators", Electron.Lett., 21 , (12), pp538-539, 1985. 20/ E.O.Kane, "Thomas-Fermi approach to impure semiconductor band structure", Phys.Rev., 131 , (1), pp186-194, 1963.

21/ C.Kittel, Introduction to Solid State Physics, Wiley, 5th ed., (see Chap 9).

22/ B.I.Halperin, M.Lax, "Impurity band tails in the high density limit, I Minimum counting methods", Phys.Rev., 148 , (2), pp722-740, 1966.

23/ F.Stern, "Calculated spectral dependence of gain in GaAs", J.Appl.Phys., 47 , (12), pp5382-5386, 1976.

CHAPTER 2

2-1 Double Heterostructure Devices

The object of this introduction is to describe the physical characteristics of a semiconductor laser diode type stucture which are required to create an optical waveguide with gain. The structure must of course guide light and, in general, light is guided by a region of higher refractive index. If the device is to have optical gain then the same region which guides the light must also confine the carriers. To ensure a strong interaction between light and carriers this region must be a direct band gap semiconductor. This is the "active" region in which transitions between bands take place. Such an "active layer" can be produced by growing heterostructure layers of III-V semiconductors and forming a p-n junction. If the lattice match is good then the potential step in the semiconductor bands at boundary B, (Fig. 2-1), between the active layer and surrounding layers, ensures that there is virtually no reverse injection of electrons into the active layer. The refractive index of the surrounding layers is lower than that of the active layer and in all practical cases this means that their band gap is wider too. This ensures that light, not completely confined in the active layer, will not be absorbed by the surrounding layers. In the case of GaAs-GaAlAs structures with GaAs active layers and GaAlAs surrounding layers a highly doped GaAs contact layer is needed if an ohmic contact is to be made. The active layer must not be too close to this contact layer which would absorb the light propagating within it. In this way both light and carriers can be confined by a layered structure. (Fig 2-2).

In Chapter 4 the form of the electromagnetic fields confined by a layered slab structure is considered and the maximum active layer thickness for only

one to propagate is given in terms of the refractive indeces of the layers n_1 and n_2, the layer thickness d_2 and the free space wavenumber k_0.

$$v=(n_1^2-n_2^2)^{\frac{1}{2}}k_0 d_2<\pi \qquad (2\text{-}1.1)$$

In a GaAs-GaAlAs structure $n_1\approx 3.55$ and $n_2\approx 3.39$ so that with $\lambda\approx 0.9\mu m$

$$\frac{d_2}{2}<\frac{\pi}{2}\frac{\lambda_0}{2\pi}(n_1^2-n_2^2)^{\frac{1}{2}} \qquad (2\text{-}1.2)$$

that is

$$d_2<0.5\mu m \qquad (2\text{-}1.3)$$

A further design factor is that the active layer should be as thin as possible to increase the carrier density and hence the optical gain. However, as the electromagnetic field extends beyond the active layer, the gain for the propagating mode is maximised by maximising the product of gain and fraction of the mode within the guide. The optimum active layer thickness is between $0.2\mu m$ and $0.3\mu m$.

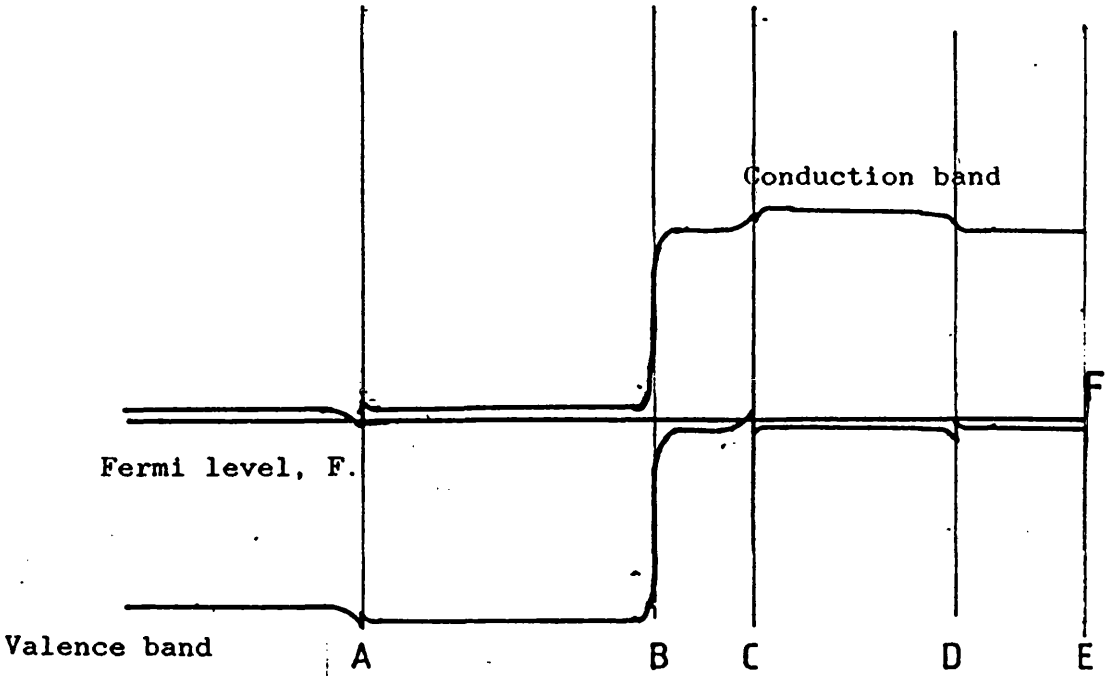

Fig. 2-1a The electron potentials of the heterostucture layers of a laser diode structure with no forward bias. The contact is made at interface E and the active region is region B-C.

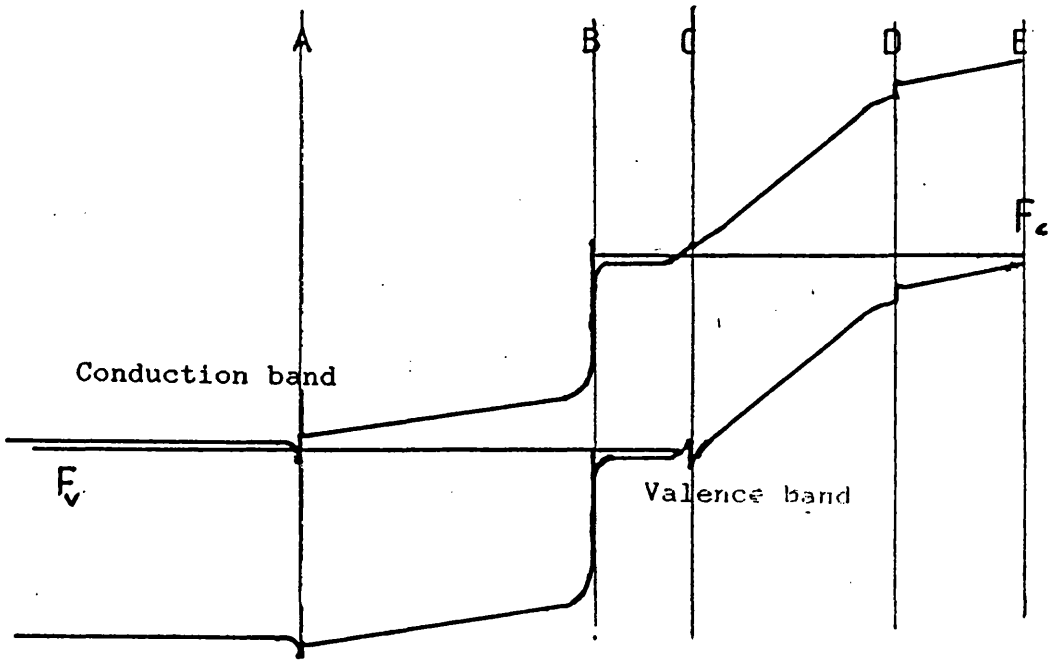

Fig. 2-1b Under forward bias the band diagram is altered and two quasi Fermi levels, F_C for electrons and F_V for holes, are required to describe the band occupancies. Net downward stimulated emission, optical gain, occurs when $F_c - F_v$ exceeds the band gap energy, E_g

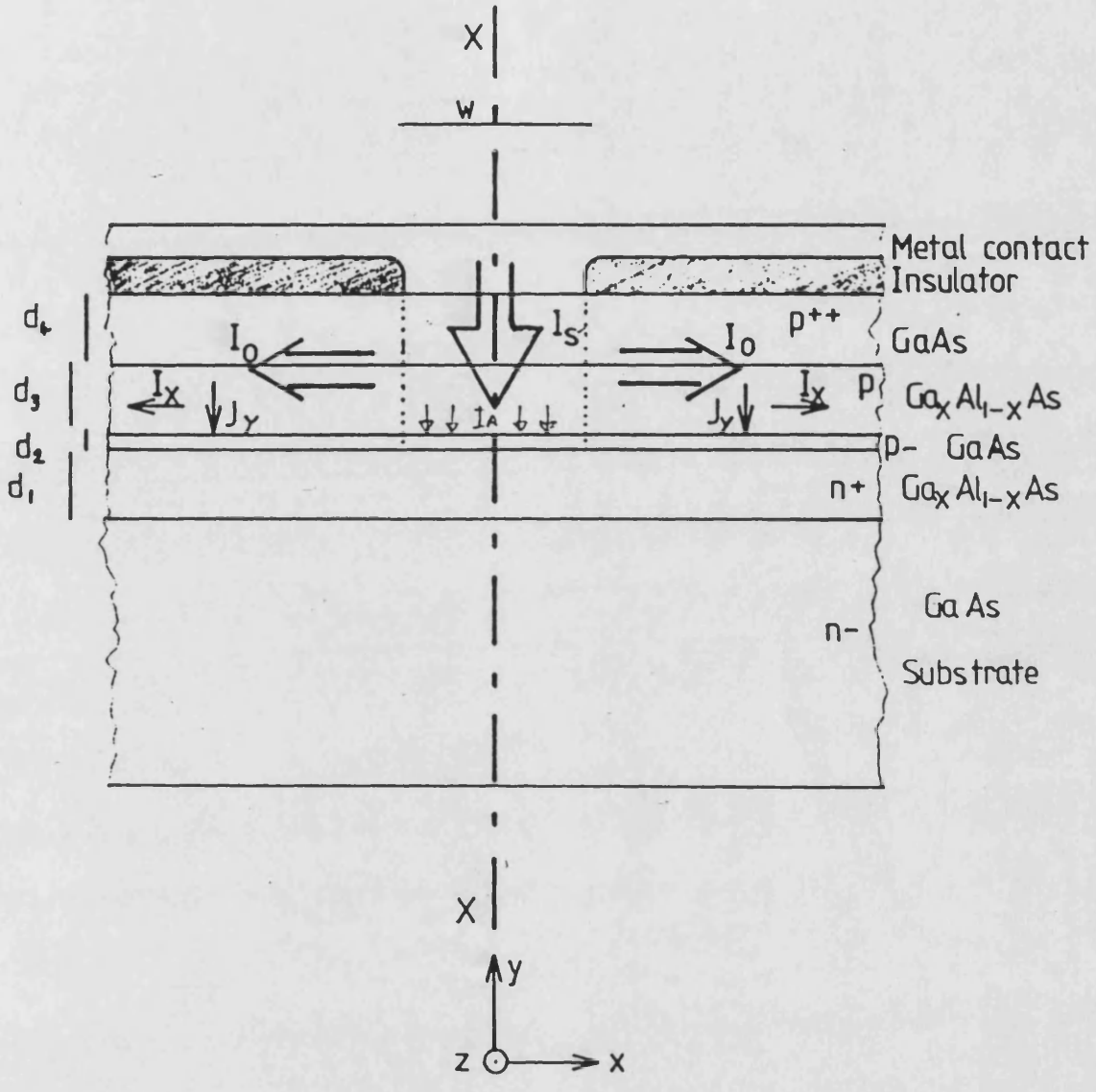

Fig. 2-2 Laser Diode Structure

Fig. 2-2 The crossection of a laser diode, perpendicular to the stripe contact, width w, is shown. The structure is symmetric about the line X-X and the active layer is the thin layer of thickness d . The current distribution in the device is shown splitting into three components, I_A directly from the contact to the active layer and I_D to either side.

2-2 Stripe Contacts

To confine the current in the lateral, x direction, the simplest approach is to confine the area of current injection. The contact then takes the form of a simple stripe. In the case of a simple planar structure the current will inevitably spread out to either side under the stripe. If the current spreads out then the current density entering the active layer is reduced. This would produce a corresponding reduction in inversion population. The optical gain of the structure is dependent on carrier density and if this can be maximised the device will perform better.

To improve the carrier confinement the areas on either side of the stripe can be proton bombarded [1] or oxygen implanted [2] (Fig. 2-3a). The crystal lattice is thereby damaged, particularly near the surface, depending on the depth to which the protons reach. There are two possible outcomes. In both cases the resistivity of the top GaAlAs layer is increased, confining the carriers to enter the active layer only under the stripe. If protons reach deep into the sample then the active layer itself will be affected. This does not totally stop carrier diffusion away within the active layer but it reduces the diffusion constant by up to 30%[3]. At the same time it reduces the carrier lifetime by a factor of twenty, leading to greater carrier loss through out diffusion. In some circumstances oxygen implantation does not greatly reduce carrier lifetime and can be used to improve device performance in this configuration [2].

Another solution to the problem of carrier confinement is to etch away the layers on either side of the stripe to form a mesa (Fig. 2-3b). If only the layers above the stripe are etched then the current spreading is controlled and the guiding mechanism is provided through the effective change in the refractive index of the active layer on either side of the stripe. If the active

layer is also etched away then the mesa would have to be very narrow if it is to form a single mode guide. Alternatively a region of semiconductor could be grown on either side which has a high resistivity and a refractive index only slightly less than that of the active layer [4]. This structure causes purely index guiding because of the refractive index step in the x direction.

Passive guiding which produces a single x directed mode requires a value of effective frequency v_x less than $\frac{\pi}{2}$. Since the width of the stripe is much greater than the thickness of the active layer this implies a smaller refractive index step in x than in y is needed to ensure a single lateral mode. A simple passive guiding structure can be produced by diffusing an impurity into the region below the stripe in a planar structure (Fig. 2-3c). The width of the diffusion will be the width of the passive guiding region and in general the stripe contact will be wider than this. The passive guiding comes from the fact that material into which the impurity has diffused has a higher refractive index than the original material [5] . So that the effective dielectric constant in the diffusion region under the stripe is higher than that on either side. However, this does not relieve the problem of current spreading.

For monomode laser operation one of the best solutions is to create a passive guide by etching a groove under the stripe and regrowing with a GaAlAs layer. If liquid phase epitaxy is used then the GaAlAs will grow preferentially in the groove leaving a curved surface over its cross section. When the active layer is grown it takes up a crescent shape profile, thicker in the centre than at the edge. It may even become detached from the GaAs layer at either side [6]. (Fig. 2-3d). This crescent shaped active layer reduces current spreading and confines the optical field to the centre.

The width of the active part of the active layer for a monomode guide can be calculated from equation (2-1.1) if the slab approximation is accepted. Even when the slab approximation is not valid the result will give the order of magnitude of the active width and so the stripe width. The step in the refractive index in the x direction is very small, of the order of 10^{-4}, which is smaller than the index step in the y direction. This implies a stripe width of the order of $10\mu m$.

The object of this thesis is not to study laser phenomena. The object is to study the effect of spontaneous emission under "below threshold" conditions and how it couples to a guided mode. The results only apply to travelling wave optical amplifier structures with anti reflection coated facets. The simplest structure is one which has no index guiding built in. The x direction guiding mechanism is governed by carriers injected into the active layer. Despite the action of current spreading and diffusion of carriers, the carrier density profile can readily be calculated and the waveguiding analysed.

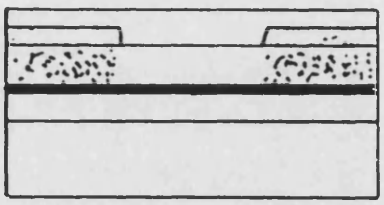

a/ Proton bombarded / oxygen implanted

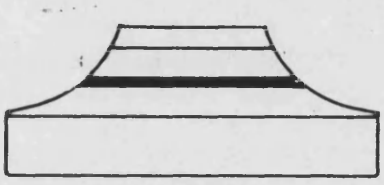

b/ Mesa

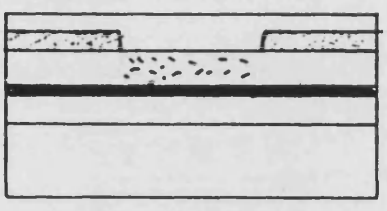

c/ Zn or impurity diffused

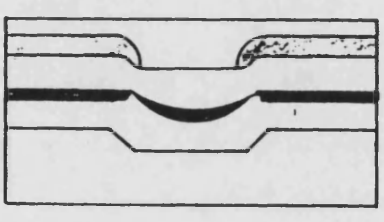

d/ Channelled substrate planar

Fig. 2-3 Lateral structures for charge and radiation confinement.

Fig. 2-3 There are several methods of improving charge and radiation confinement in heterostructure light emitting diode structures. Some of these are illustrated here. The active layer in all cases is the thin shaded region.

2-3 The Model Under The Stripe

In broad stripe contact devices ($w > 15\mu m$) the injected current can be considered as entering the active layer only under the stripe contact. Current spreading and carrier diffusion do not greatly increase the width of the active section of the active layer which is important. In narrow stripe devices, except for mesa or non continuous active layers, the carriers spread out under the stripe due to current spreading below the stripe and diffusion in the active layer (Fig. 2-2).

The problem of current spreading has been treated analytically in several ways. [7,8,9,10] A full solution would involve an analysis of the potential variation in the layers above the active layer and a model of the p-n junction effect in that layer. Such an analysis would yield mainly numerical results. The theory proposed by Yonezu et al. [14] and followed by Tsang [8], gives an insight into how the carrier density in the active layer is affected and is closely followed here. The total current through the stripe is I_S but this splits into two components, I_A into the active layer and I_X parallel to the junction in each direction, so that

$$I_S = I_A + 2I_X \tag{2-3.1}$$

The current density entering the active layer J_A, is assumed to be uniform in the region beneath the stripe, because of the close proximity of the stripe contact. Outside the stripe, however, the current density must vary with position.

Consider an elemental region at a position x where $x >> \frac{w}{2}$.

The change in the current flowing in the x direction is due to the current flowing across the p-n junction of the active layer. Then referring to Fig.2-2,

$$-dI_X = J_Y(x)\, L\, dx \tag{2-3.2}$$

Where L is the length of the contact. Since J_Y is the current across a p-n junction, it is related to the junction voltage by

$$J_Y = J_{sat}\,(\exp(\beta V_j) - 1) \tag{2-3.3}$$

The voltage drop in the x direction is related to the resistance of the layers above the active layer and the current flowing in them.

$$-\frac{dV_X(x)}{dx} = R_S\, I_X \tag{2-3.4}$$

Where $\frac{1}{R_S} = \frac{d_3}{\rho_3} + \frac{d_4}{\rho_4}$ and ρ_3, ρ_4 and d_3, d_4 are the sheet resistivities and thicknesses of layers three and four. (See Fig. 2-2 and Fig. 2-4)

Differentiating equation (2-3.3) and substituting for J_{sat}, and for $\frac{dV}{dx}$ from (2-3.4), since the junction voltage $V_X = V_j$ and assuming $\exp(\beta V_j) >> 1$, gives

$$\frac{d^2 I_X}{dx^2} = -\beta R_S I_X \frac{dI_X}{dx} \tag{2-3.5}$$

Which has the solution for x directed current flow

$$I_X(x) = \frac{I_X\left(\frac{w}{2}\right)}{1 + \frac{x - w/2}{l_0}} \tag{2-3.6a}$$

$$l_0 = \frac{2}{\beta R_S I_X(\frac{w}{2})} \tag{2-3.6b}$$

Differentiating this and comparing with (2-3.2) gives the y directed current

density J_Y as a function of x

$$J_Y(x) = \frac{J_A}{\left[1+\frac{x-w/2}{l_0}\right]^2} \qquad x > \frac{w}{2} \tag{2-3.7a}$$

$$= J_A = \frac{I_X(w/2)}{Ll_0} \qquad |x| < \frac{w}{2} \tag{2-3.7b}$$

This implies that $I_A = J_A wL = I_X(w/2)\frac{w}{l_0}$ which allows $I_X(\frac{w}{2})$ to be substituted for in (2-3.1), using (2-3.6b)

$$I_S = I_A + 2\left[\frac{2I_A}{w\beta R_S}\right]^{1/2} \tag{2-3.8}$$

It is convenient at this point to convert to current densities since J_A is the quantity required from this analysis. A new constant J_Q with dimensions of current density is now defined as $J_Q = (\beta R_S L^{1/2} w^2)^{-1}$ so that

$$J_S = J_A + 2(J_A J_Q)^{1/2} \tag{2-3.9}$$

From which it follows that

$$J_A = J_S - 2J_Q\left[\left[1+\frac{J_S}{J_Q}\right]^{1/2} - 1\right] \tag{2-3.10}$$

For wide stripes J_Q is small, and J_A tends to J_S.

The characteristic spreading distance can also be written in terms of J_Q

$$l_0 = \frac{w}{2}\left[2\frac{J_Q}{J_A}\right]^{1/2} = \left[\frac{2}{\beta R_S L J_A}\right]^{1/2} \tag{2-3.11}$$

which is large when J_Q is large but does not increase in proportion to stripe width.

To illustrate the behaviour of J_A with J_S these quantities have been normalised to J_Q and plotted in Fig. 2-5a . For an efficient device J_A should be nearly equal to J_S but this relies on J_S being much greater than J_Q . J_Q itself is dependant on both material properties and device structure. A plot of $\frac{l_0}{w}$ against $\frac{J_S}{J_Q}$. is also shown.

A plot of the y directed current density as a function of its position x for J_S equal to 10, 20 and 30 J_Q is shown in Fig. 2-5b. to illustrate current density profiles.

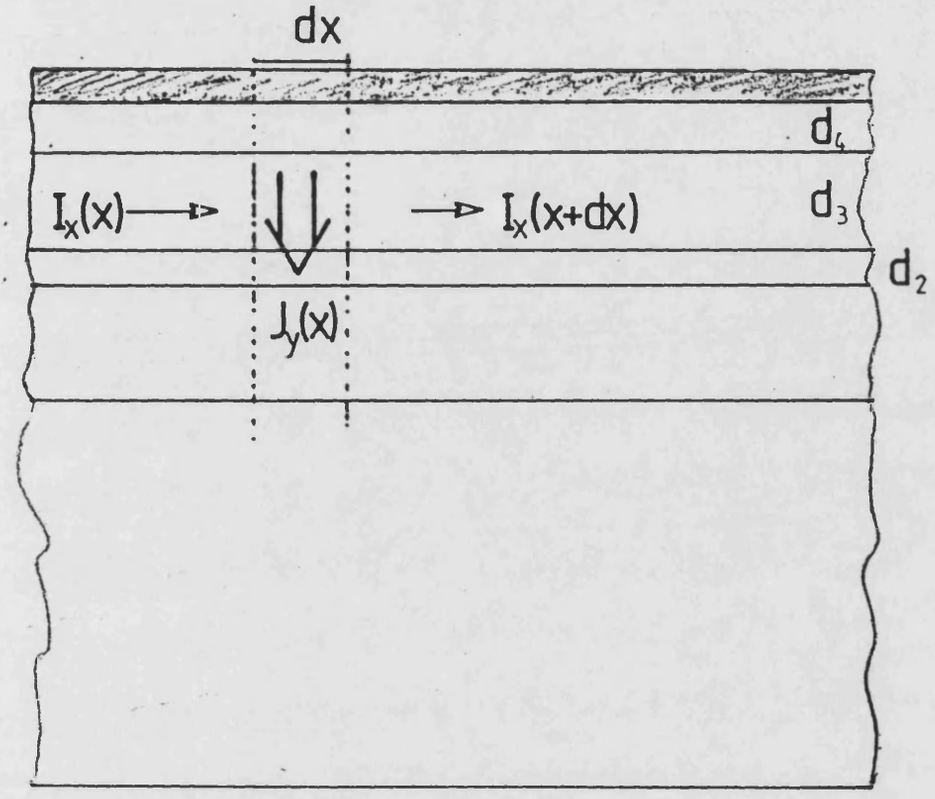

Fig 2-4 Current flow in elemental region of width dx.

Fig. 2-4 The current flow parallel to the junction, I_x, gives rise to a finite current density into the active layer, $J_Y(x)$, on either side of the stripe contact.

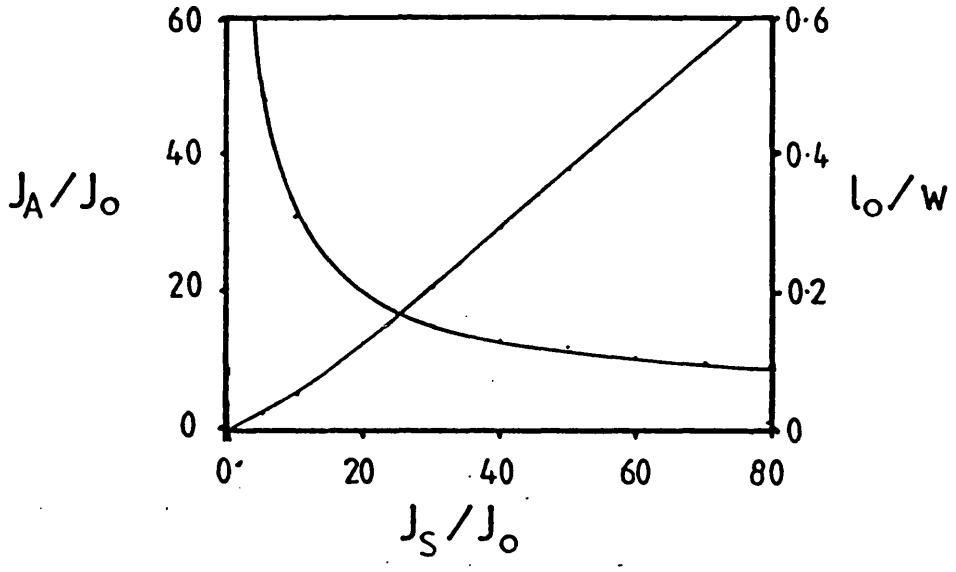

Fig. 2-5a Normalised active layer current density and normalised current spreading length vs. normalised injection current density. This shows that the active layer current density is almost linearly dependent on injection current density for $J_S >> J_o$ and that the diffusion length decreases as J_S increases.

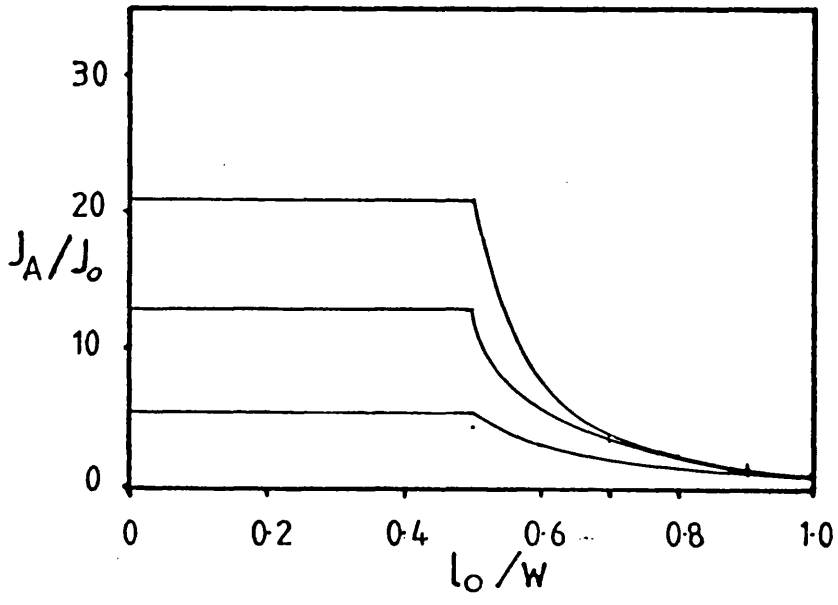

Fig 2-5b Stripe injection current density

The model used assumes that the current density under the stripe contact is constant but decays inversly as x squared outside the active layer. Three different levels of injection are illustrated to show the effect of the change in current spreading length on the tails of the current density distribution.

2-4 Diffusion of Carriers

The carriers are initially injected through the stripe and some current spreading may occur above the active layer. In the active layer the carriers diffuse away from their initial position because of their random thermal motion. The one dimensional diffusion equation takes the form

$$D\frac{d^2N}{dx^2} - \frac{N}{\tau_s} + \frac{J}{qd_2} = gP(h\nu) \qquad (2\text{-}4.1)$$

Where g is the optical power gain and $P(h\nu)$ is the optical power. If the photon density is small then the term $gP(h\nu)$ may be ignored. $N(x)$ is the density of charge carriers, D is the diffusion coefficient, x is the distance from the centre of the guide, $J_Y(x)$ is the current density, q is the electronic charge and d_2 is the guide thickness. The spontaneous electron lifetime is τ_s. An analytic solution is possible if τ_s is assumed constant and the current density $J_Y(x)$ has the profile

$$J_Y(x) = J_A \qquad |x| < \frac{w}{2} \qquad (2\text{-}4.2a)$$

$$J_Y(x) = 0 \qquad |x| \geq \frac{w}{2} \qquad (2\text{-}4.2b)$$

This has the solution shown below in equation (2-4.3) (see fig. 2-6a)

$$N(x) = \frac{J_A\tau_s}{qd_2}\left[1 - \exp\left(-\frac{w}{2l_s}\right)\cosh\left(\frac{x}{l_s}\right)\right] \qquad |x| \leq \frac{w}{2} \qquad (2\text{-}4.3a)$$

$$N(x) = \frac{J_A\tau_s}{qd_2}\sinh\left(\frac{w}{2l_s}\right)\exp\left(\frac{-|x|}{l_s}\right) \qquad |x| > \frac{w}{2} \qquad (2\text{-}4.3b)$$

Where $l_s = (D\tau_s)^{-\frac{1}{2}}$. In fact the spontaneous lifetime of electrons depends on the carrier density

$$\tau_s^{-1} = B(N + p_0) \qquad (2\text{-}4.4a)$$

The exact solution of (2-4.1) is no longer simple but a stepwise numerical approximation can be found. If a number of discrete regions of carrier density are considered with different values of τ_s then τ_s for region r is given by

$$\tau_r^{-1} = B(N_r + p_0) \qquad (2\text{-}4.4b)$$

The second derivative term of N in (2-4.1) can be replaced by the central difference formula

$$D\frac{d^2N_r}{dx^2} = \frac{N_{r+1} - N_r}{\tau_D} + \frac{N_{r-1} - N_r}{\tau_D} \qquad (2\text{-}4.5)$$

Where $D\tau_D = (\Delta x)^2$ and Δx is the width of each elemental region. The diffusion equation (2-4.1) now becomes

$$\frac{N_r}{\tau_r} + \frac{N_r - N_{r-1}}{\tau_D} + \frac{N_r - N_{r+1}}{\tau_D} - \frac{J_r}{qd} = 0 \qquad (2\text{-}4.6)$$

The values of J_r can be determined from the current spreading properties discussed in section 2-3 and can have any distribution required.

To solve (2-4.6) by numerical methods a set of recurrence relations for N_r is now derived. To do this the boundary conditions must be considered. Since the problem is symmetrical only one side of the distribution needs to be calculated. If N_1 is the value of N nearest the stripe centre and N_0 the value to the left then $N_1 = N_0$ (See Fig. 2-6b). At the other extreme, since N cannot actually be zero for large x, (only $x \to \infty$), the choice of $\frac{dN}{dx}$ tends to zero for x tends to infinity is made. i.e. $N_n = N_{n+1}$, so that with

$$x_r = \left[\tau_D \left[\frac{1}{\tau_r} + \frac{2}{\tau_D}\right]\right]^{-1} \qquad (2\text{-}4.7a)$$

$$y_r = \frac{J_r}{qd\left[\frac{1}{\tau_r} + \frac{2}{\tau_D}\right]} \qquad (2\text{-}4.7b)$$

giving

$$N_r - x_r(N_{r+1} + N_{r-1}) - y_r = 0 \qquad (2\text{-}4.8)$$

Substituting the second boundary condition gives for $r = n$

$$N_n(1 - x_n) = x_n N_{n-1} + y_n \qquad (2\text{-}4.9a)$$

$$N_n = x_n' N_{n-1} + y_n' \qquad (2\text{-}4.9b)$$

Where $x_n' = \frac{x_n}{1 - x_n}$ and $y_n' = \frac{y_n}{1 - x_n}$ Now for the next region, $r = (n-1)$ from (2-4.8) and (2-4.9)

$$N_r - x_r((x_{r+1}' N_r + y_{r-1}') + N_{r-1}) - y_r = 0$$

i.e.

$$N_r = x_r' N_{r-1} + y_r' \qquad (2\text{-}4.10)$$

Where

$$x_r' = \frac{x_r}{1 - x_r x_{r+1}'} \qquad (2\text{-}4.11a)$$

$$y_r' = \frac{y_r + x_r y_{r+1}'}{1 - x_r x_{r+1}'} \qquad (2\text{-}4.11b)$$

And so (2-4.10) is identical in form to (2-4.9) and (2-4.10) and (2-4.11)

represent general recurrence relations for $(n-1)\geqslant r\geqslant 2$

Finally the boundary condition at $x=0$ gives, from (2-4.8)

$$N_1 = x_1(N_2+N_0)+y_1$$

but from (2-4.10) with $r=2$ it follows that

$$N_1 = \frac{y_1+x_1y_2'}{1-x_1x_2'-x_1} = y_1' \qquad (2\text{-}4.12)$$

So, this analysis has resulted in two sets of recurrence relations, the first in x_r and y_r and the second in N_r. The solution for constant τ_s is simply found by using the recurrence relations in x_r and y_r to establish y_1' and hence N_1 and so all values of N_r. When τ_s is dependent on N it is necessary to start by finding a solution with constant τ_s and then calculating τ_r and so x_r and y_r from the result. This procedure can be repeated until the solution converges to the required accuracy.

Solutions found in this way are useful in considering the shape of the carrier profile for devices where current spreading is also important, and have the further advantage of including a variable τ_s.

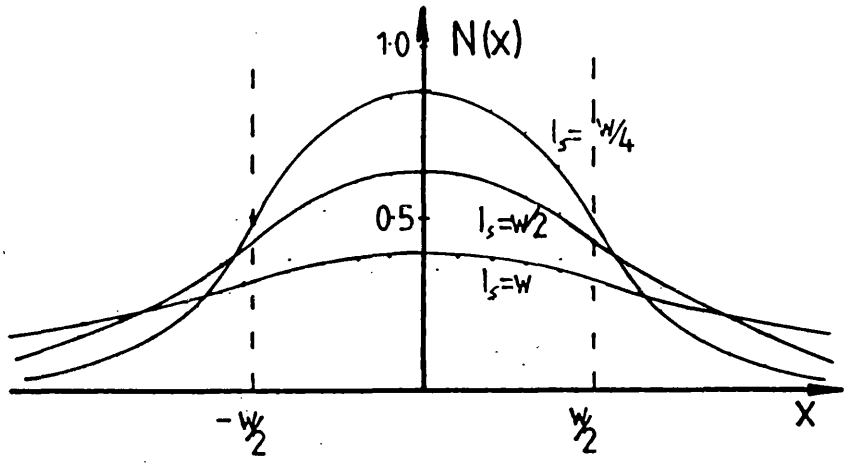

Fig 2-6a Carrier profile for τ_s constant

Fig. 2-6a The carrier profile can be calculated for the case where the diffusion time is constant and the current density on either side of the stripe contact is zero. The three curves represent different diffusion lengths as indicated.

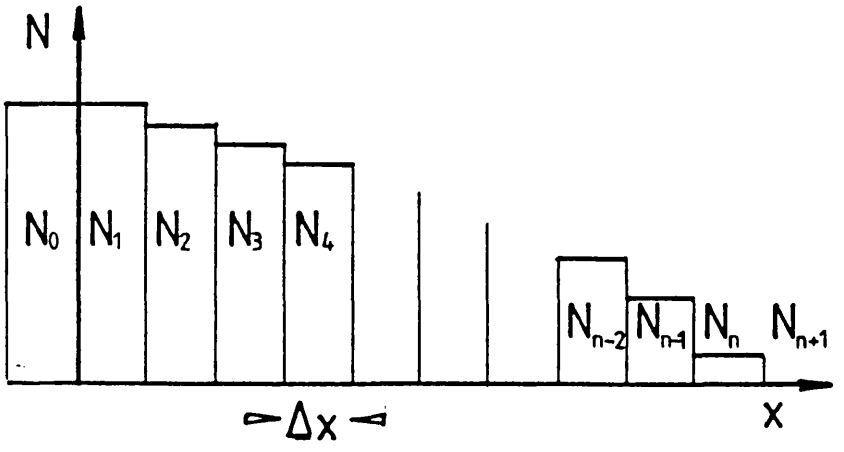

Fig 2-6b Regions of carrier density

Fig. 2-6b In order to solve the diffusion equation for an arbitrary current density profile and a variable diffusion time the active layer is split into a number of elemental regions, each with a different carrier concentration.

2-5 Appropriate Diffusion Profiles

In general, it is easier to find an approximation to the carrier profile in the active layer than to use a computer calculated profile. The simplest way to do this is to consider a three layer slab waveguide with three regions of constant refractive index, and hence constant carrier density. Obviously, the carrier density will be expected to be some kind of average value over each region. These values can be calculated by letting Δx, the width of an elemental region in the numerical solution of the diffusion equation, be equal to the stripe width, or half the stripe width, (Fig. 2-7). If $\Delta x = \frac{w}{2}$ then the boundary conditions can be set at $x = 0$ and for $x \to \infty$.

At $x = 0$ $\frac{dN}{dx} = 0$ and so $N_1 = N_0$, and for $x \to \infty$ $\frac{dN}{dx} = 0$. This implies that $N_2 = N_3$ (See Fig. 2-7a). However, the mode profile for a bound mode of such a slab results in a field which tends to zero exponentially as x tends to infinity. In practice, N becomes very small for large x but with this boundary condition N has a constant value. A better approximation might to be to let $N \to 0$ as $x \to \infty$. i.e. $N_3 = 0$. For the case of $\Delta x = w$ (Fig 2-7b) the boundary conditions occur for $x \to \pm \infty$ and can be either of these two discussed. These solutions are tabulated in Table 2-1 for the case where the current density enters the active layer only under the stripe. In principle the analysis can be extended to the situation where J_2 is also non zero. In fact this simple analysis has some important drawbacks. The solutions of the diffusion equation (2-4.3) with a constant spontaneous electron lifetime τ_s should provide similar results for the average value of N in each region. The maximum value N_{max} at $x = 0$ for (2-4.3) is given by $N_{max} = \frac{J\tau_s}{qd}(1 - \exp(\frac{w}{2l_s}))$. For $\tau_s = 4\text{ns}, l_s = 3.5\mu\text{s}$ and $w = 7\mu\text{m}$ the value of

N_{max} is $0.63\frac{J\tau_s}{qd}$. The average value under the stripe, for the same numerical values, is $0.51\frac{J\tau_s}{qd}$. The solutions in Table 2-1 are for the same numerical values but three of the four give an average value of N which is greater than this value of N_{max}. A more realistic solution can be obtained by changing the ratio of τ_s and τ_D, but another approach might be more reliable.

The carrier profile can be calculated as described for a large number of elementary regions. The average values required for the slab model can then be found by simply calculating the average in each region. In this way the effect of any current profile can be included and the value of N can still be calculated. Using this method the actual position of the slab boundary is no longer necessarily the stripe edge. An effective slab width can be defined on any number different principles. One possiblilty would be to let the effective slab boundary be at the position where $N = \frac{N_{max}}{2}$

The electromagnetic fields do not have to be derived from slab boundary conditions if another set of orthogonal functions can be found which represent the electromagnetic field ditribution [12,13,14]. The solution of the diffusion equation for a symmetric stripe guide leads to diffusion profiles which are symmetric, $N(x)$ is an even function. The Lorentz distribution and a $\cosh^{-2}\left(\frac{x}{w}\right)$ profile would have the correct behaviour as $x \to \infty$. If the electromagnetic fields are closely bound to the area under the stripe then the carrier profile need only match the numerically calculated values under the stripe. In this situation a parabolic [14] or a $\cos^{-2}\left(\frac{x}{w}\right)$ [13] type profile might be considered. To compare these different approximations each of these curves can be normalised so as to coincide with the calculated profile at the stripe

centre and the stripe edge. Those distributions which tend to zero for $x \to \infty$ could be further adjusted so that they tend to some finite limit but this has not been done.

These carrier profile functions that have been plotted are tabulated in Table 2-2 along with the expressions for the normalisation width of each. N_2 is the value of N at the stripe edge and N_0 the value at the stripe centre. These profiles are plotted in Fig. 2-8.

All these suggested profiles can be expected to fit the carrier profile reasonably well close to the stripe but only profiles 3 and 4 show the correct behaviour for $x \to \infty$. For this reason profiles 3 and 4 would seem to be the best for a discussion of weakly bound active modes.

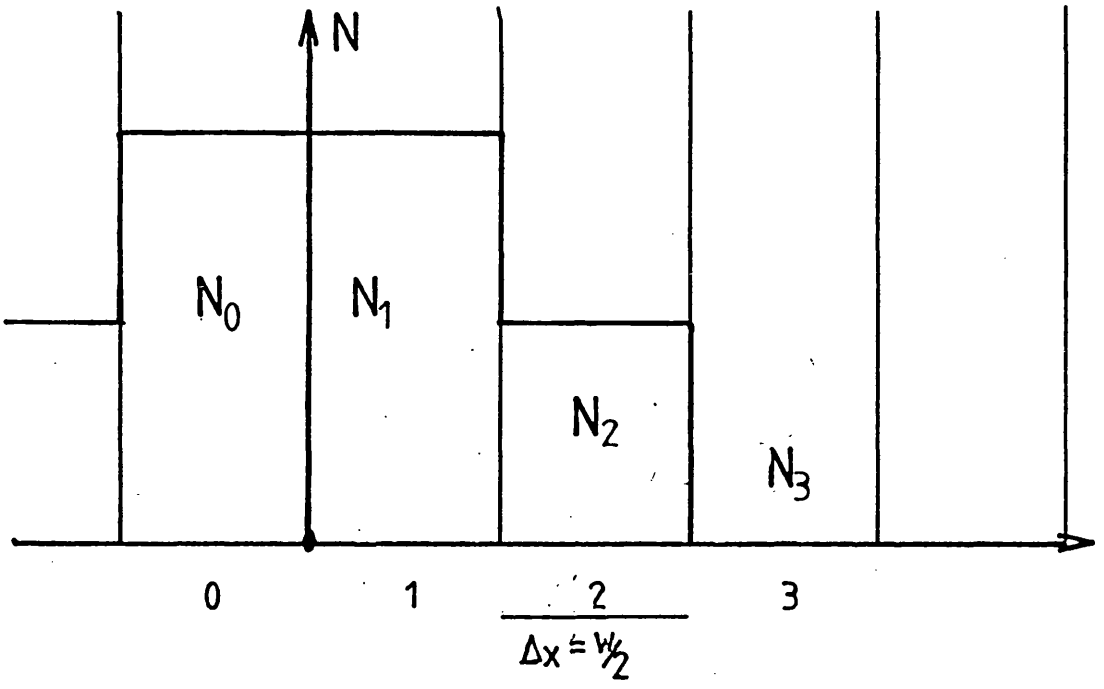

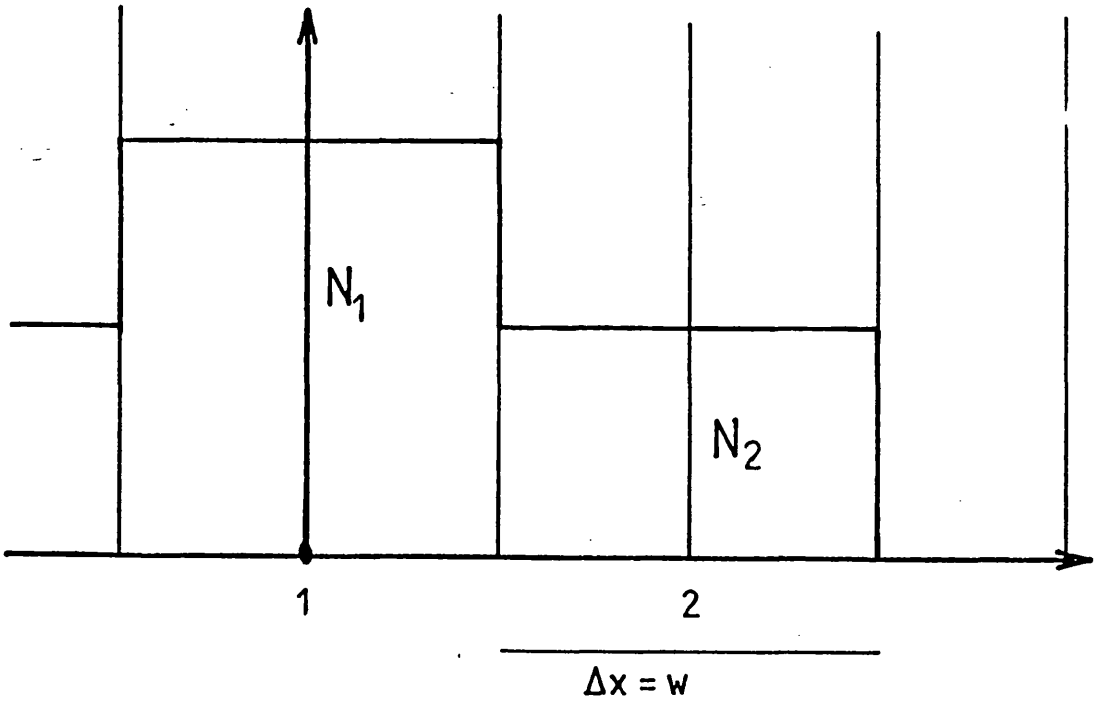

Fig 2-7 Simple slab carrier profiles

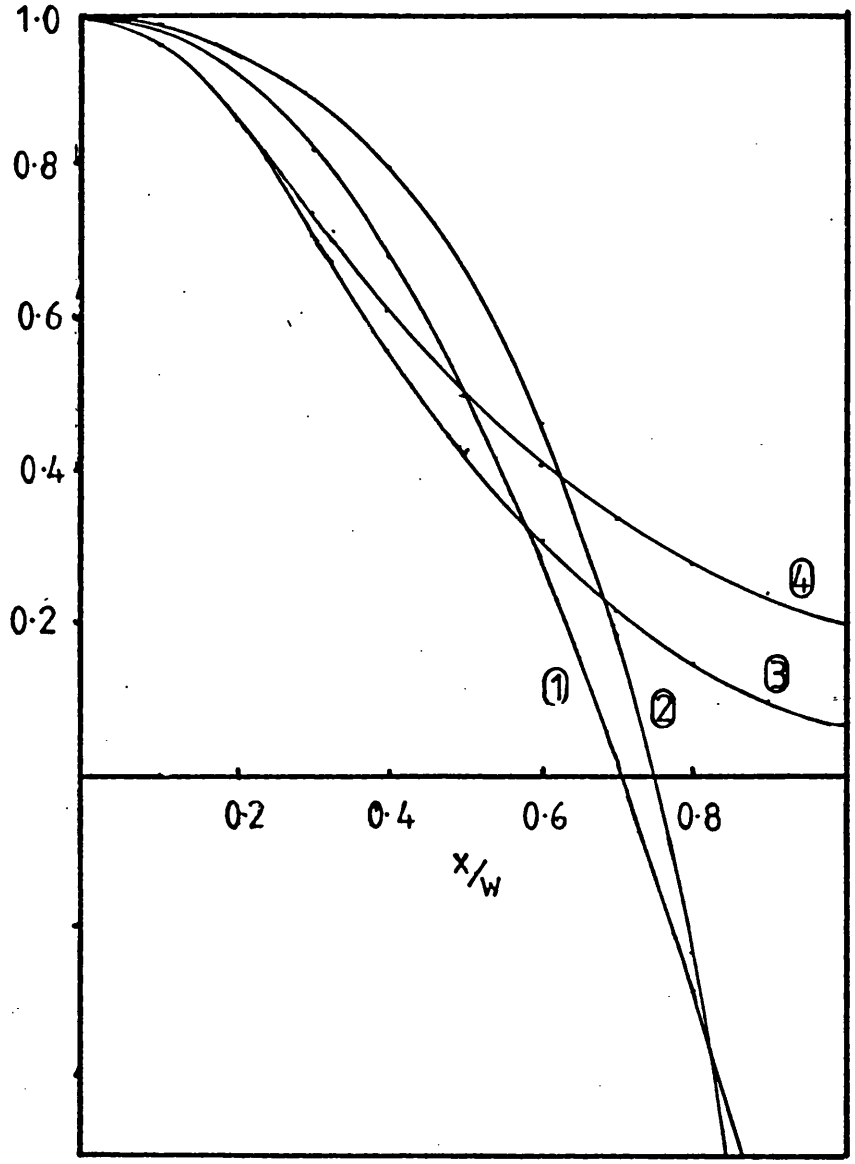

Fig 2-8 Approximate diffusion profiles

1/ $1 - 2x^2$

2/ $1 - \tan^2(\pi/3\ x)$

3/ $\cosh^2(2x)$

4/ $(1-(2x)^2)^{-1}$

Table 2-1

Table 2-1 gives the solutions for N_1 and N_2 for several sets of boundary conditions. These are the width, Δx, of the layers and the boundary condition for $J_1 = J$ and $J_2 = J_3 = 0$.

Three layer slab solutions							
Width Δx	Limit for $x \to \infty$	Density $N_1\left(\frac{J\tau_s}{qd}\right)^{-1}$	Density $N_2\left(\frac{J\tau_s}{qd}\right)^{-1}$	$\frac{N_1}{N_2}$ *		$N_{\Delta x}\left(\frac{J\tau_s}{qd}\right)^{-1}$	
				τ_s = 4ns	8ns	τ_s = 4ns	8ns
$\frac{w}{2}$	$\frac{dN}{dx} = 0$	$\frac{\tau_s + \tau_D}{2\tau_s + \tau_D}$	$\frac{\tau_s}{2\tau_s + \tau_D}$	2	1.5	0.67	0.6
$\frac{w}{2}$	$N = 0$	$\frac{\tau_D(2\tau_s + \tau_D)}{\tau_s^2 + 3\tau_s\tau_D + \tau_D}$	$\frac{\tau_s\tau_D}{\tau_s^2 + 3\tau_s\tau_D + \tau_D}$	3	2.5	0.6	0.45
w	$\frac{dN}{dx} = 0$	$\frac{\tau_D + \tau_s}{3\tau_s + \tau_D}$	$\frac{\tau_s}{3\tau_s + \tau_D}$	5	3	0.71	0.53
w	$N = 0$	$\frac{\tau_D(2\tau_s + \tau_D)}{3\tau_s^2 + 4\tau_s\tau_D + \tau_D}$	$\frac{\tau_s\tau_D}{3\tau_s^2 + 4\tau_s\tau_D + \tau_D}$	6	4	0.89	0.53

* The numerical values in this part of the table were calculated using the values, $w = 7\mu m$ and $D = 3.3\times10^{-3} m^2 s^{-1}$ so that $\tau_D = (\Delta x)^2 D^{-1}$, i.e. $\tau_D \approx 4ns$ for $\Delta x = \frac{w}{2}$ and $\tau_D \approx 16ns$ for $\Delta x = w$. Two sets of values are given in the numerical part of the table corresponding to τ_s = 4ns and τ_s = 8ns.

Table 2-2

Approximate Profiles

	Distribution	Normalisation	at $x = \frac{w}{2}$	at $x = w$
1	$N = N_0 \left\lvert 1 - 2 \left\lvert \frac{x}{w_1} \right\rvert^2 \right\rvert$	$w_1 = \frac{w}{2} \left\lvert \frac{2}{1 - N_2/N_0} \right\rvert^{1/2}$	$N = 0.5 N_0$	$N = -N_0$
2	$N = N_0 \left\lvert 1 - \tan^2 \left\lvert \frac{\pi}{3} \frac{x}{w_2} \right\rvert \right\rvert$	$w_2 = w \frac{\pi}{6} \left\lvert \arctan \left\lvert (1 - N_2/N_0)^{1/2} \right\rvert \right\rvert^{-1}$	$N = 0.42 N_0$	$N = -2 N_0$
3	$N = N_0 \left\lvert \cosh \left\lvert \frac{2x}{w_3} \right\rvert \right\rvert^{-2}$	$w_3 = w \left\lvert \operatorname{artanh} \left\lvert (1 - N_2/N_0)^{1/2} \right\rvert \right\rvert^{-1}$	$N = 0.67 N_0$	$N = 0.07 N_0$
4	$N = N_0 \left\lvert 1 + \left\lvert \frac{2x}{w_4} \right\rvert^2 \right\rvert^{-1}$	$w_4 = w \left\lvert \frac{N_0}{N_2} - 1 \right\rvert^{-1/2}$	$N = 0.5 N_0$	$N = 0.2 N_0$

References for Chapter 2

1/ J.C.Dyment, L.A.D'Asaro, J.C.North, B.I.Miller, J.E.Ripper, " Proton bombardment formation of stripe geometry heterostructure lasers for 300K cw operation ", Proc.IEEE.(Lett.), 60 , pp726-728, 1972.

2/ J.M.Blum, J.C.McGruddy, P.G.McMullin, K.K.Shih, A.W.Smith, J.F.Ziegler, " Oxygen-implanted double heterojunction GaAs/GaAlAs injection lasers ", IEEE.J.Q.Electron., QE-11 , pp413-418, 1975.

3/ B.W.Hakki, " Carrier and gain spatial profiles in GaAs stripe geometry lasers ", J.Appl.Phys., 44 , (11), pp5021-5028, 1973.

4/ W.T.Tsang, R.A.Logan, M.I.Legems, " High power fundamental-transverse-mode stripe buried heterostructure lasers with linear light-current characteristics ", Appl.Phys.Lett., 32 , pp311-314, 1978.

5/ T.E.Rozzi, J.H.C.van Heuven, G.H.in't Veld, " A new D.H. laser configuration with passive transverse field confinement ", Electron.Lett., 14 , (4), pp87-88, 1978.

6/ P.A.Kirby, G.B.H.Thompson, " Channelled substrate buried heterostructure GaAs-(GaAl)As injection lasers", J.Appl.Phys., 47 , pp4578-4589.

7/ B.W.Hakki, " GaAs double heterostructure lasing behaviour along the junction plane ", J.Appl.Phys., 46 , (1), pp292-302, 1975.

8/ W.T.Tsang, " The effects of lateral current spreading carrier out-diffusion, and optical mode losses on the threshold current density of GaAs-GaAlAs stripe-geometry D.H. lasers ", J.Appl.Phys., 49 , (3), pp1031-1044, 1978.

9/ W.B.Joyce, " Current-crowded carrier confinement in double-heterostructure lasers ", J.Appl.Phys., 51 , (5), pp2394-2401, 1980.

10/ H.Yonezu, I.Sakuma, K.Kobayashi, T.Kamejima, M.Ueno, Y.Nannichi, " A GaAs-AlGaAs double heterostructure planar stripe laser ", Jap.J.Appl.Phys.,

12 , (10), pp1585-1592, 1973.

11/ K.A.Shore, T.E.Rozzi, G.H.in't Veld, " Semiconductor laser analysis: general method for characterising devices of various cross-sectional geometries ", IEE.Proc., 27 , (5), pp221-229, 1980.

12/ W.Streifer, D.R.Scifres, R.D Burnham, " Analysis of gain-induced waveguiding in stripe geometry diode lasers ", IEEE.J.Q.Electron, QE-14 , (6), pp418-427, 1978.

13/ W.Streifer, R.D.Burnham, D.R.Scifres, " Symmetrical and asymmetrical waveguiding in very narrow conducting stripe lasers ", IEEE.J.Q.Electron, QE-15 , (3), pp136-141, 1979.

14/ F.R.Nash, " Mode guidance parallel to the junction plane of double-heterostructure GaAs lasers ", J.Appl.Phys., 44 , (10), pp4696-4707, 1973.

CHAPTER 3

3-1 Light Emission in Direct Band Gap Semiconductors

Spontaneous and stimulated emission in semiconductors are of prime importance for optoelectronic devices. Consequently calculations of these phenomena in III-V semiconductors, and in particular GaAs, have been made. [1,2,3] In many cases the object has been to find the maximum gain and corresponding spontaneous emission over a narrow band for comparison with the performance of D-H lasers. In the study of active guides where lasing does not occur, gain is important because it forms the guided mode. For a spectral treatment of active guides it is therefore important to know the gain and corresponding spontaneous emission strength over a wide range of wavelengths. Such a detailed set of results has not appeared in the literature to date and for this reason some calculation is necessary. Several approximate models have been developed [4,5,6] but none include any band tailing which is characteristic of degenerate impure semiconductors. [7,8] The band tails occur at energies within the band gap of the pure crystal and contribute to the output spectrum of any device, particularly at low levels of injection.

Light is emitted in semiconductors as the result of a transition of an electron between the conduction and valence bands. In thermal equilibrium there are a few occupied states in the conduction band and similarly a few empty states in the valence band. An electron in the conduction band has a certain probability of falling into one of the empty valence band states. In doing so a photon is created, the energy of which is the energy difference between the two states.

Should a photon of suitable energy pass through the semiconductor there is a possibility that it might cause a electron transition. In thermal

equilibrium this has a greater probability of being an upward transition because there are few occupied states in the conduction band. In this process the photon is absorbed. If the photon should cause a downward transition then a new photon is created with the same energy and in phase with the original. If, by some means, the number of electrons in the conduction band can be made to exceed the number of holes in the valence band then the number of stimulated emissions can be made greater than the number of absorptions.

The theory of band to band transitions gives the basic equations with which to derive a working approximation for the spectral radiation characteristics of GaAs. The approximations must be as simple as possible and yet still show the same behaviour as experimental results. Although attempts by this author to measure gain and spontaneous emission profiles were unsuccessful this has been done by other authors[9], and the results are in agreement with those of Stern[3]. The spectral characteristics of the radiation are dependent upon the conduction and valence band shapes. The simplest model considered is based on parabolic band shapes. The calculations of Marinelli [6] are combined with approximations for the Fermi-levels proposed by Joyce and Dixon [5]. This analysis provides an analytic model for gain and spontaneous emission in terms of the inversion population.

The effect of band tails on the basic parabolic band shapes is investigated. Theoretically derived band tail lengths depend on screening lengths for an electron. Since the screening length changes with inversion population the band tail lengths change too. This is easiest to see in the expressions for the Kane band tail [7]. (3-3.2,3) The screening length $1/k_s$ is proportional to $N_{AV}^{-1/6}$ and so varies very little over an order of magnitude of N_{AV}. Consequently, for the sake of simplicity, a model based on fixed band tail lengths is considered. A computer program has been written which can be used to produce gain and

spontaneous emission spectra for any band tail shapes. Of most interest here are Kane band tails and an exponential band tail. Exponential-like band tails have been reported [10] and analysed [4] and are within the range of possible band tail shapes predicted by Halperin and Lax [11]. Comparisons between these functions, parabolic bands and the analytic model are made.

3-2 Summary of the Physics of Band to Band Transitions

This section is a brief review of the transition probabilities between energy levels in semiconductors which is needed before calculations can be made.

Planck's Law for thermal radiation [10,12] states that the photon density emitted from a black body is given by

$$P(h\nu)=\frac{8\pi n^2\bar{n}(h\nu)^2}{(hc)^3(\exp(h\nu/kT)-1)} \tag{3-2.1}$$

Where n is the refractive index and $\bar{n}=n+\frac{h\nu\ dn}{d(h\nu)}$. The process of stimulated recombination and generation of photons by a two level, $(N_1.N_2)$, system can be described by

$$-\frac{dN_{E1}}{dt}=B_{12}N_{E1}P(h\nu)=\frac{dN_{E2}}{dt} \tag{3-2.2}$$

$$-\frac{dN_{E2}}{dt}=B_{21}N_{E2}P(h\nu)=\frac{dN_{E1}}{dt} \tag{3-2.3}$$

and the process of spontaneous emission can be described by

$$-\frac{dN_{E2}}{dt}=A_{21}N_{E2}=\frac{dN_{E1}}{dt} \tag{3-2.4}$$

Where $B_{12}.B_{21}$ and A_{21} are the Einstein transition probabilities [12]. In equilibrium, with all processes occuring simultaneously

$$B_{12}N_{E1}P(h\nu)=A_{21}N_{E2}+B_{21}N_{E2}P(h\nu) \tag{3-2.5}$$

If N_{E1} and N_{E2} are given by Boltzmann statistics with Fermi level F then at an energy level E_1

$$N_{E1} = N_{E0}\exp((F-E_1)/kT) \tag{3-2.6}$$

and similarly for N_{E2}. Combining these two results it becomes apparent that $B_{21} = B_{12} = B$ and by rearranging (3-2.5) $P(h\nu)$ can be given as

$$P(h\nu) = \frac{A_{21}/B}{\exp((E_2-E_1)/kT)-1} \tag{3-2.7}$$

This is clearly Plank's Law for thermal radiation with $A = ZB$ where Z is the number of modes per unit volume and

$$Z = \frac{8\pi n^2 \bar{n}(h\nu)^2}{(hc)^3} \tag{3-2.8}$$

If either A or B can be calculated then the other follows. [13,14]. The transition coefficient B is calculated by Stern. The analysis starts with the Schroedinger wave equation.

$$-\frac{\hbar^2}{2m}\nabla^2\phi + V\phi = j\hbar\frac{\partial\phi}{\partial t} \tag{3-2.9}$$

Where $|\phi|^2$ is the probability function describing the position of an electron. The solution for ϕ can be given in terms of orthogonal spatial field functions u_k with amplitude coefficients A_k and frequency $E_k/\hbar$.

$$\phi = \sum_k A_k u_k \exp\left(\frac{-jE_k t}{\hbar}\right) \tag{3-2.10}$$

If the system of one atom is perturbed by an electric field E then Schroedinger's wave equation is perturbed. Only an electric dipole transition need be considered. If q is the electronic charge and $\mathbf{r}_0$ the electron position relative to the atomic centre then

$$j\hbar\frac{\partial\phi}{\partial t} = -\frac{\hbar^2}{2m}\nabla^2\phi + V\phi + \mathbf{E}.q\mathbf{r}_0 \qquad (3\text{-}2.11)$$

The solution can now be expressed with additional time dependencies $a_k(t)$.

$$\phi = \sum_k a_k(t)u_k \exp\left[\frac{-jE_k t}{\hbar}\right] \qquad (3\text{-}2.12)$$

Substituting this in equation (3-2.11) and simplifying using the orthogonality properties of u_k gives

$$j\hbar\frac{da_n}{dt} = e^{j\omega_{bb}t}\int\phi_n^*\mathbf{E}.\mathbf{r}_0\, q\phi_k\, d\tau \qquad (3\text{-}2.13)$$

Where $\omega_{nk} = \omega_{bb} = (E_2 - E_1)/\hbar$ corresponding to a transition between energy levels E_2 and E_1 or energy states n and k. If the electric field is a plane wave of the form $\hat{\mathbf{x}}E_0\cos(\omega t - kz)$ and energy density $P(h\nu) = \frac{1}{2}E_0^2$ this simplifies to

$$a_n = -\left[\frac{P(h\nu)}{2\epsilon\hbar^2}\right]^{\frac{1}{2}}|D_x|^2\left[\frac{\exp[j(\omega_{bb}+\omega)t]-1}{\omega_{bb}+\omega} + \frac{\exp[j(\omega_{bb}-\omega)t]-1}{\omega_{bb}-\omega}\right] \qquad (3\text{-}2.14)$$

The dipole moment D_x is the x component of $\mathbf{D}$.

$$\mathbf{D} = \int\phi_m^*\mathbf{r}_0\, q\phi_k\, d\tau \qquad (3\text{-}2.15)$$

Only one of the terms in the brackets is significant at any one time, when $\omega_{bb} = \pm\omega$. By integrating $|a_n|^2$ over all frequency, provided the final state into which the electron transits exists, the probability of an absorption in time t is

$$|a_n(t)|^2 = \frac{\pi}{2}\frac{|\mathbf{D}|^2}{3}\frac{P(\omega_{bb})}{\epsilon\hbar^2}t \qquad (3\text{-}2.16)$$

Where the assumption is made that $|D_x|^2$ can be replaced by $|\mathbf{D}|^2/3$. The rate

of transitions is proportional to the number of electrons in the upper state, N_1 and the probability of a transition. The rate of power emission R_{stim} is also proportional to the photon energy so that

$$R_{stim} = \hbar\omega \frac{\pi}{2} \frac{|\mathbf{D}|^2}{3} P(\hbar\omega) N_1 \tag{3-2.17}$$

Stern [15] refers to the band to band transition matrix |M| and not the dipole transition element |D| but these are related by

$$\int \phi_n^* \mathbf{E}.\mathbf{r}_0 q \phi_m \, d\tau = \frac{q}{m} A_0 \, |\mathbf{M}| = E_0 \, |\mathbf{D}| \tag{3-2.18}$$

so that

$$R_{stim} = \frac{hq^2 |\mathbf{M}|^2}{6\epsilon m^2 \hbar\omega} P(h\nu) N_1 \tag{3-2.19}$$

The Einstein coefficient B is then given by

$$B = \frac{hq^2 |\mathbf{M}|^2}{6\epsilon m^2 \hbar\omega} \tag{3-2.20}$$

The value of the band to band transition matrix $|\mathbf{M}_{bb}|^2$ is given by Stern [2,15] as

$$\frac{|\mathbf{M}_{bb}|^2}{3} = \frac{m^2 E_g}{2m_c} \tag{3-2.21}$$

Where E_g is the band gap and m_c is the effective electron mass. A more complex analysis by Kane [7,16] includes spin orbit splitting in the valence band giving

$$< |\bar{\mathbf{M}}_{bb}|^2 >_{av} = \frac{m^2 E_g}{2m_c} \left| \frac{\Delta + E_g}{2\Delta + 3E_g} \right| \tag{3-2.22}$$

Where Δ is the spin orbit splitting. The extra Δ term is only a small correction for GaAs since $\Delta << E_g$. Where multiple energy levels are present in a semiconductor not all energy levels are necessarily filled. In the limit for high impurity concentrations the bands are degenerate. This is assumed in following calculations and approximations.

3-3 Band Shapes and Emission Profiles

This section considers approximations to semiconductor band shapes and presents the equations for calculating spontaneous and stimulated transition profiles. The shape of semiconductor bands is parabolic in the simplest approximation with density of states function

$$\rho_c = \frac{\sqrt{2m_c^3 E_c}}{\pi^2 \hbar} \tag{3-3.1}$$

Where E_c is the energy relative to the band edge and m_c is the effective electron mass. In practice band shapes deviate from this, with extra states near the band edge due to impurities. Several authors show the difficulty of producing a function which reflects the shape of bands in semiconductors. [17,18] Two of note are Kane [7] and Halperin and Lax [11,19]. Halperin and Lax predict band tails which decay at the bands edge as $\exp(-E^n/kT)$ where n varies between 0.5 and 2.0, but their results are hard to use, being discontinuous near the band edge. Kane finds a band tail approximation which is Gaussian well into the band gap and parabolic well into the band. The length of these band tails depends on the screening length for an electron and is sufficiently different between these two methods that Stern calculated band tails from the Halperin and Lax analysis and fitted a Kane band tail shape to it. Kane band tails are given by

$$y(x) = \frac{1}{\sqrt{\pi}} \int_{-\infty}^{x} (x-z)^{1/2} \exp(-z^2)\, dz \tag{3-3.2}$$

Where $x = h\nu/\eta$ and Kane defines the band tailing parameter, η as

$$\eta = \left[\frac{q^2}{\epsilon}\right]\left[\frac{4\pi N_D}{k_s}\right]^{1/2} \tag{3-3.3a}$$

and

$$k_s^2 = \frac{m_c q^2}{\pi \epsilon \hbar^2} \left(\frac{3N_{AV}}{\pi} \right)^{\frac{1}{3}} \qquad (3\text{-}3.3b)$$

Here k_s is the Thomas-Fermi screening length, m_c the electronic mass and N_D the doping density.

The electron and hole densities can be calculated from the density of states functions with effective masses m_c and m_v and the occupation factors f_c and f_v. These are given by Fermi-Dirac statistics with quasi-Fermi levels F_c and F_v. The electron density is given by the integral over all conduction band states [10]

$$N = \int \rho_c(E_c) f_c(E_c)\, dE_c \qquad (3\text{-}3.4)$$

The hole density is given by

$$P = \int \rho_v(E_v)[1 - f_v(E_v)]\, dE_v \qquad (3\text{-}3.5)$$

The total spontaneous transition rate at a given frequency, and photon energy, depends on the number of starting and finishing states that can be found with the correct energy separation and the probability of a transition. The transition probability, B, depends on $|M|^2$. If this is the same for all initial and final states then the spontaneous transition coefficient is given by

$$r_{spon} = B \int \rho_c(E_c) \rho_v(E_v) f_c(E_c)[1 - f_v(E_c - h\nu)]\, dE_c \qquad (3\text{-}3.6)$$

Where $E_v = h\nu - E_g - E_c$. The rate of spontaneous emission is $Z\, r_{spon}$ where z is the number of modes per unit volume. The nett stimulated transition rate is given similarly by

$$r_{stim} = B\int \rho_c(E_c)\,\rho_v(E_v)\,[f_c(E_c) - f_v(E_c - h\nu)]\,dE_c \qquad (3\text{-}3.7)$$

The rate of stimulated emission is $P(h\nu)\,r_{stim}$. The total spontaneous emission R_{spon} is given by integrating $Z\,r_{spon}$ over $h\nu$. By changing the variable of integration this becomes

$$R_{spon} = A\iint \rho_c(E_c)\,\rho_v(E_v) f_c(E_c)\,[1 - f_v(E_g - E_v)]\,dE_c\,\,dE_v$$

$$= A\,N\,P \qquad (3\text{-}3.8)$$

Where N and P are the electron and hole densities. If no external carriers are injected then the recombination rate is AN_0P_0. In the excited state this becomes

$$R_{net} = A[(N + N_0)(P + P_0) - N_0P_0] \qquad (3\text{-}3.9)$$

and in equilibrium $N = P$ gives the spontaneous lifetime of the carriers, τ_s as

$$\tau_s^{-1} = A\,(N + N_A - N_D) \qquad (2\text{-}3.10)$$

Where $(N_A - N_D)$ is the difference in doping densities and equal to $(P_0 - N_0)$. This links the Einstein coefficient A with the spontaneous lifetime coefficient, B_r, in Chapter 2.

The ratio $(f_c - f_v)/(f_c(1 - f_v))$ depends only on the difference between E_c and E_v and so is independent of E_c and E_v beacause the two energy levels are always separated by the photon energy hv. Multiplying r_{spon} in equation (3-3.6) by this factor and rearranging gives

$$\frac{r_{stim}}{r_{spon}} = \frac{(f_c - f_v)}{f_c(1 - f_v)} = 1 - \exp\left[\frac{h\nu - F_c + F_v}{kT}\right] \qquad (3\text{-}3.11)$$

This is independent of the variable of integration, E_c, and shows quite clearly

that there are only nett stimulated downward transitions when $(F_c - F_v) > h\nu$.

3-4 Approximate Solutions

Several authors [4,5,6] have studied approximate models for optical gain in semiconductors, and in particular in GaAs. In general the object of these papers has been to try to derive expressions for lasing phenomena in laser diodes. Analytic models tend not to include band tailing effects but have the advantage of producing more tractable results than computational methods. A computer model is to be used here to include band tailing effects. However, to gain some insight into the processes some analytic approximations are also developed. Marinelli [1] derives an approximate analytic solution by considering the bands to be parabolic and defines the stimulated transition rate to be

$$r_{stim}(h\nu) = C \int_0^{h\nu - E_g} E_c^{1/2} E_v^{1/2} (f_c - f_v)\, dE_c \qquad (3\text{-}4.1)$$

The band shapes are given simply by $E_c^{1/2}$ and $E_v^{1/2}$, and C is a multiplying constant including all other constants. E_c is the energy level above the conduction band edge and E_v is the corresponding energy level in the valence band. The following analysis uses similar approximations to those used by Marinelli but in this analysis the spontaneous transition coefficient, r_{spon}, is derived. The value of r_{stim} will then follow from (3-3.7).

$$r_{spon}(h\nu) = C \int_0^{h\nu - E_g} E_c^{1/2} E_v^{1/2} f_c (1 - f_v)\, dE_c \qquad (3\text{-}4.2)$$

The occupation factor term $f_c(1-f_v)$ follows from Fermi-Dirac statistics.

$$\Phi(E_c) = f_c(1-f_v) =$$

$$= \frac{\tfrac{1}{2}\exp[(F_c - F_v - h\nu)/2kT]}{\cosh[(2E_c - h\nu - F_v - F_c)/2kT] + \cosh[(h\nu + F_v - F_c)/2kT]} \qquad (3\text{-}4.3)$$

The value of the integral in (3-4.2) is found by a change of variable to $\frac{1}{2}(h\nu - E_g)x = E_c - \frac{1}{2}(h\nu - E_g)$, the integral then becomes

$$r_{spon}(h\nu) = \frac{C}{4}(h\nu - E_g)^2 \int_{-1}^{1} \Phi(x)\sqrt{1-x^2}\, dx \qquad (3\text{-}4.4)$$

Marinelli argues that if $h\nu < F_c - F_v << 2kT$ then Φ is a slowly varying function for $|x| << 1$ and that for $|x| \to 1$ the $(1-x^2)^{\frac{1}{2}}$ term tends to zero. Then by expanding $\Phi(x)$ in powers of x near $x = 0$ and taking only the first term the integral can be approximated and

$$r_{spon} = \frac{C}{4}(h\nu - E_g)^2 \, \Phi\left|\frac{h\nu - E_g}{2}\right| \int_{-1}^{1} \sqrt{1-x^2}\, dx \qquad (3\text{-}4.5)$$

Evaluating the remaining integral gives the result $\pi/2$, so by changing C for C_1.($C_1 = C\pi/4$), r_{spon} can be written

$$r_{spon} = \frac{C_1 \, \frac{1}{2}(h\nu - E_g)^2 \exp[(F_c - F_v - h\nu)/2kT]}{\cosh[(F_v + F_c)/2kT] + \cosh[(h\nu + F_v - F_c)/2kT]} \qquad (3\text{-}4.6)$$

Re-arranging this gives the result

$$r_{spon}(h\nu) = \frac{C_1(h\nu - E_g)^2}{(\exp[(h\nu + 2F_v)/2kT] + 1)(\exp[(h\nu - 2F_c)/2kT] + 1)} \qquad (3\text{-}4.7)$$

Which could have been derived from Marinelli's form of r_{stim} and equation (3-3.7). It is generally more useful when solving waveguide problems to have r_{spon} and r_{stim} as functions of the carrier concentration N. An approximation for quasi-Fermi levels in terms of electron and hole densities N and P has been derived by Joyce and Dixon. [5]

In the notation of this section the analysis is outined below. The normalised carrier concentration $N' = N/N_0$ is the Fermi-Dirac transform of the band

shape function ρ_c

$$N' = \int_0^\infty \frac{\rho_c(E_c')}{(\exp(E_c' - F_c') + 1)} \, dE_c' \qquad (3\text{-}4.8)$$

Where E_c' and F_c' are normalised to kT. If this is expanded in terms of $\exp(E_c' - F_c')$ then

$$N' = g_1 \exp(F_c') - g_2 \exp(2F_c') + \cdots \qquad (3\text{-}4.9)$$

With

$$g_n = \int_0^\infty \rho_c(E_c)/\exp(nE_c) \, dE_c \qquad (3\text{-}4.10)$$

Joyce and Dixon construct a power series for F_c' from this in terms of N'/g_1

$$F_c' = \ln\left(\frac{N'}{g_1}\right) + \frac{g_2}{g_1}\left(\frac{N'}{g_1}\right) + \left(\frac{3g_2^2 - 2g_1 g_2}{2g_1^2}\right)\left(\frac{N'}{g_1}\right)^2 + \cdots \qquad (3\text{-}4.11)$$

Taking only the first term in the series results in the Boltzmann expression for N' when $F_c' < 0$ with the multiplicative factor g_1

$$N' = g_1 \exp(F_c') \qquad (3\text{-}4.12)$$

Taking the first two terms greatly improves the result, extending the range of validity of F_c' to $(-\infty, 2.1)$, to an accuracy of about 1 meV and for carrier densities up to $N' = 2.97 g_1$. Rearranging (3-4.11) then gives

$$g_1 \exp(F_c') = N' \exp\left(\frac{g_2 N'}{g_1^2}\right) \qquad (3\text{-}4.13)$$

For parabolic bands, from equation (3-4.10) it follows that $g_m = m^{-\frac{3}{2}}\Gamma\left[\frac{3}{2}\right]$ so that $g_1 = \frac{1}{2}\sqrt{\pi}$ and $g_2 = \frac{1}{4}\sqrt{\frac{1}{2}\pi}$. The carrier concentrations N and P are then given by

$$\frac{N}{N_0}\exp\left[\frac{N}{2\sqrt{2}N_0}\right] = \exp\left[\frac{F_c}{kT}\right] \qquad (3\text{-}4.14a)$$

$$\frac{P}{P_0}\exp\left[\frac{P}{2\sqrt{2}P_0}\right] = \exp\left[\frac{F_v}{kT}\right] \qquad (3\text{-}4.14b)$$

These expressions can now be used to derive spontaneous and stimulated emissions in terms of N and P , not F_c and F_v. The combination of these two approximations seems to be a new and useful result. The spontaneous transition coefficient can be rearranged as

$$r_{spon} = \frac{C_1(h\nu - E_g)^2}{(\exp[(\frac{1}{2}h\nu - F_c)/kT]+1)(\exp[(\frac{1}{2}h\nu + F_v)/kT]+1)} \qquad (3\text{-}4.15)$$

The value of $\frac{h\nu}{kT}$ is greater than fifty for lasers and $h\nu$ is greater than or approximately equal to E_g . F_c on the other hand is only a few kT and F_v approximately $-E_g$. Of the two terms in the denominator of (3-4.15) the first is then $\exp[(\frac{1}{2}h\nu - F_c)/kT]$ and the second is close to unity. The equation then gives

$$r_{spon} = C_1\frac{N}{N_0}(h\nu - E_g)^2\exp\left[\frac{N}{2\sqrt{2}N_0}\right]\exp\left[-\frac{h\nu}{2kT}\right] \qquad (3\text{-}4.16)$$

The calculated spontaneous emission rate contains the term ZB, where Z and B are given by (3-2.8) and (3-2.20) respectively. Since Z is proportional to $(h\nu)^2$ and B to $(h\nu)^{-1}$ the spontaneous emission rate is given by

$$w_{spon} = Zr_{spon} \tag{3-4.17}$$

$$\alpha \quad \frac{N}{N_0} h\nu (h\nu - E_g)^2 \exp\left[\frac{N}{2\sqrt{2}N_0}\right] \exp\left[-\frac{h\nu}{2kT}\right]$$

This equation is separable in N and $h\nu$ so that the total spontaneous transition rate R_{tot} is

$$R_{tot} = \int w_{spon}\, d(h\nu) \;\alpha\; \frac{N}{N_0} \exp\left[\frac{N}{2\sqrt{2}N_0}\right] \tag{3-4.18}$$

Equation (3-3.9) predicts a linear relationship between R_{tot} and N for $N << (N_A + N_D)$ and a square law for $N >> (N_A + N_D)$. This expression predicts a linear relationship for $N << N_0 2\sqrt{2}$ but for $N >> N_0 2\sqrt{2}$ the exponential term dominates. The expression in equation (3-3.9) predicts that R_{tot} increases with N^2 so that a better approximation for w_{spon} might be found by expanding the exponential and taking only the first two terms

$$w_{spon} \;\alpha\; \frac{N}{N_0} h\nu (h\nu - E_g)^2 \left[1 + \frac{N}{2\sqrt{2}N_0}\right] \exp\left[-\frac{h\nu}{2kT}\right] \tag{3-4.19}$$

The relationship between r_{stim} and r_{spon}, (3-3.11), can be written in terms of N using (3-4.13) and (3-4.14) to give

$$r_{stim} \;\alpha\; \left[1 - \exp\left[\frac{h\nu - F_c + F_v}{kT}\right]\right] \exp\left[\frac{F_c - h\nu}{kT}\right] \frac{(h\nu - E_g)^2}{h\nu} \tag{3-4.20}$$

$$r_{stim} \;\alpha\; \frac{(h\nu - E_g)^2}{h\nu} \exp\left[-\frac{h\nu}{2kT}\right] - \tag{3-4.21}$$

$$\left[\frac{N}{N_0} \exp\left[\frac{N}{2\sqrt{2}N_0}\right] - \frac{P_0}{N} \exp\left[\frac{h\nu - E_g}{kT}\right]\right]$$

So that for a fixed value of photon energy the optical gain is

$$g \propto \left| \frac{N}{N_0} \exp\left(\frac{N}{2\sqrt{2}N_0} \right) - \gamma \frac{P_0}{N} \right| \qquad (3\text{-}4.22)$$

Where

$$\gamma = \exp\left(\frac{h\nu - E_g}{kT} \right)$$

In terms of quasi-Fermi levels the onset of optical gain occurs when $F_c - F_v = h\nu$, or in terms of N this is

$$\gamma = \frac{N^2}{N_0 P_0} \exp\left[\frac{N}{2\sqrt{2}} \left(\frac{1}{N_0} + \frac{1}{P_0} \right) \right] = \exp\left(\frac{h\nu - E_g}{kT} \right) \qquad (3\text{-}4.23)$$

Since, in GaAs $P_0 \approx 20N_0$ in most cases of interest this can be simplified to

$$2\ln(N) - \ln(N_0 P_0) + \frac{N}{2\sqrt{2}N_0} = \frac{h\nu - E_g}{kT} \qquad (3\text{-}4.24)$$

Since the logarithm is a small slowly varying function it can be replaced by an average value for $N^2 < N_0 P_0$ so that over a large range of N the photon energy at which optical gain is zero is linearly related to inversion population.

$$h\nu(g=0) = E_g + \frac{kT}{2\sqrt{2}N_0} \left[N + 2\sqrt{2}N_0 \ln\left(\frac{N_{AV}^2}{N_0 P_0} \right) \right] \qquad (3\text{-}4.25)$$

Fig.3-1 shows some of the features of these approximations. A spectrum of values of gain from (3-4.22) is shown in Fig.3-1a and values of w_{spon} are shown in Fig.3-1b. A range of value of N have been used which are multiples of N_0. These approximate solutions of w_{spon} from (3-4.17) show that the

peak spontaneous emission occurs at the same wavelength for all values of inversion population. This is not the case in real devices. [7]

These formulae are useful in considering the overall effect of the inversion population on the gain and spontaneous emission and their relationship to photon energy. In real devices, however, the effect of band tails is important [3,6,8] for low levels of injection.

Fig. 3-1 Approximate Emission Profiles.

a) Stimulated Emission vs. Photon Energy for different values of normalised inversion population.

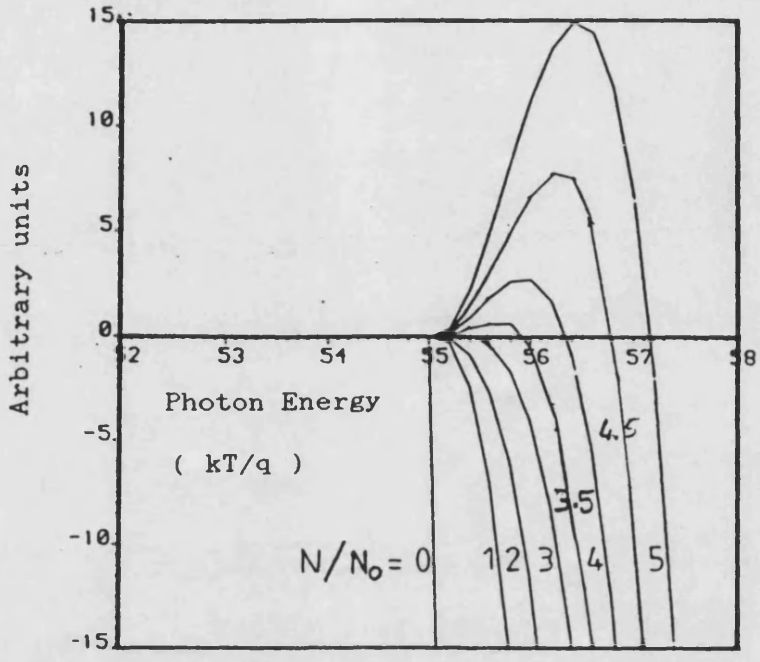

b) Spontaneous Emission vs. Photon Energy for different values of normalised inversion population.

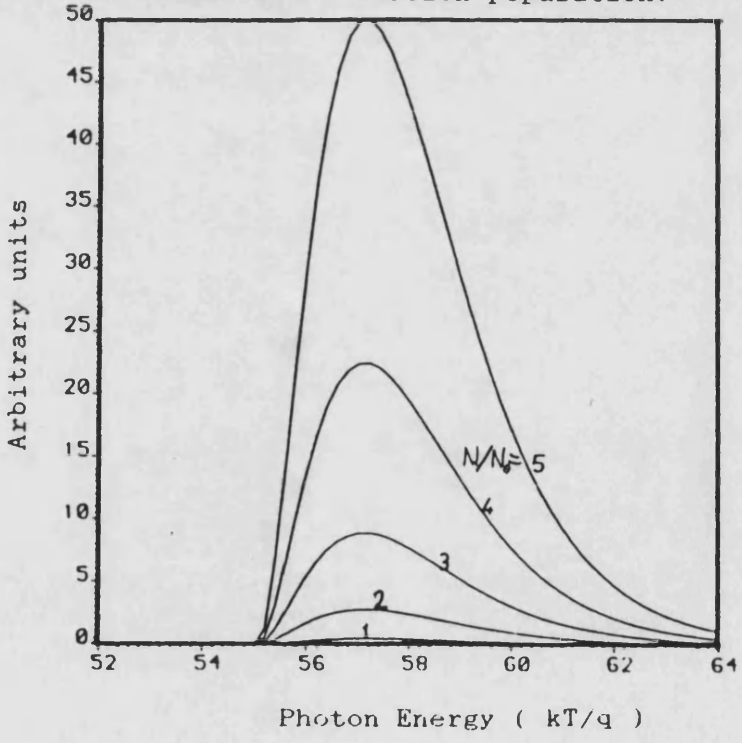

3-5 Computer Solution

The solution of the equations described so far using a digital computer was accomplished in a program written in 'pascal'. The solution falls into two parts. The first section is concerned with the calculation of the quasi-Fermi levels for each of the energy bands and the second with calculating the emission spectra.

The quasi-Fermi levels govern the occupation of the states in semiconductor bands. To calculate the Fermi level for the conduction band for a level of carrier density, N_x, a reasonable approximation is first found for F_c. This value, F_1 is near the conduction band edge. This is used to calculate a first approximation for N. The n^{th} approximation, F_n, can be found from previous values of N using a first order interpolation routine.

$$F_{n+1} = F_n + \frac{(F_n - F_{n-1})}{(N_n - N_{n-1})}(N_n - N_x) \qquad (3\text{-}5.1)$$

Where N_n is given by (3-3.4). This procedure converges after a few iterations so that $N_n \rightarrow N_x$ as $(F_{n+1} - F_n) \rightarrow 0$. The Fermi level can be found to any required accuracy. The hole concentration, P, can be found in a similar way from (3-3.5) for the equilibrium condition $N = P$.

The density of states functions ρ_c and ρ_v are defined in separate procedures and can be represented by any functional or numerical profile. Two band tail profiles were evaluated using this program. The Kane band tail function [7] (3-3.2,3), involves the evaluation of the integral of (3-3.2). Because it is so well behaved around the band edge this is the preferred profile over that calculated by Halperin and Lax. However, calculation of this integral to find each value of $y(x)$ is impractical so it is evaluated at a number of points and values of $y(x)$ are interpolated from this data. Well into the band tail the

shape is assumed to be Gaussian. For most of the range of values of x near the band edge where tabulated values exist, a third order polynomial is used to calculate $y(x)$ from the data. Well into the band $y(x)$ is assumed to be $\sqrt{x}$, i.e. a parabolic band.

The parabolic bands with exponential band tails [4,10] are defined by

$$y(x) = \sqrt{(x)} \qquad x \geqslant \eta' \tag{3-5.3a}$$

$$= \sqrt{\eta}\exp\left|\frac{x-\eta}{2\eta}\right| \qquad x < \eta \tag{3-5.3b}$$

This band tail is arranged so that at $x = \eta$ the function $y(x)$ and its first derivative are continuous.

Having calculated the Fermi levels, equation (3-4.2) allows r_{spon}, the spontaneous emission coefficient, to be calculated by integration over the conduction band for a given photon energy, $h\nu$. The stimulated emission coefficient, r_{stim}, immediately gives the gain or absorption at the given photon energy but the spontaneous emission rate is given by Zr_{spon}, where Z is defined by (3-2.8). The sequence of equations is

$$r_{spon} = \int_{-5.5\eta}^{\infty} \frac{(m_c^3 m_v^3)^{1/2} y(E_c)\, y(h\nu - E_g - E_c)}{[\exp(E_c - F_c)+1][\exp(E_g + E_c - h\nu)+1]}\, dE_c \tag{3-5.4}$$

$$w_{spon} = Z\ r_{spon}$$

$$= 3.2646\times 10^{7}(h\nu)^2 E_g \left|\frac{kT}{q}\right|^6 n^4 r_{spon}\, \mu m^{-3} \quad eV^{-1} \tag{3-5.5}$$

$$g = (1-\exp(h\nu - F_c + F_v))r_{spon}\, 2.4787 n E_g \left|\frac{kT}{q}\right|^4 \tag{3-5.6}$$

In all the computer solutions values of energy have been normalised to $\frac{kT}{q}$ to speed up the calculations. The considerations of (3-3.3) lead to N being normalised by N_{norm}

$$N_{norm} = 6.8108\times10^{3}\left|\frac{kT}{q}\right|^{3} \qquad (3\text{-}5.7)$$

The value of E_g, the band gap, was approximated from[20]

$$E_g = 1.519\frac{q}{kT} - \frac{6.2724}{1+0.017579\frac{q}{kT}} \qquad (3\text{-}5.8)$$

For comparison with the approximate analytic solutions and to evaluate the effect of the band tails the solution for parabolic bands was first calculated. This is shown in Fig.3-2. Four graphs are plotted to show the results. The first is stimulated gain against photon energy for a number of values of N in intervals of $0.5\times10^{23}\mathrm{m}^{-3}$. The second, (Fig.3-2b), is a similar plot for spontaneous emission. These two plots are closely comparable with Fig.3-1a,b and show how closely the approximate solutions agree. Fig.3-2c and 3-2d show gain and stimulated emission as a function of inversion population for several values of photon energy.

The major difference between the analytic approximation and the results of the computer model is the shift in the peak spontaneous model to higher energies as the inversion population increases. The plots of stimulated emission, (3-2a, 3-2c), show how the optical gain varies almost linearly with increasing N. Similar plots to (3-2) have been drawn for parabolic bands with exponential band tails with $\eta = 0.2q/kT$, and $q/kT = 25\mathrm{meV}$, in Fig.3-3 and for Kane band tails with $\eta = 1.0q/kT$ in Fig.3-4. These band tail lengths are marginally longer than those used to model real devices by Middlemast et al. [21,22]

but serve to show the changes to the emission spectra that band tails introduce.

The first thing to notice is that the spontaneous emission spectrum is much wider than the stimulated gain spectrum. In fact, there is still considerable output at $h\nu = 1.6$eV This corresponds to a wavelength, λ_0, of about 775 nm and is near the visible range. The value of E_g, the nominal band gap energy, is rather small here to correspond to the material grown for Bath University by the University of Sheffield. The peak gain occurs at about 1.425 eV or 870 nm. For a peak gain around 830 nm this analysis would predict light output around 730 nm, at the red end of the visible spectrum. Many 830 nm semiconductor laser diodes do in fact radiate sufficient power at the red end of the spectrum (i.e. $\lambda < 730$nm), to be clearly visible. Further, this visible light is radiated at angles approaching 90° to the normal and is therefore mainly spontaneous in nature and not due to stimulated gain.

The change that the band tails produce on the spontaneous emission is only slight. The sharp cut off at the band edge, seen in in Fig.3-2b is removed to produce a gentle roll off of emission. There is a slight increase in spectrum width accompanied by a slight shift to lower energies. The peak spontaneous emission is reduced and the change of wavelength of the peak with N is also increased.

The changes induced in the gain spectrum are far more significant. The reduction in the effective band gap due to the inclusion of the band tail states considerably widens the gain spectrum as well as shifting it to lower energies. At low levels of injection optical gain is first achieved at energies within the nominal band gap. The inversion population required to turn optical absorption to optical gain is reduced since the Fermi level separation required is less. Although the gain is higher for low values of N the rate of increase of peak

gain with N is reduced. The change in the wavelength of the peak gain with N is, however, increased. The results for Kane band tails and exponential band tails are different only in detail so that both seem to reasonable approximations. Middlemast [21,22] has used these curves to model superluminescent light emitting diodes, SLEDs, and Fabry-Perot laser amplifiers. When characterising SLEDs the best predictions of device performance were made using Kane band tails with $\eta \approx 0.6$. These calculations provide a set of curves for gain and spontaneous emission which closely resemble those of more complicated analyses [3] and experimental results. [9]

Fig. 3-2 Spontaneous and Stimulated Emission vs. Photon Energy for different values of inversion population, (in units of 10^{24} m^{-3}). The band gap energy is 55.1kT/q, the band shapes are parabolic with no band tails.

3-2a Stimulated Emission vs. Photon Energy

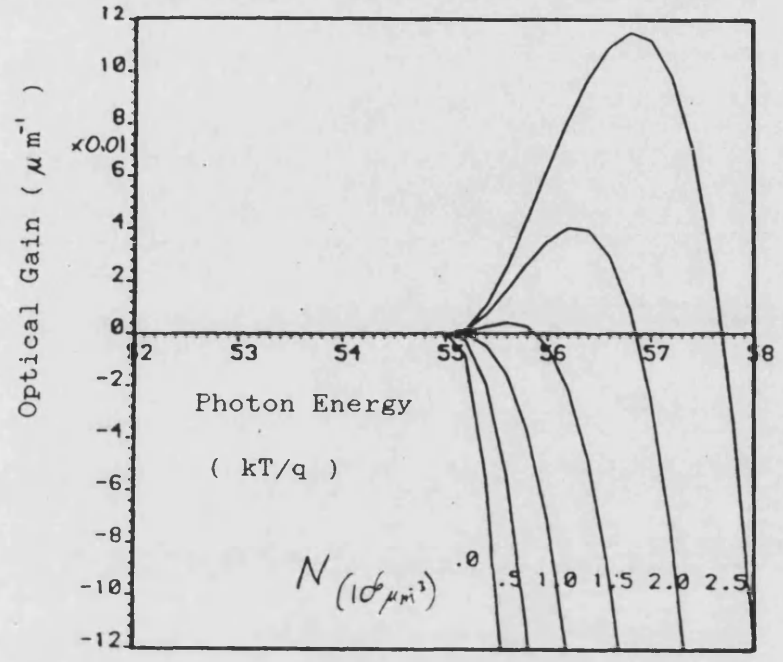

3-2b Spontaneous Emission vs. Photon Energy

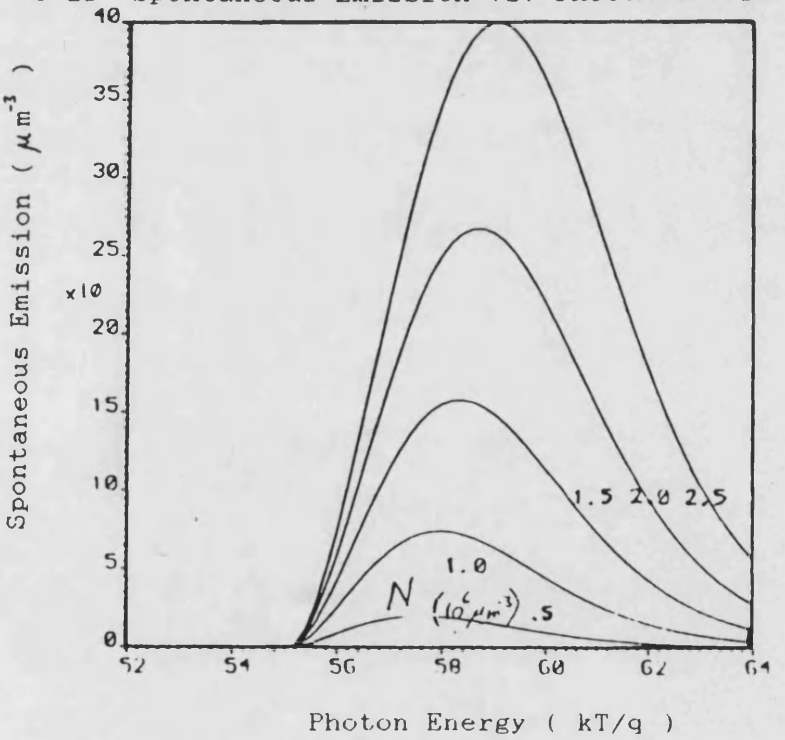

Fig. 3-2 Spontaneous and Stimulated Emission vs. Inversion Population, for different values of Photon Energy (in units of q/kT). The band gap energy is 55.1kT/q, the band shapes are parabolic with no band tails.

3-2c Stimulated Emission vs. Inversion population

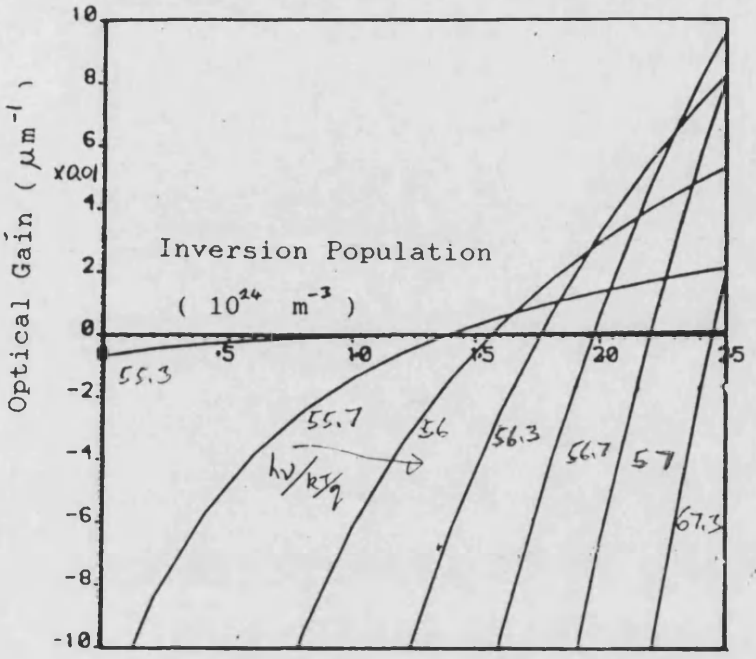

3-2d Spontaneous Emission vs. Inversion Population

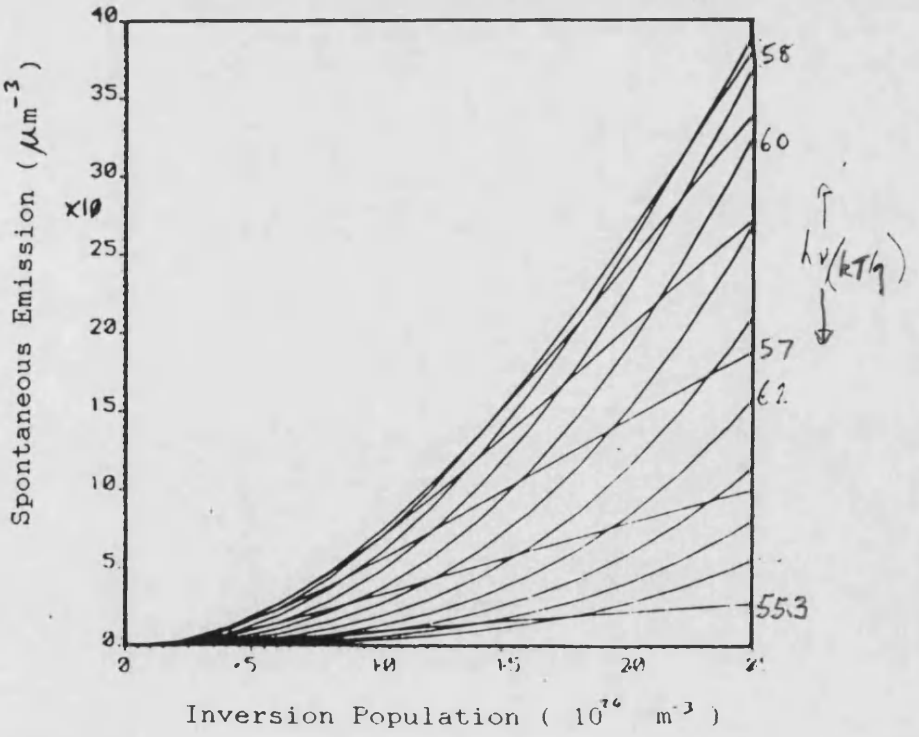

Fig. 3-3 Spontaneous and Stimulated Emission vs. Photon Energy for different values of inversion population, (in units of $10^6 \mu m^{-3}$). The band gap energy is 55.1kT/q, the band shapes are parabolic with exponential band tails. (η=0.2kT/q)

3-3a Stimulated Emission vs. Photon Energy

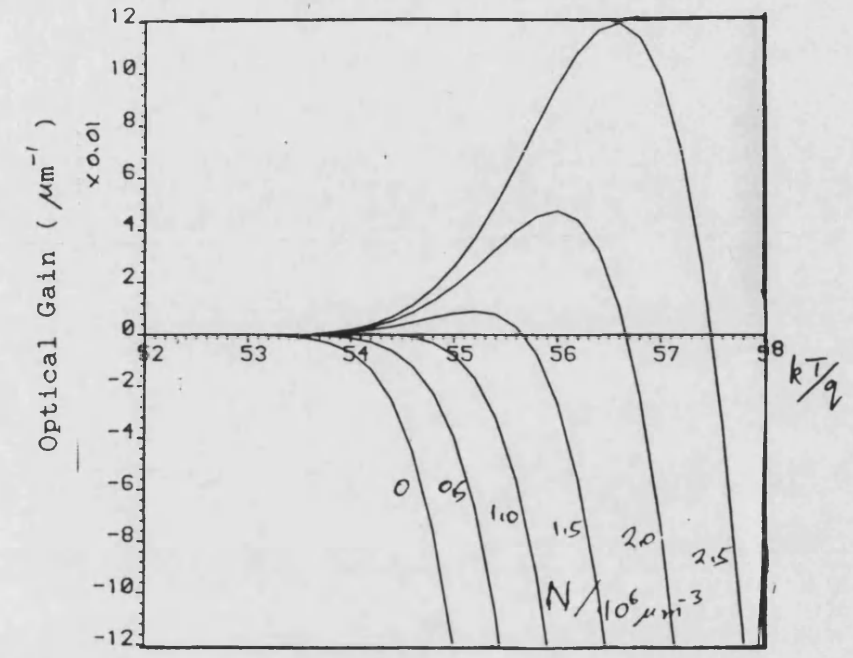

3-3b Spontaneous Emission vs. Photon Energy

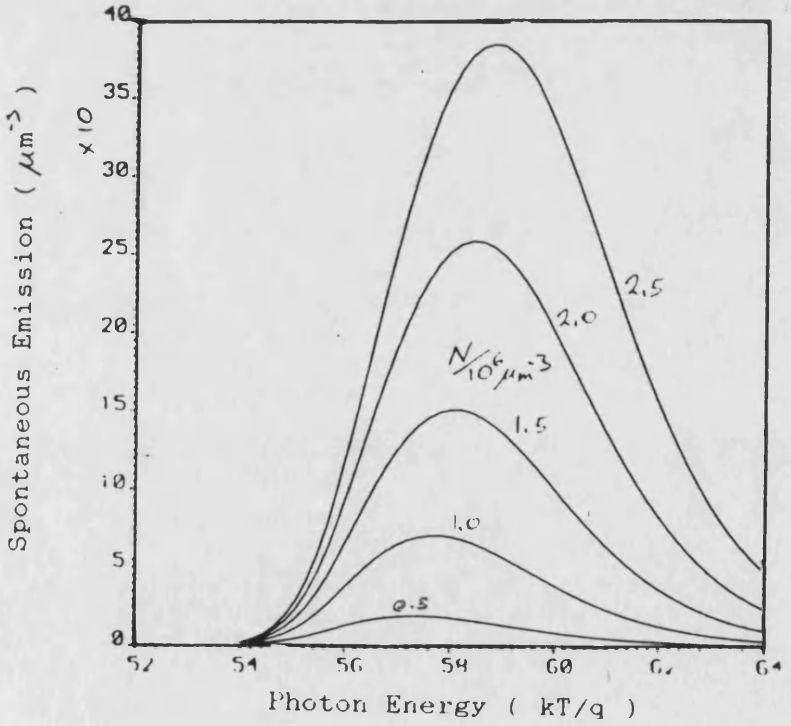

Fig. 3-3 Spontaneous and Stimulated Emission vs. Inversion Population, for different values of Photon Energy (in units of q/kT). The band gap energy is 55.1kT/q, the band shapes are parabolic with exponential band tails. ($\eta = 0.2\ kT/q$)

3-3c Stimulated Emission vs. Inversion Population

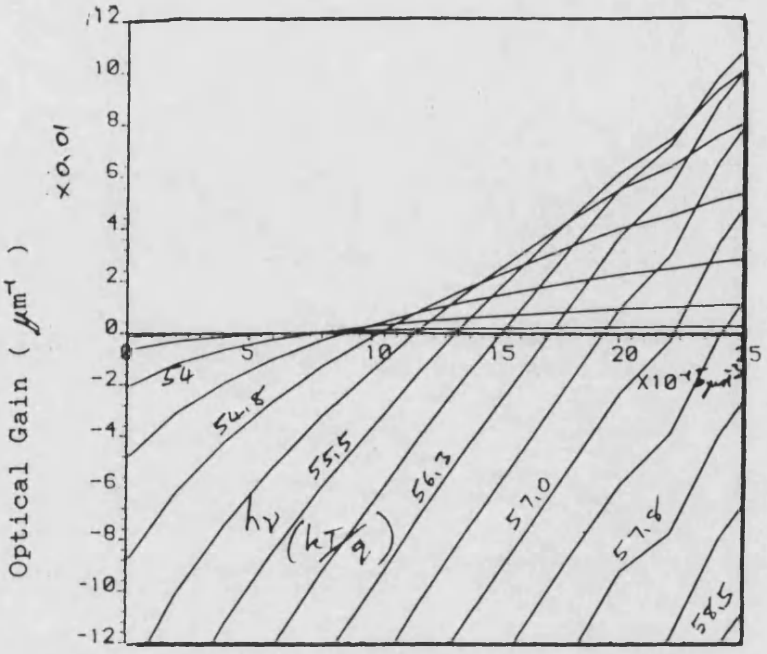

3-3d Spontaneous Emission vs. Inversion Population

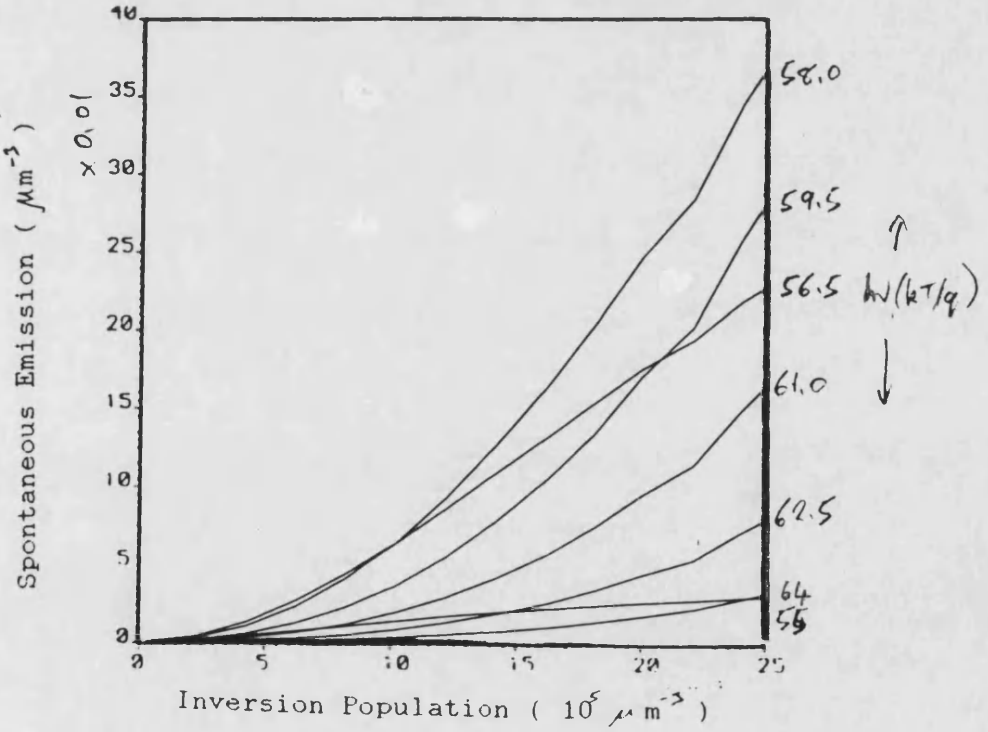

Fig. 3-4 Spontaneous and Stimulated Emission vs. Photon Energy for different values of inversion population, (in units of $10^6 \mu m^{-3}$). The band gap energy is 55.1kT/q, the bands have Kane band tails. (η=1.0 kT/q)

3-4a Stimulated Emission vs. Photon Energy

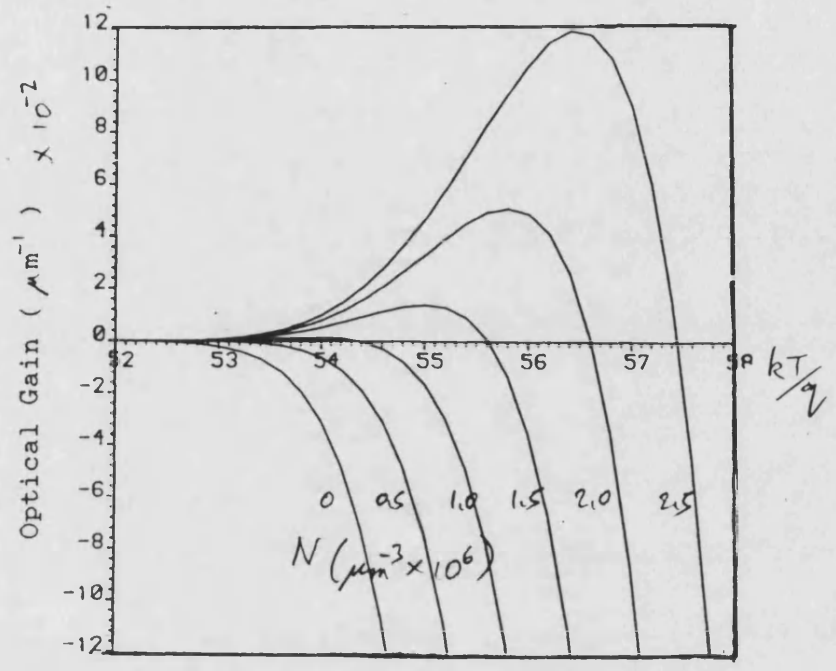

3-4b Spontaneous Emission vs. Photon Energy

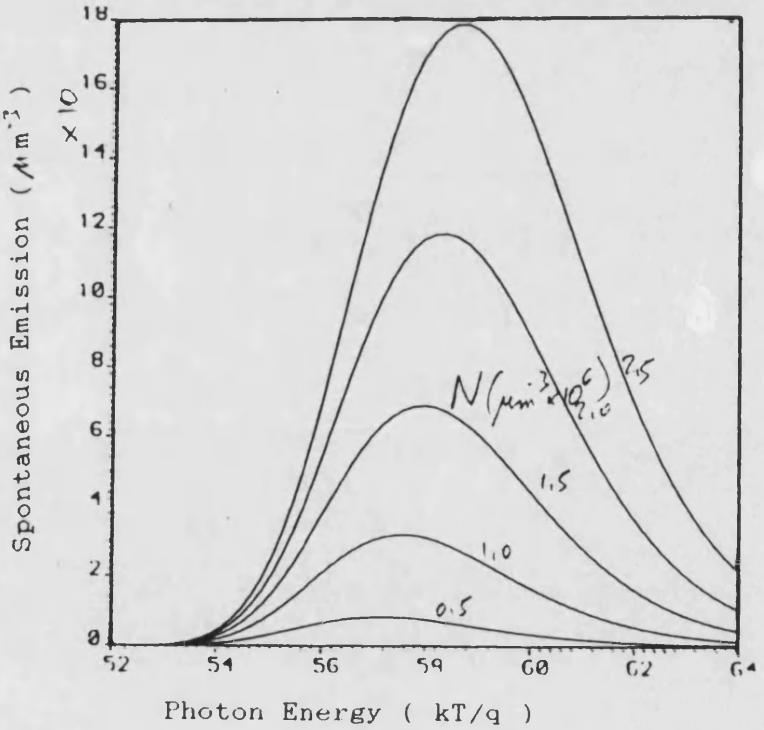

Fig. 3-4 Spontaneous and Stimulated Emission vs. Inversion Population, for different values of Photon Energy (in units of q/kT). The band gap energy is 55.1kT/q, the bands have Kane band tails. (η=1.0kT/q).

3-4c Stimulated Emission vs. Inversion population

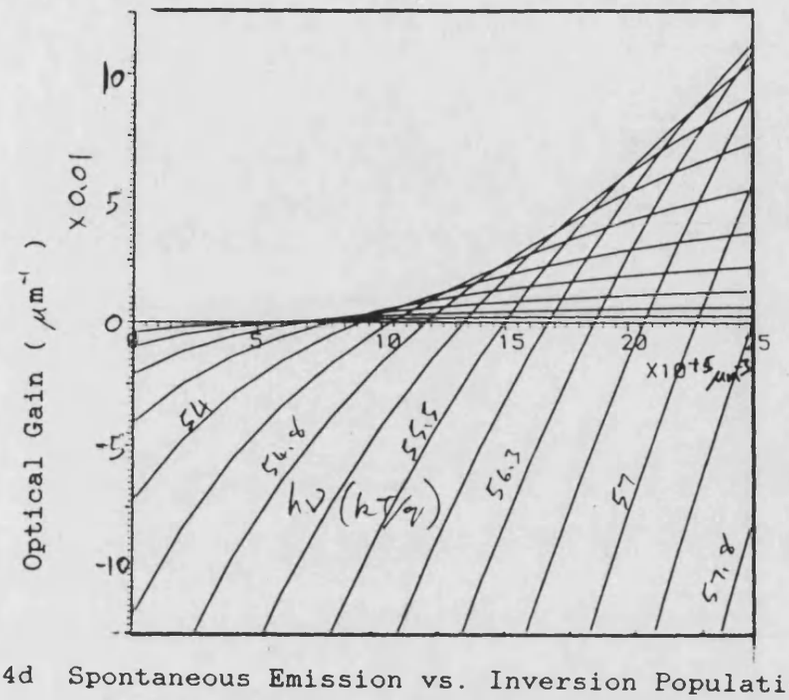

3-4d Spontaneous Emission vs. Inversion Population

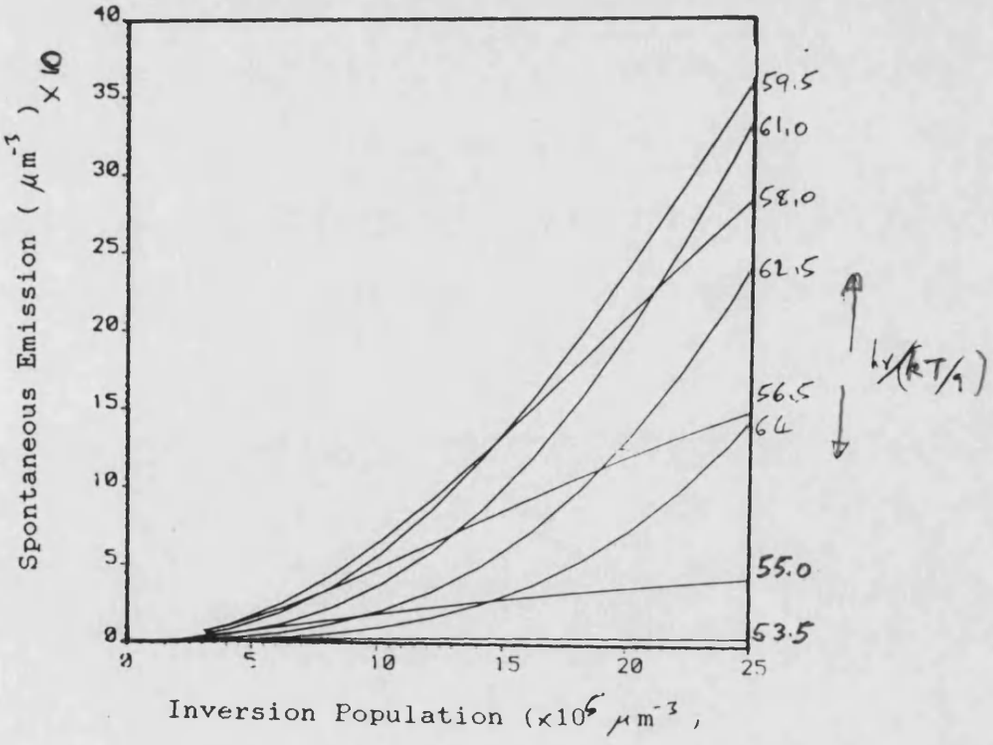

References for Chapter 3

1/ C.J.Hwang, " Properties of spontaneous and stimulated emission in GaAs Junction lasers. II Temperature dependence of theshold current and excitation dependence of superradiance spectra " . Phys.Rev.B, **12** , (10), pp4126-4134, 1970.

2/ G.Lasher, F.Stern, " Spontaneous and stimulated recombination radiation in semiconductors ", Phys.Rev., **133** , (2A), pp553-565, 1964.

3/ F.Stern, " Calculated spectral dependence of gain in GaAs ", J.Appl.Phys., **47** , (12), pp5382-5386, 1976.

4/ D.J.Morgan, M.J.Adams, " Quantum noise in semiconductor lasers ", Phys.Stat.Sol.(a), **11** , pp243-253, 1972.

5/ W.B.Joyce, R.W.Dixon, " Analytic approximations for the Fermi energy in an ideal Fermi gas ", Appl.Phys.Lett., **32** , pp354-356, 1977.

6/ F.Marinelli, " Approximate calculation of the spectral function for the stimulated recombination radiation in semiconductors ", S.S.Electron, **8** , pp939-942, 1965.

7/ E.O.Kane, " Thomas-Fermi approach to impure semiconductor band structure ", Phys.Rev., **131** , (1), pp79-88, 1963.

8/ F.Stern, " Effect of band tails on stimulated emission of light in semiconductors ", Phys.Rev., **148** , (1), pp186-194, 1966.

9/ C.H.Henry, R.A.Logan, F.R.Merrit, " Measurement of gain and absorption spectra in AlGaAs buried heterostructure lasers ", J.Appl.Phys., **51** , (6),pp3042-3050, 1980. 10/ G.H.B.Thompson, Physics of semiconductor laser devices, Wiley, 1980

11/ B.I.Halperin, M.Lax, " Impurity band tails in the high density limit, I Minimum counting methods", Phys.Rev., **148** , (2), pp722-740, 1966.

12/ F.H Read, Electromagnetic Radiation, Wiley, 1980.

13/ J.L.Martin, Basic Quantum Mechanics, Oxford Physics Series, 1981.

14/ L.I.Shiff, Quantum Mechanics, 2nd ed., McGraw-Hill, 1955.

15/ F.Stern, " Elementary theory of the optical properties of solids ", Solid State Physics, 15 , Academic Press Inc., 1963.

16/ E.O.Kane, " Band structure of Indium Antimonide ", J.Phys.Chem.Solids, 1 , pp249-261, 1957.

17/ C.J.Hwang, " Properties of spontaneous and stimulated emission in GaAs junction lasers. I Densities of states in the active regions ", Phys.Rev.B, 2 , (10), pp4117-4125, 1962.

18/ P.A.Wolff," Theory of the band structure of very degenerate semiconductors ", Phys.Rev., 126 , (2), pp405-412, 1962.

19/ M.Lax, B.I.Halperin, " Impurity band tails in degenerate semiconductors :, J.Phys.Soc.Jap., 21 , Supplement, pp218-223, 1966.

20/ H.C.Casey,M.B.Panish, Heterostructure Lasers, Academic Press, 1978.

21/ I.Middlemast, J.Sarma, T.Kambayashi, " A comprehensive study and characterisation of superluminescent light emitting diodes ", IEEE, TELD '82, Ottowa, Canada, 1982

22/ I.Middlemast, J.Sarma, " Computer simulation of Fabry-Perot laser amplifiers", IoP, SILA '84, UWIST, Cardiff, Wales, 1984.

CHAPTER 4

Dielectric Slab Analysis

4-1 Introduction

This chapter aims to review the analysis of the electromagnetic fields in a dielectric slab. The slab is analysed as being an infinite layer of refractive index n_1 (for $|y|<d$ thickness $2d$, between two semi-infinite half spaces of refractive index n_2. (See Fig 4-1). Propagation is considered only along the z-axis, parallel to the slab interface. Such a slab is a convenient representation of the layered structure of a semiconductor laser diode. The slab is symmetric in y as the semi-infinite half spaces have equal refractive indeces.

The slab is an open waveguide so that the electromagnetic fields are not totally confined by the dielectric boundaries. Unlike closed waveguides, such as hollow metallic waveguides, the fields cannot be expressed as a summation of an infinite series of discrete eigenmodes. In the case of a dielecric slab a series of bound modes must be defined to which a continuous spectrum of radiation modes must be added [1,2,3]. The surface modes are required to be square integrable over the infinite y co-ordinate so that no mode may carry infinite power and the field decays to zero at infinity. The continuous spectrum must only obey the weaker boundary condition that the field of any mode must be finite at infinity. For any physically realisable source a continuum of continuous spectrum modes are excited and the field is expressed as an integral over the continuous spectrum and the radiation condition is met by this integral being finite.

In a dielectric slab surface waves represent a situation in which a plane wave is travelling at an angle to the slab surface, and is reflected at each

boundary in turn at intervals along its path. For a pure surface wave the reflection is a total internal reflection and, although some power propagates outside the slab, there is no net power flow away from the interface. at the surface. In this case the field intensity outside the slab decays with distance from the boundary. In this sense the mode is a bound mode of the slab.

Physically not all discrete modes are necessarily bound modes of the slab but may belong to a class of modes known as leaky modes. These modes travel along the slab but at each reflection some power flows out of the slab. The power in a leaky wave decays as it propagates, but decays faster inside the slab than along some angles outside. At any given cross-section, z= const., the intensity increases away from the slab boundary. There is a connection between leaky waves and the modes of the continuous spectrum. If the radiation contribution from the continuous spectrum is evaluated by contour deformation then isolated singularities occur in the complex plane. Each of these singularities represents the contribution from a leaky wave. In structures where the predominant guiding mechanism is the difference in the imaginary part of the refractive indices of successive layers no pure surface waves can exist. In this case a class of gain guided modes exists which are similar to leaky waves but still bound to the slab.

In a situation where the complex refractive indices imply optical gain within the medium the power may increase in magnitude as it propagates along z, even when energy is continuously leaked out. For a situation where both regions are lossy the power decreases as it propagates but it can still be considered as a bound mode if the fields decay with $|y|$ outside the slab.

4-2 Slab Boundary Conditions and Surface Waves

This section derives the form of bound modes in a dielectric slab. From Maxwell's Equations [4] in a source free region, ($\mathbf{J} = \rho = 0$), assuming a piecewise homogeneous dielectric, (Fig. 4-1), with $\nabla \cdot \epsilon_r = 0$ the wave equation of the electric and magnetic fields with time dependancies of $e^{j\omega t}$ are

$$\nabla^2 \mathbf{E} + n^2 k_0^2 \mathbf{E} = 0 \tag{4-2.1a}$$

$$\nabla^2 \mathbf{H} + n^2 k_0^2 \mathbf{H} = 0 \tag{4-2.1b}$$

Where $n^2 k_0^2 = \epsilon_r \epsilon_0 \mu_0 \omega^2$.

There are several ways to construct the solutions for **E** and **H**. The most convenient here is to construct a solution in terms of longitudinal section electric (LSE) and magnetic (LSM) modes, i.e. TE and TM to y. The electric field is then given by the general form [5]

$$\mathbf{E} = \nabla \times \hat{\mathbf{y}} \psi + \nabla \times \nabla \times \hat{\mathbf{y}} \chi \tag{4-2.2}$$

Where ψ and χ are two functions yet to be determined, but which have z dependencies $e^{-j\beta_e z}$ and $e^{-j\beta_m z}$ respectively. For an infinite slab neither function is dependent on x so that

$$\mathbf{E} = j\beta_e \psi \hat{\mathbf{x}} + \beta_m^2 \chi \hat{\mathbf{y}} - j\beta_m \frac{\partial \chi}{\partial y} \hat{\mathbf{z}} \tag{4-2.3a}$$

$$\mathbf{H} = \frac{\beta_e}{j\omega\mu} \left(\beta_e \psi \hat{\mathbf{y}} - j \frac{\partial \psi}{\partial y} \hat{\mathbf{z}} \right) + \omega \epsilon \beta_m \chi \hat{\mathbf{x}} \tag{4-2.3b}$$

The TE, (LSE), modes are described by ψ and the TM, (LSM), modes by χ

In an infinite homogeneous slab these are separable with

$$\frac{\partial^2 \mathbf{E}}{\partial z^2} + \beta^2 \mathbf{E} = 0 \tag{4-2.4a}$$

$$\frac{\partial^2 E}{\partial y^2} + \sigma_y^2 E = 0 \qquad (4\text{-}2.4b)$$

The separation constants are related by

$$n_1^2 k_0^2 = \beta^2 + \sigma_y^2 \qquad |y| < d \qquad (4\text{-}2.5a)$$

$$n_2^2 k_0^2 = \beta^2 + \rho_y^2 \qquad |y| > d \qquad (4\text{-}2.5b)$$

The boundary conditions at $y = \pm d$ are that tangential electric and all magnetic fields must be continuous. A further constraint is that the fields must not increase as y tends to infinity. For surface waves, where it is possible to excite only one mode, the mode must not carry infinite power and so must decay to zero at infinity.

The solution of the wave equation in a piecewise homogeneous medium are sines and cosines or exponentials. For a bound mode the solution within the slab will be either a sine or cosine but outside it will be a decaying exponential. These solutions can be divided into odd and even modes by considering the symmetry of the fields about $y = 0$. Consider the boundary conditions as applied to the TM solutions. [6,7,8] For an even mode, with a maximum at $y = 0$

$$\chi = a\cos(\sigma_y y) \qquad |y| \leq d \qquad (4\text{-}2.6a)$$

$$= b\exp(-j\rho_y(|y| - d)) \qquad |y| \geq d \qquad (4\text{-}2.6b)$$

Since H_x and E_z are both continuous across the boundary at $y = d$ it follows that $b = a(\epsilon_1/\epsilon_2)\cos(\sigma_y d)$ and the boundary conditions are met if

$$\sigma_y \sin(\sigma_y d) = \frac{\epsilon_1}{\epsilon_2} j\rho_y \cos(\sigma_y d) \qquad (4\text{-}2.7)$$

For an odd mode where χ has a zero at $y=0$ the boundary conditions are met if $B=A(\epsilon_1/\epsilon_2)\sin(\sigma_y d)$ and

$$\sigma_y \cos(\sigma_y d) = -\frac{\epsilon_1}{\epsilon_2} j\rho_y \sin(\sigma_y d) \qquad (4\text{-}2.8)$$

It is convenient to normalise to the guide half thickness d, i.e. $u=\sigma_y d$ and $w=-j\rho_y d$ then these equations (4-2.7/8) become

$$u\tan(u) = w\frac{\epsilon_1}{\epsilon_2} \quad \text{and} \quad u\cot(u) = -w\frac{\epsilon_1}{\epsilon_2} \qquad (4\text{-}2.9)$$

From the conservation of wave numbers (4-2.5) the effective frequency v can be defined as

$$(\epsilon_1-\epsilon_2)k_0^2 d^2 = u^2+w^2 = v^2 \qquad (4\text{-}2.10)$$

Solutions for TE fields can be obtained in a similar fashion and using the same normalisation. The analagous relations to (4-2.9) are

$$u\tan(u) = w \quad \text{and} \quad u\cot(u) = -w \qquad (4\text{-}2.11)$$

Graphical solutions of these equations are shown [6,7] in (Fig. 4-2). If w is plotted against u for pure surface waves, (u and w real), then (4-2.10) is the equation of a circle centred at the origin, with radius v and (4-2.11) takes the form of modified tangent curves. In both cases it is clear that the tangent-like curves intersect any circle at only a finite number of points so that for any finite v there are a finite number of solutions. Guided mode solutions have $w>0$. The cut off condition is that $w=0$, i.e. that $v=n\pi$ for the n^{th} mode. The lowest order mode has no cut off.

For active guides v is complex and solutions are best illustrated by

plotting the modulus and argument of v^2 on the u plane, (Fig. 4-3,4). The solution outside the slab is $e^{-j\rho(|y|-d))}$, the modulus of which decays with $(|y|-d)$ for $\rho''<0$ but increases for $\rho''>0$. Cut off conditions must now be given by $\mathrm{Re}(v)=0$ or $\mathrm{Im}(\rho)=0$. This is equivalent to

$$u'\sin(2u')=u''\sinh(2u') \qquad (4\text{-}2.12)$$

and this is plotted for TE modes on Fig.s 4-3 and 3-4. Guided mode solutions occur within the dotted lines.

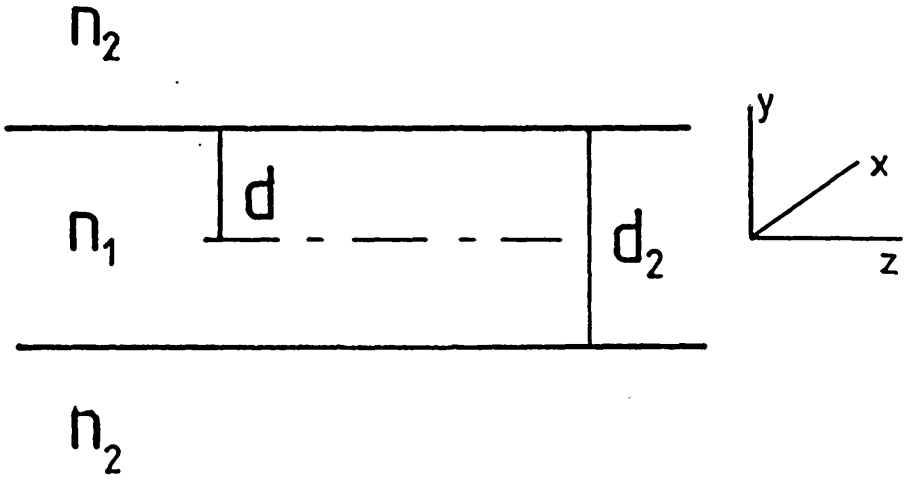

Fig 4-1 Piecewise homogeneous dielectric slab

Fig. 4-1 Piecewise homogeneous dielectric slab. The dielectric slab is an infinite slab of refractive index n and thickness 2d in the x-z plane between two semi-infinte half spaces of refractive index n .

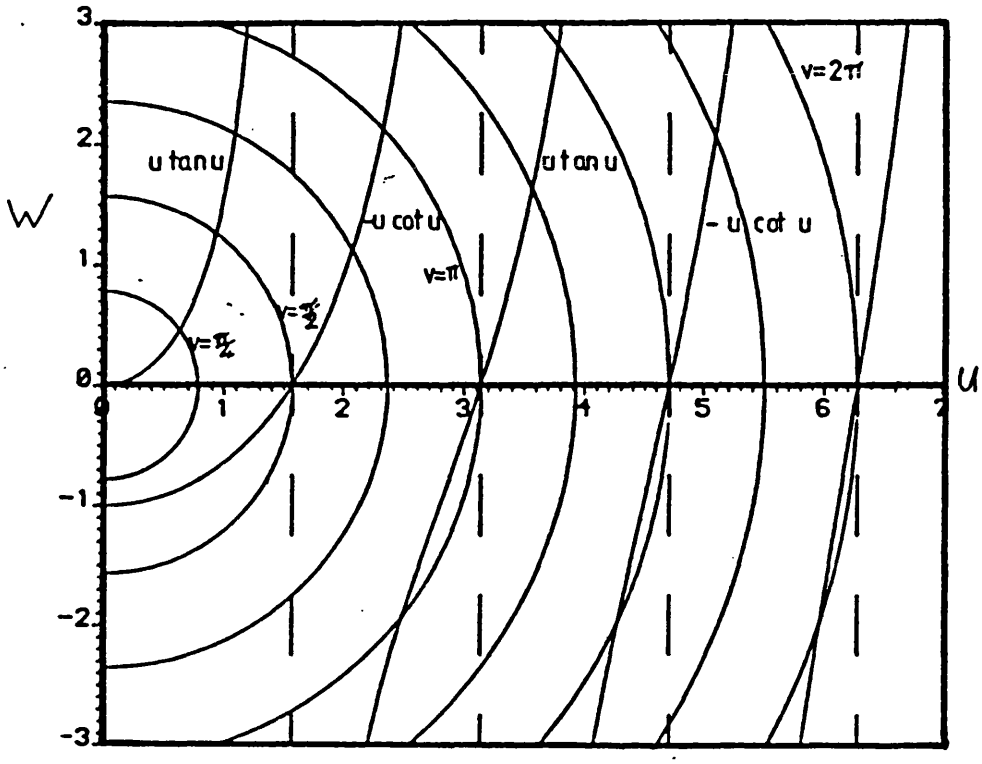

Fig 4-2 Solutions for TE modes of a lossless slab

Fig. 4-2 The solutions of the wave equation for propagation in an infinite lossless dielectric slab are expressed graphically. The effective frequency of the slab waveguide in question defines a single circle, centre the origin, in the w vs. u plane, a number of which are shown for different effective frequencies. The solutions for normalised y-directed propagation and decay constants can be read from the graph of w vs. u as the intersections of the u tan(u) and -u cot(u) with the circle representing the relevant value of effective frequency.

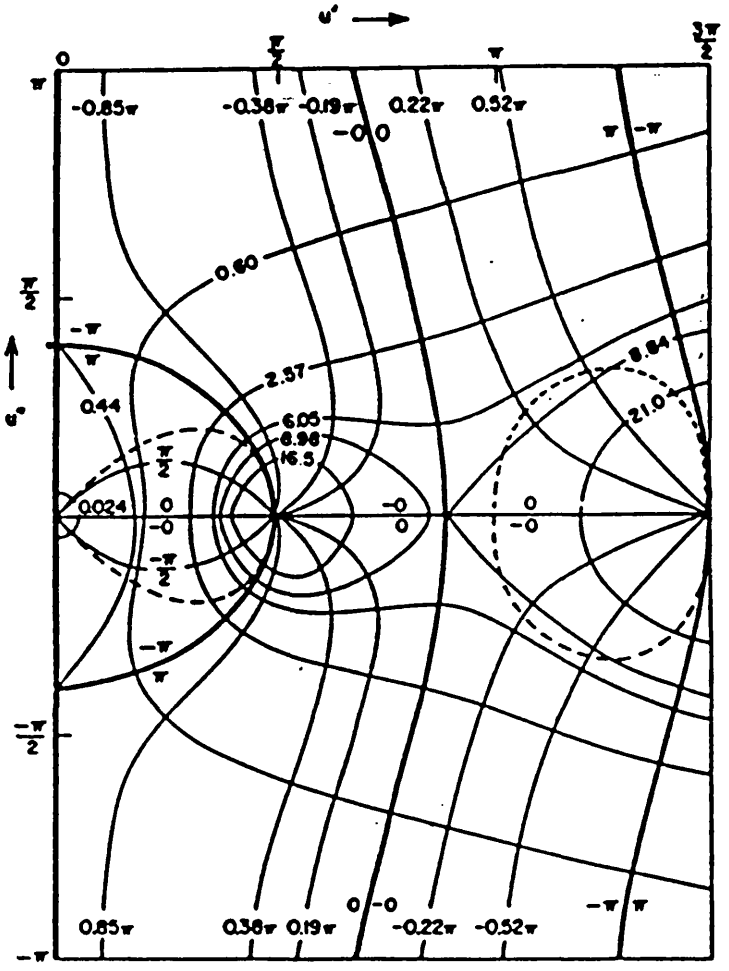

Fig. 4-3 Solutions for the normalised complex y-directed propagation constant within the slab described in equations (4-2.11a) and (4-2.10) for even TE modes are shown graphically on the complex u plane. Contour lines for modulus and phase of the square of the complex effective frequency are shown. The double lines divide the plane into domains in each of which v takes all possible values. Roots lying outside the dashed cut off curves correspond to complex surface waves. Roots lying outside these curves yield leaky wave solutions.

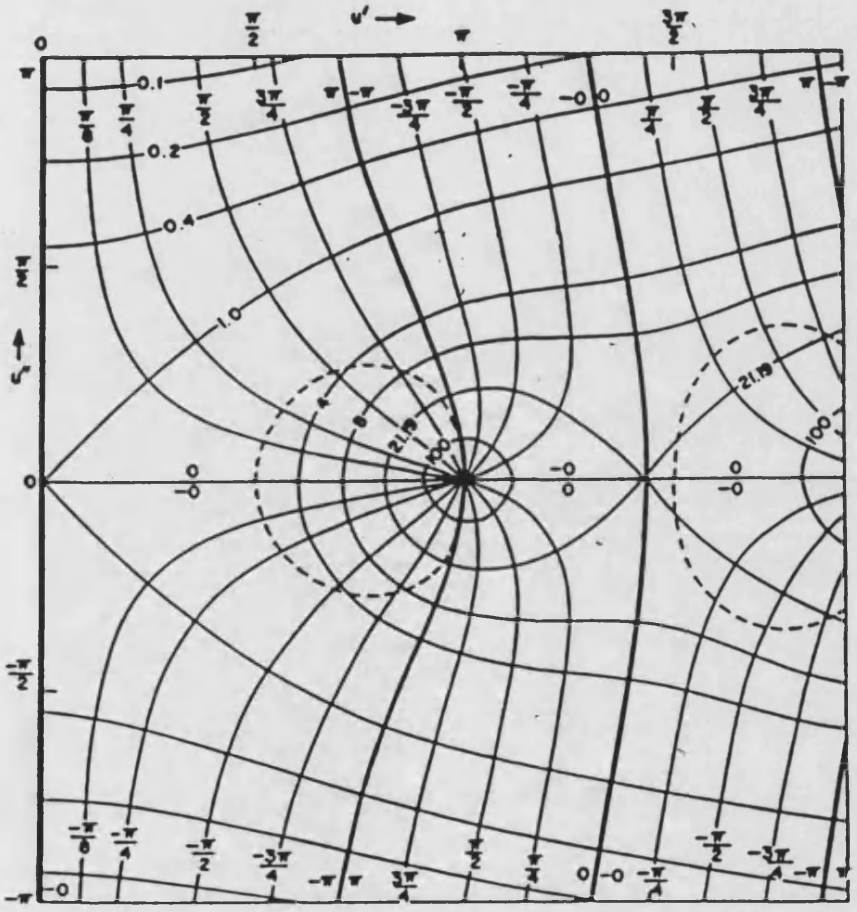

Fig. 4-4 Solutions for the normalised complex y-directed propagation constant within the slab described in equations (4-2.11b) and (4-2.10) for odd TE modes are shown graphically on the complex u plane. Contour lines for modulus and phase of the square of the complex effective frequency are shown. The double lines divide the plane into domains in each of which v takes all possible values. Roots lying outside the dashed cut off curves correspond to complex surface waves. Roots lying outside these curves yield leaky wave solutions.

4-3 Modal Orthogonality and Normalisation

The properties of orthogonality and normalisation of the modes in 4-2 will now be derived.

For a TE mode the one dimensional y directed wave equation for the field function ψ can be written as

$$\frac{d^2\psi}{dy^2}+k^2=0 \tag{4-3.1}$$

Where $k=\sigma_y$ for $|y|<d$ and $k=\rho_y$ for $|y|>d$ and the form of χ in each case is assumed to be as shown in the previous section.

If two separate functions ψ_1 and ψ_2, which both satisfy the wave equation are considered, then the wave equation in ψ_1, say, can be multiplied by ψ_2 to give

$$\psi_2\frac{d^2\psi_1}{dy^2}+k_1^2\psi_2\psi_1=0 \tag{4-3.2}$$

and similarly for ψ_1 and ψ_2 interchanged. Subtracting the resulting two equations gives

$$\psi_2\frac{d^2\psi_1}{dy^2}-\psi_1\frac{d^2\psi_2}{dy^2}=-(k_1^2-k_2^2)\psi_1\psi_2 \tag{4-3.3}$$

Now, bearing in mind that $n_1^2k_0^2=\sigma_y^2+\beta^2$ and $n_2^2k_0^2=\rho_y^2+\beta^2$ it follows that $(k_1^2-k_2^2)=(\beta_2^2-\beta_1^2)$ Substituting this in (4-3.3) and integrating both sides between $y=\pm\infty$

$$\int_{-\infty}^{\infty}\left(\psi_2\frac{d^2\psi_1}{dy^2}-\psi_1\frac{d^2\psi_2}{dy^2}\right)dy=-(\beta_2^2-\beta_1^2)\int_{-\infty}^{\infty}\psi_1\psi_2dy \tag{4-3.4}$$

$$=\left[\psi_2\frac{d\psi_1}{dy}-\psi_1\frac{d\psi_2}{dy}\right]_{-\infty}^{\infty}-\int_{-\infty}^{\infty}\left(\frac{d\psi_1}{dy}\frac{d\psi_2}{dy}-\frac{d\psi_2}{dy}\frac{d\psi_1}{dy}\right)dy \tag{4-3.5}$$

For a bound mode both the field and its derivative tend to zero at infinity and the integral above is identically zero so that

$$(\beta_2^2-\beta_1^2)\int_{-\infty}^{\infty}\psi_1\psi_2 dy=0$$

If $\psi_1\neq\psi_2$ and β_2 is not equal to β_1 so that the orthonormality property can be written as

$$\int_{-\infty}^{\infty}\psi_m\psi_n\,dy=\delta_{m,n} \qquad (4\text{-}3.6)$$

Where $\delta_{m,n}$ is the Kronecker delta. For $m=n$ the normalisation constant a, can be found by integration of the fields in equation (4-2.6) giving,

$$a^2=\frac{j\rho}{j\rho d+\xi(\rho^2-\sigma^2)/(\rho^2-\xi\sigma^2)} \qquad (4\text{-}3.8)$$

For TE modes, $\xi=1$. The same argument applies for TM modes with $\xi=\epsilon_2/\epsilon_1$.

The surface waves of a slab do not form a complete set and the continuous spectrum of radiation must also be considered.

The continuous spectrum is represented as an integral of one the propagation constants (β ,σ orρ). The complete field expansion for an arbitrary TM function X including the integral of the continuous spectrum over ρ is then

$$X=\sum_n b_n\psi_n(y)+\int_0^{\infty}b(\rho)\psi(y,\rho)\,d\rho \qquad (4\text{-}3.9)$$

Where ψ_n are discrete mode functions and $\psi(y,\rho)$ is the continuous spectrum field function. The constants b_n and $b(\rho)$ are the magnitude components defining X. For even TE modes [1],

$$\psi(y,\rho) = a(\rho)\cos(\sigma_y y) \qquad |y| \leq d \qquad \text{(4-3.10a)}$$

$$= \xi a(\rho)\frac{\cos(\sigma_y d)}{\cos(\alpha)}\cos(\rho_y(y-d)+\alpha) \qquad |y| \geq d \qquad \text{(4-3.10b)}$$

Where $\tan(\alpha) = -\frac{\sigma_y}{\rho_y}\tan(\sigma_y d)$ and $\xi = 1$. For even TE modes the coefficient $a(\rho)$ is given by

$$a^2(\rho) = \qquad \text{(4-3.12)}$$

$$\frac{n_2^2 k_0^2 - \beta^2}{[j\rho_y\cos(\sigma_y d)+\xi\sigma_y\sin(\sigma_y d)][j\rho_y\cos(\sigma_y d)-\xi\sigma_y\sin(\sigma_y d)]}$$

With $\xi = 1$ and for odd modes sine and cosine terms are interchanged. Expressions for TM modes are given by the same formulae with $\xi = \frac{\epsilon_2}{\epsilon_1}$.

References for Chapter 4

1/ V.V.Chevshenko, Continuous transitions in open waveguides, Golem Press, 1971.

2/ T.Tamir, A.A.Oliner, " Guided complex waves I.", Proc.IEE, **110** , (2), pp310-324, 1963.

3/ T.Tamir, A.A.Oliner, " Guided complex waves II.", Proc.IEE, **110** , (2), pp325,334, 1963.

4/ For example, J.D.Kraus, K.R.Carver, " Electromagnetics ", 2nd Ed., McGraw-Hill Kogakusha, 1973.

5/ P.M.Morse, H.Feshbach, Methods of Theoretical Physics, McGraw Hill, 1953, (See Chapt. 13).

6/ G.H.B.Thompson, " Physics of semiconductor laser devices ", Wiley, 1980.

7/ J.J.Burke, " Propagation constants of resonant waves on homogeneous, isotropic slab waveguides ", Appl.Opt., 9 , (11), pp2444-2452, 1970.

8/ N.S.Kapany, J.J.Burke, Optical Waveguides, Academic Press, 1972.

CHAPTER 5

5-1 Active Optical Waveguides

The guiding mechanism for electromagnetic fields in the vertical, y direction, is easily explained in terms of the refractive indices, n_1 and n_2. (See Fig.5-1). The refractive indeces are real with $n_1 > n_2$. It is not immediately clear why the electromagnetic fields should be confined in the lateral, x direction. The injection of carriers causes a reduction in the real part of the refractive index so that it is higher at the edge of the guide. This is an antiguiding phenomenon. The guiding mechanism can only be expained in terms of complex refractive indeces. [1] If the variation in refractive index in the lateral direction is approximated by an equivalent slab then, for a guided mode, the effective frequency, v, is given by, $v^2 = \sigma^2 - \rho^2$. The real and imaginary parts of the lateral propagation constant have the same sign inside the guide, i.e. $\sigma'\sigma'' > 0$, and opposite outside, i.e. $\rho'\rho'' < 0$. So that the imaginary part of v^2 must be greater than zero.

$$\mathrm{Im}(v^2) = \mathrm{Im}(n_1^2 - n_3^2) k_0^2 d^2 > 0 \qquad (5\text{-}1.1)$$

that is

$$n_1' n_1'' > n_3' n_3'' \qquad (5\text{-}1.2)$$

Since n_1' is approximately equal to n_3' the guided mode can exist only if $n_1'' > n_3''$. (Although this in itself is not sufficient.) This phenomenon is referred to as gain guiding. It should be noted that if n_1'' and n_3'' are both negative, such that the local gain in each region is negative, gain guiding can still occur. It is the presence of carriers described in Chapter 2 that causes optical gain, as shown in Chapter 3.

The electromagnetic field is considered to have a z dependence of $e^{-j\beta z}$ and is described by a number of modes of gain g_m and propagation constants β_m. The value of β_m for any mode is complex with imaginary part $\beta_m'' = \frac{g_m}{2}$. Because of the extension of the fields out from under the stripe each value of g_m is less than the local gain g calculated in Chapter 3, i.e. $\beta_m'' \leq n_1'' k_0$.

In the vertical slab analysis the cross-section considered was one dimensional and the cross-section function was easy to describe. In this chapter a two dimensional cross-section function is developed. It is convenient to separate the x and y variations and so the effective dielectric constant, edc, method is used. This method is only applicable to guiding structures with large aspect ratios and some of the approximations made are discussed.

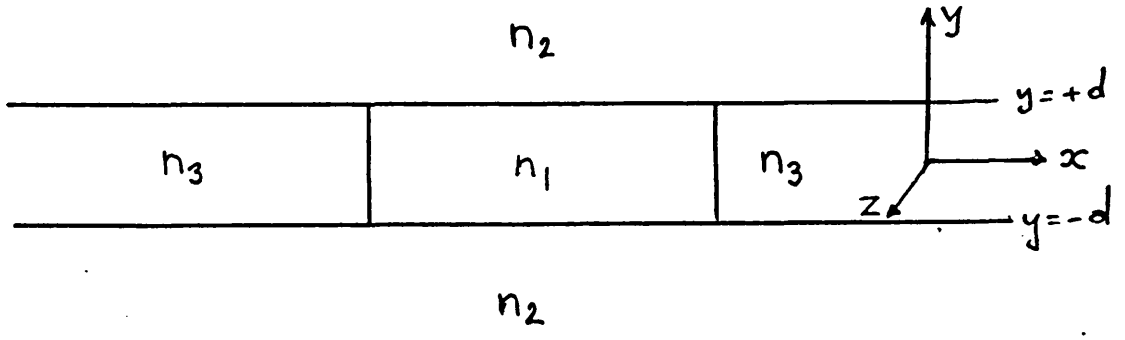

Fig. 5-1 The analysis of a waveguide requires an extension of the nomenclature of the dielectric slab. In addition to the regions of refractive index n_1 and n_2, two further regions of refractive index n_3 are added on either side of the guide centre, within the guiding layer. In a slab model the centre region may be the same width as the stripe contact but when the refractive index is considered to be a function of x the refractive index n_3 may be the limiting value for large x.

5-2 The Effective Dielectric Constant Method

The dielectric constant in the active layer is dependent on its position, i.e. it is a function of x. This is due to the injection of carriers. If the amplitudes of the electromagnetic fields are small so that they do not affect the refractive index then the analysis is simplified.

It is convenient to represent the electric field

$$\mathbf{E} = \nabla \times \hat{\mathbf{y}}\psi + \nabla \times \nabla \times \hat{\mathbf{y}}\chi \tag{5-2.1}$$

with *spi* and χ as solutions of the wave equation. The two orthogonal polarisations represented by ψ and χ are TE and TM to $\hat{\mathbf{y}}$ and are longitudinal section modes, LSE and LSM. Expanding **E** gives

$$\mathbf{E} = \frac{\partial \psi}{\partial x}\hat{\mathbf{z}} + \frac{\partial \psi}{\partial z}\hat{\mathbf{x}} + \frac{\partial^2 \chi}{\partial x \partial y}\hat{\mathbf{x}} - \left(\frac{\partial^2 \chi}{\partial x^2} + \frac{\partial^2 \chi}{\partial z^2}\right)\hat{\mathbf{y}} + \frac{\partial^2 \chi}{\partial z \partial y}\hat{\mathbf{z}} \tag{5-2.2}$$

And so, from Maxwell's equations

$$-j\omega\mu\mathbf{H} = \frac{\partial^2 \psi}{\partial x \partial y}\hat{\mathbf{x}} + \frac{\partial^2 \psi}{\partial z \partial y}\hat{\mathbf{z}} - \left(\frac{\partial^2 \psi}{\partial x^2} + \frac{\partial^2 \psi}{\partial z^2}\right)\hat{\mathbf{y}} + n^2 k_0^2 \left(\frac{\partial \chi}{\partial x}\hat{\mathbf{z}} - \frac{\partial \chi}{\partial z}\hat{\mathbf{x}}\right) \tag{5-2.3}$$

Where it is assumed that χ and ψ are solutions of the scalar wave equation and separable in x, y and z. Hence

$$n^2 k_0^2 \chi + \frac{\partial^2 \chi}{\partial x^2} + \frac{\partial^2 \chi}{\partial y^2} + \frac{\partial^2 \chi}{\partial z^2} = 0 \tag{5-2.4}$$

The basic premise of the edc method is that the guide is large in the x direction so that $\frac{\partial \chi}{\partial x}$ or $\frac{\partial \psi}{\partial x}$ terms are small with respect to the others. Then

$$\mathbf{E} = \frac{\partial \psi}{\partial z}\hat{\mathbf{x}} + n_f^2 k_0^2 \chi\, \hat{\mathbf{y}} + \frac{\partial^2 \chi}{\partial z \partial y}\hat{\mathbf{z}} \tag{5-2.5}$$

$$j\omega\mu\mathbf{H} = \frac{\partial^2\psi}{\partial z\partial y}\hat{\mathbf{z}} + n_e^2 k_0^2\psi\,\hat{\mathbf{y}} - n^2 k_0^2\frac{\partial\chi}{\partial z}\hat{\mathbf{x}} \tag{5-2.6}$$

Where

$$n_e^2 k_0^2\psi = n^2 k_0^2\psi + \frac{\partial^2\psi}{\partial y^2} = -\frac{\partial^2\psi}{\partial x^2} - \frac{\partial^2\psi}{\partial z^2}$$

and similarly for χ and n_f. With this reduced set of fields the LSE modes are now TE to $\hat{\mathbf{z}}$ and LSM are TM to $\hat{\mathbf{z}}$. It is frequently convenient to restrict attention only to TE and TM mode components. Bearing in mind that ϵ is a function of x Maxwell's equations can be used to investigate the wave equation.

$$\nabla\times\nabla\times\mathbf{H} = -j\omega(\nabla\times\epsilon\mathbf{E})$$

$$-\nabla^2\mathbf{H} = n^2 k_0^2\mathbf{H} + j\omega\left[E_z\frac{\partial\epsilon}{\partial x}\hat{\mathbf{y}} - E_y\frac{\partial\epsilon}{\partial x}\hat{\mathbf{z}}\right] \tag{5-2.7}$$

The TE components on the right hand side of this equation are $j\omega\epsilon n_e^2 k_0^2\psi$ from H_y and $j\omega\frac{\partial\phi}{\partial x}\frac{\partial\epsilon}{\partial x}$ from E_z. The E_z term is small compared to the H_y term and so the equation (5-2.7) for H_y can be expressed as

$$\nabla^2 H_y + n^2 k_0^2 H_y = 0 \tag{5-2.8}$$

However ψ is a solution of the wave equation and $j\omega\mu H_y = n_e^2 k_0^2\psi$. In order that H_y should be a solution of the same wave equation, H_y must be represented by an average value of n_e, n_{ea}. Since $n_e \approx 3.6$ and varies only by about 1% overall this is a reasonable approximation. The other TE fields follow

$$H_y = \frac{n_{ea}^2 k_0^2\psi}{j\omega\mu} \tag{5-2.9a}$$

$$E_x = \frac{n_{ea}^2}{n_e^2}\frac{\partial \psi}{\partial z} \tag{5-2.9b}$$

$$H_z = \frac{1}{-j\omega\mu}\frac{\partial^2 \psi}{\partial z \partial y} \tag{5-2.9c}$$

The ratio n_{ea}^2/n_e^2 used to describe E_x could be approximated to unity but including it means that E_x is discontinuous if n_e is used and only D_x is continuous. The LSE fields have five components, the other two are

$$E_z = \frac{\partial \psi}{\partial x} \tag{5-2.9d}$$

$$H_x = \frac{1}{-j\omega\mu}\frac{\partial^2 \psi}{\partial x \partial y} \tag{5-2.9e}$$

The TM fields can be derived in a similar fashion. From Maxwell's equations

$$\nabla \times \nabla \times \mathbf{E} = \nabla(\nabla \cdot \mathbf{E}) - \nabla^2 \mathbf{E} = n^2 k_0^2 \mathbf{E} \tag{5-2.10}$$

However $\nabla(\nabla \cdot \mathbf{E}) \neq 0$ since $\nabla \cdot \mathbf{D} = 0$, in fact

$$\nabla^2 \mathbf{E} + n^2 k_0^2 \mathbf{E} + \nabla E_x \frac{1}{\epsilon}\frac{\partial \epsilon}{\partial x} + \hat{\mathbf{x}}\left[\frac{\partial \epsilon}{\partial x}\frac{1}{\epsilon^2}\frac{\partial \epsilon}{\partial x}E_x - \frac{1}{\epsilon}\frac{\partial^2 \epsilon}{\partial x^2}E_x\right] = 0 \tag{5-2.11}$$

So, consider E_y, a TM component with no corresponding E_x.

$$\nabla^2 E_y + n^2 k_0^2 E_y = 0 \tag{5-2.12}$$

Again if χ is a solution of the scalar wave equation and $E_y = n_f^2 k_0^2 \chi$ then an average value of n_f must be chosen for E_y to be a solution of the same wave equation. If this is n_{fa} then

$$E_y = n_{fa}^2 k_0^2 \chi \tag{5-2.13a}$$

$$H_x = \frac{-n_a^2 k_0^2}{-j\omega\mu}\frac{\partial\chi}{\partial z} \qquad (5\text{-}2.13b)$$

$$E_z = \frac{\partial^2\chi}{\partial z\partial y} \qquad (5\text{-}2.13c)$$

and the remaining LSM fields are

$$H_z = \frac{n_a^2 k_0^2}{-j\omega\mu}\frac{\partial\chi}{\partial x} \qquad (5\text{-}2.13d)$$

$$E_z = \frac{n_a^2}{n^2}\frac{\partial^2\chi}{\partial x\partial y} \qquad (5\text{-}2.13e)$$

The value of n has been replaced by an average value for some of these fields and n^2E_x is continuous in x, no matter what profile of n is chosen. For a slowly varying, almost constant n the ratio $n_a^2{:}n^2$ might be approximated to 1.

The solutions presented here rely on the variation of n in x being small. From the representation of H and Maxwell's equations E is given by

$$n^2k_0^2\mathbf{E} = \frac{\partial}{\partial z}\left(\frac{\partial^2\psi}{\partial y^2} - n_{ea}^2k_0^2\psi\right)\hat{\mathbf{x}} + \frac{\partial}{\partial x}\left(n_{ea}^2k_0^2\psi - \frac{\partial^2\psi}{\partial y^2}\right)\hat{\mathbf{z}} \qquad (5\text{-}2.14)$$

$$+ n_a^2k_0^2\frac{\partial^2\chi}{\partial x\partial y}\hat{\mathbf{x}} - n_a^2k_0^2\left(\frac{\partial^2\chi}{\partial x^2} + \frac{\partial^2\chi}{\partial z^2}\right)\hat{\mathbf{y}} + n_a^2k_0^2\frac{\partial^2\chi}{\partial z\partial y}\hat{\mathbf{z}}$$

Comparing this with (5-2.2) and (5-2.5) allows the approximations to be investigated. For LSE modes this reduces to saying that $(\sigma_y^2 - \sigma_{ya}^2)$ is very much less than $n^2k_0^2$, where, σ_{ya} is an average value of σ_y. This is undoubtedly true. For LSM modes, considerations for E_y dictate that $n^2n_{fa}^2 = n_a^2n_f^2$, which is likely to be true since the variation of n and n_f with x is only small and the two are closely related.

The two dimensional cross-sectional functions have similar y dependencies to those discussed in Chapter 4. In that case, since n_1, the active layer refractive index is a function of x so is the y directed propagation constant σ_y. If the z propagation is exponential, i.e. $e^{-j\beta z}$ then from (4-2.4)

$$\frac{\partial^2 H_y}{\partial x^2} + \left(n^2 k_0^2 - \sigma_y^2 - \beta^2\right) H_y = 0 \qquad (5\text{-}2.15)$$

or since H_y is proportional to ψ

$$\frac{\partial^2 \psi}{\partial x^2} + (n_e^2 k_0^2 - \beta^2)\psi = 0 \qquad (5\text{-}2.16)$$

Similarly from (5-2.12) for E_y

$$\frac{\partial^2 \chi}{\partial x^2} + \left(n_f^2 k_0^2 - \beta^2\right)\chi = 0 \qquad (5\text{-}2.17)$$

It is the solution of these equations which is considered in the next section.

5-3 Solutions of the Active Slab Problem

In (5-2) the principle of edc was stated and the approximations involved were demonstrated. However, approximations made in justifying the boundary conditions rely on the x variation of the refractive index being small. The solution of the diffusion equation in (2-3) shows this variation. A three layer slab model for the x variation should be convenient but there is no guarantee that it would produce a reasonable solution. Numerical solutions using edc and involving a transverse transmission line analysis [2] have been used to calculate field shapes in D-H laser structures where inversion population changes with light intensity. For the purpose of this thesis such numerical solutions do not give the required insight into the mechanisms of gain guiding structures.

Several approximate carrier profiles are shown in Fig.2-8 but only those which yield tractable analytic field shapes are useful in this context. The exclusion of photon intensity from the calculation of carrier density limits the range over which these solutions are valid. The profiles which are of interest here are

$$n = n_0 + \left[\eta_{01} - \eta_1 \left(\frac{x}{w_1}\right)^2\right] \qquad |x| < w_1 \qquad (5\text{-}3.1)$$

$$n = n_0 + \left[\eta_{02} - \eta_2 \tan^2\left(\frac{\pi}{3}\frac{x}{w_2}\right)\right] \qquad |x| < \frac{3w_2}{4} \qquad (5\text{-}3.2)$$

$$n = n_0 + \left[\eta_{03} - \eta_3 \tanh^2\left(\frac{2x}{w_3}\right)\right] \qquad |x| < \infty \qquad (5\text{-}3.3)$$

The three layer slab approximation will also be investigated. Profiles (5-3.1,2,3) have been previously investigated in the literature [3,4]. In each case n_0 is the background refractive index before it is modified by carriers. The values

of η_1, η_2, η_3, are proportional to the change in refractive index with N, and includes the changes in both real and imaginary parts. The constant η_{0i} is included to keep the refractive index at the limiting value of $|x|$ the same in all cases. In the case of (5-3.1,2) the equations are only valid for a specified region under the stripe. Solutions of the type (5-3.3) have been modified [5] to include asymmetric refractive index profiles. This is not felt necessary here in view of the limited range of photon intensities considered, and the symmetrical nature of stripe boundary conditions.

In this section the one dimensional wave equation in an active slab is analysed by using these three approximate profiles and the equivalent slab analysis.

The reduced wave equation in one dimension is

$$\frac{d^2X}{dx^2} + \left[n^2 k_0^2 - \beta^2\right] X = 0 \qquad (5\text{-}3.4)$$

If the magnitude of the variation of the refractive index in the x direction is small and $n_3 = n_0 + \eta_{0i}$ then, in each case the refractive index can be expressed as

$$n = n_3 - \eta_i f(x) \qquad (5\text{-}3.5)$$

it follows from (5-3.4) that

$$\frac{d^2X}{dx^2} + \left[\left[n_3 - \eta_i f(x)\right]^2 k_0^2 - \beta^2\right] X = 0 \qquad (5\text{-}3.6)$$

and, neglecting terms in $f^2(x)$

$$\frac{d^2X}{dx^2} + \left[\left[n_3^2 - 2n_3\eta_i f(x)\right] k_0^2 - \beta^2\right] X = 0 \qquad (5\text{-}3.7)$$

The case of the parabolic index profile can be considered by substituting (5-3.1) into (5-3.7) giving

$$\frac{d^2X}{dx^2}+\left[\left[n_3^2-2n_3\eta_1\frac{x^2}{w_2^2}\right]k_0^2-\beta^2\right]X=0 \qquad (5\text{-}3.8)$$

This has solutions which are Gaussian Hermite orthogonal polynomials [6,7] of the form

$$X(x)=b_p\exp(-\tfrac{1}{2}\xi x^2)H_p(\xi^{1/2}x) \qquad (5\text{-}3.9a)$$

$$\xi^2=\frac{2n_3\eta_1k_0^2}{w_1^2} \qquad (5\text{-}3.9b)$$

$$\beta^2=n_3^2k_0^2-\xi(2p+1) \qquad (5\text{-}3.9c)$$

The polynomials are normalised over the interval $x:(-\infty,\infty)$, with normalisation coefficient for the p^{th} polynomial, b_p, given by

$$b_p^{-2}=\sqrt{\pi}\ 2^p\,p! \qquad (5\text{-}3.10a)$$

Gaussian Hermite polynomials are defined by

$$H_0=1,\quad H_1(z)=2z,\quad H_2(z)=4z^2-2,\quad \text{etc.} \qquad (5\text{-}3.10b)$$

The Gaussian term $\exp(-\xi x^2/2)$ ensures that all these functions decay for large x when the positive root of (5-3.9b) is used for ξ. Although the modal field shapes seem well enough behaved the refractive index profile used in finding these solutions is parabolic, not just near the guide, but for all x, implying a field decay that is far too strong away from the stripe.

The square tangent profile gives the differential equation

$$\frac{d^2X}{dx^2}+\left[\left[n_3^2-2n_3\eta_2\tan^2\left(\frac{\pi}{2}\frac{x}{w_2}\right)\right]k_0^2-\beta^2\right]X=0 \qquad (5\text{-}3.11)$$

This has solutions which are Gegenbauer (Ultraspherical) polynomials given by [8]

$$X(x)=b_p \cos^{\mu}\left|\frac{\pi}{2}\frac{x}{w_2}\right| C_p^{(\mu)}\left|-\sin(\frac{\pi}{3}\frac{x}{w_2})\right| \qquad (5\text{-}3.12a)$$

Where

$$\mu(1-\mu)=-2n_3\eta_2 k_0^2\left|2\frac{w_2}{\pi}\right|^2 \qquad (5\text{-}3.12b)$$

and the z directed propagation constant is given by

$$\beta_p^2=n_3^2k_0^2-(p^2+2p\mu+\mu^2)\left|\frac{\pi}{3w_2}\right|^2 \qquad (5\text{-}3.12c)$$

Gegenbauer polynomials are defined by

$$C_0^{(\mu)}=1, \quad C_1^{(\mu)}(z)=2z\mu \qquad (5\text{-}3.13a)$$

and

$$(p+1)C_{p+1}^{(\mu)}(z)=2z(p+\mu)C_p^{(\mu)}(z)-(p+2\mu-1)C_{p-1}^{(\mu)}(z) \qquad (5\text{-}3.13b)$$

Gegenbauer polynomials are usually normalised for x:$(-1,1)$ so that these functions are only useful when the fields are confined near the stripe boundaries. Further, the refractive index variation suggested by (5-3.2) describes a profile which approaches infinity as x approaches $2w_2$. Solutions can be found, however, by matching the fields at $z=\pm\sin(\pi/4)$ to an exponetial, but matching and ensuring modal orthogonality is awkward. Solutions of the squared hyperbolic tangent profile are for refractive index variations which closely resemble the actual solution of the diffusion equation. The refractive index changes slowly from its value at the centre to a constant limit value for

increasing x. The differential equation for this profile is

$$\frac{d^2X}{dx^2}+\left[\left[n_3^2-2n_3\eta_3\tanh^2\left[2\frac{x}{w_3}\right]\right]k_0^2-\beta^2\right]X=0 \qquad (5\text{-}3.14)$$

This also has solutions which are Gegenbauer polynomials.

$$X(x)=b_p\cosh^{\mu}\left[2\frac{x}{w_3}\right]C_p^{(\mu)}\left[j\sinh\left[2\frac{x}{w_3}\right]\right] \qquad (5\text{-}3.15a)$$

Where

$$\mu(1-\mu)=-2n_3\eta_3k_0^2\frac{w_3^2}{2} \qquad (5\text{-}3.15b)$$

and the z directed propagation constant is given by

$$\beta_p^2=n_3^2k_0^2+(p^2+2p\mu+\mu^2)\left[\frac{2}{w_3}\right]^2 \qquad (5\text{-}3.15c)$$

the Gegenbauer polynomials are defined by (5-3.13). The solutions of this are odd or even depending on the value of p and only decay for increasing x if $(p+\mathrm{Re}(\mu))<0$. For $(p+\mathrm{Re}(\mu))<0$ the solutions represent bound modes and for $(p+\mathrm{Re}(\mu))>0$ the amplitudes increase with x away from the stripe as with leaky wave solutions of the slab waveguide.

Representing the x directed variation of the refractive index by means of a three layer slab requires a boundary to be drawn between inner and outer regions. Solutions then take the form of slab waveguide solutions, illustrated in Fig.4-3,4. The boundaries for this slab can be drawn at the stripe edge but this make no allowance for any effective stripe width used in the other models. It is perhaps better to define an effective stripe width, w_{eff}, which depends on the inversion population profile and not the stripe width. A suitable point

might be the value of x at which $N(x) = \frac{1}{2}N_{max}$. The value of N_1 within the slab then becomes the average value of $N(x)$ between $x = 0$ and $x = w_{eff}$. The value of N_3, outside the slab becomes the average between w_{eff} and some further boundary ,w_f. This in effect defines a five layer slab, although only a three layer model is needed to give the field solutions. Although it is clear that w_f is bigger that w_{eff} it is not clear where this second boundary should be.

All of these solutions can only be calculated after current spreading and carrier out diffusion have been used to calculate the refractive index profile. The three approximate solutions for continuously varying refractive index rely on a linear relationship between real and imaginary parts of the refractive index. This assumes that n'', the imaginary part of n, and hence the local gain have a more or less linear dependency on N. (Since n' varies almost linearly with N^{8}). Calculations of gain in Chapter 3 do not bear this out. Consequently, to apply these solutions the ratio between the real and imaginary parts of the refractive index must be approximated. This ratio will depend on wavelength as well as inversion population as the imaginary part will depend on optical gain and the real part is derived from Ref 9.

Several field shapes for x directed zeroth order modes are shown in Fig.5-2,3,4,5 for the diffusion profile in Fig.5-1. This was calculated for a current density of $40 Acm^{-2}$ and a $7\mu m$ stripe width and active layer thickness $0.3\mu m$. The x directed field profiles that have been plotted correspond to four different values of gain, ($g = \alpha N - \beta$), where α and β were chosen to represent different wavelengths.

The slab solutions were derived by calculating average refractive indeces between the guide edge, $w/2$, and the origin and between $w/2$ and w. Three slab profiles are shown corresponding to slab boundaries at the stripe edge (1-1), at the point where the inversion population reaches half its maximum

value (1-2), and where it reaches 30% of its maximum value (1-3). The exponential tails on these functions are very long and the shape hardly varies at all within the slab boundaries, even for very small values of α when the solution should approximate a plane wave. The field shapes derived from the approximate refractive index variations behave more as expected. The fields being confined to the centre of the guide only when α, the gain parameter, is large. The squared tangent profile [3] and the parabolic index profile [2] do not represent the variations in refractive index profile calculated in Chapter 2, (Curve 0 in Fig.5-1), except under the stripe. This must lead to the field shapes being too tightly confined for low values of α. The hyperbolic cosine profile is the only profile for which the generating carrier profile approximates the calculated one for low levels of injection. For low levels of injection the field shape it produces approximates a plane wave. This is the preferred profile and will be concentrated on in following Chapters.

Fig. 5- Approximate Carrier Profiles

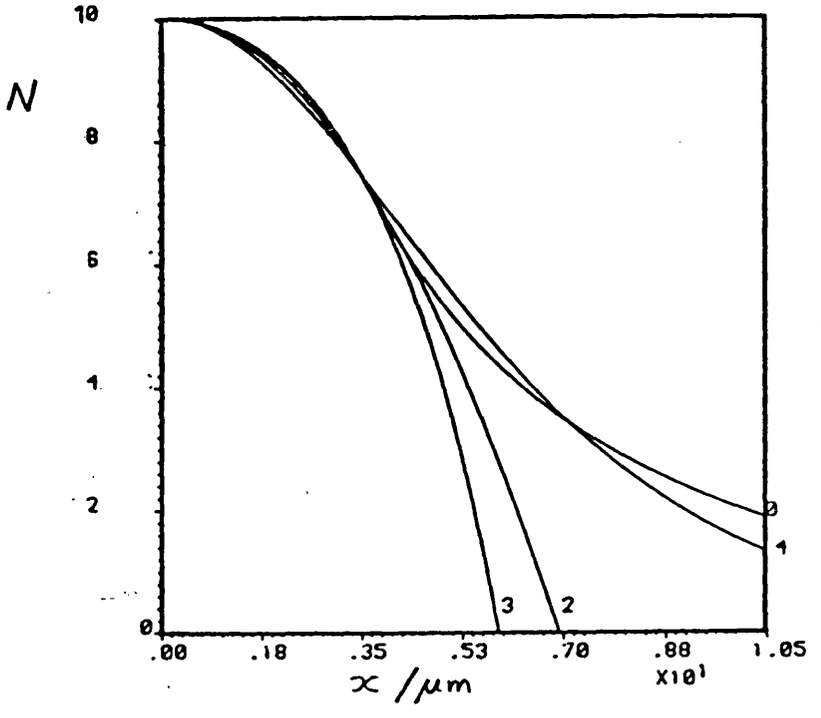

Fig. 5-2 Approximate Carrier Profiles.
An example of the approximate carrier profiles is shown where the profiles have been matched at the centre of the structure and at the edge of the stripe, (x=3.5μm).
The profiles illustrated are:-

0	Numerically calculated profile
2	Tangent squared profile
3	Parabolic profile
4	Inverse hyperbolic cosine squared profile

The slab approximations considered have not been shown.

Fig. 5-3 Field Profiles for Approximate Profiles.
The following graphs show the fundamental mode field profiles calculated using the approximate carrier profiles shown in Fig.5-2 and three calculated from the slab approximations discussed in the text. There are four graphs in the series and they show the variation in field profiles with different ratios of real and imaginary parts of the refractive index. The cahnge in this ratio represents a change in inversion population or difference in wavelength.

Fig.5-3a Very Good Field Confinement

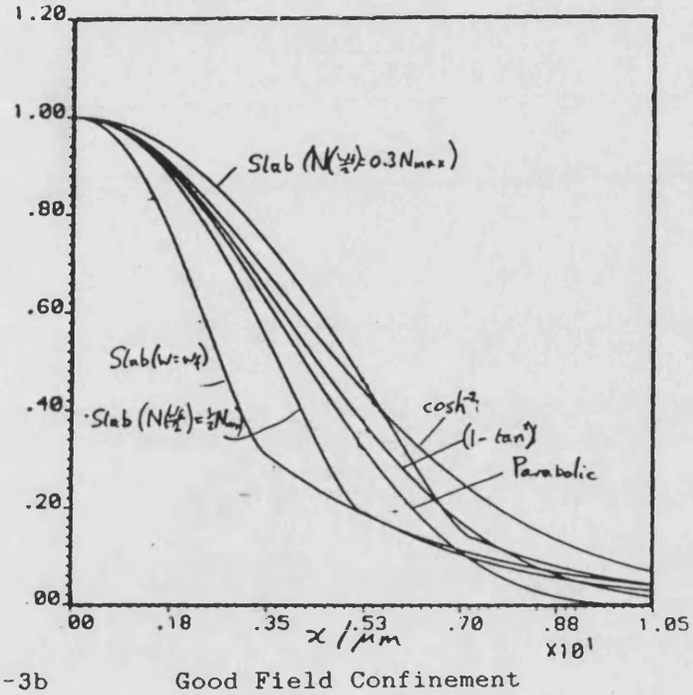

Fig.5-3b Good Field Confinement

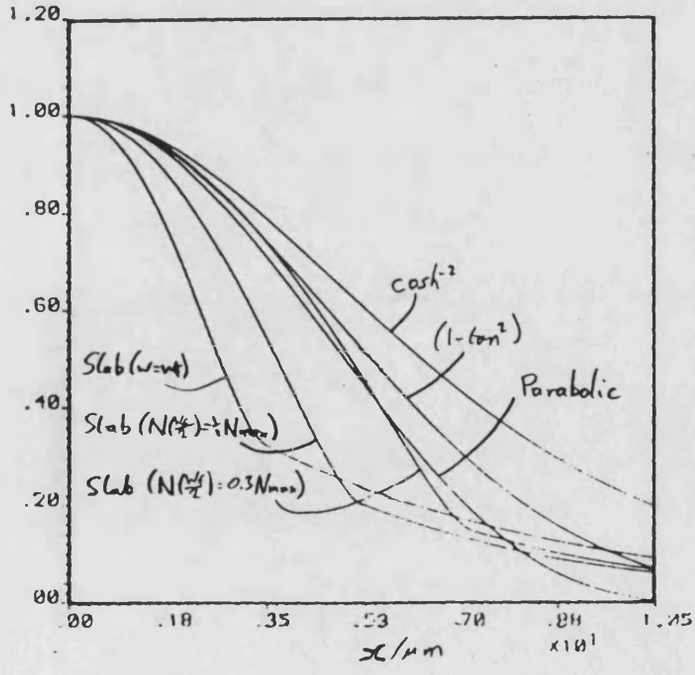

Field Profiles for Approximate Carrier Profiles

Fig.5-3c Poor Field Confinement

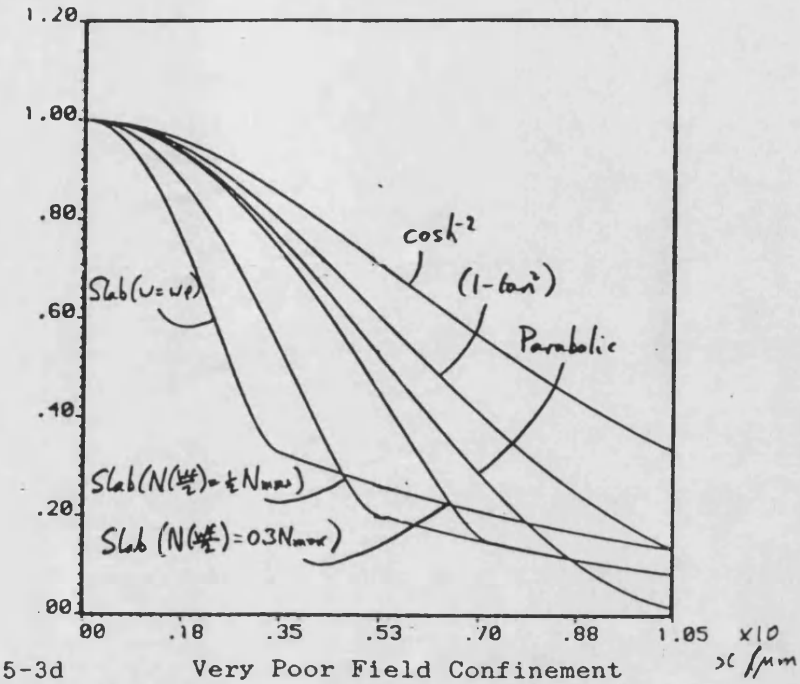

Fig.5-3d Very Poor Field Confinement

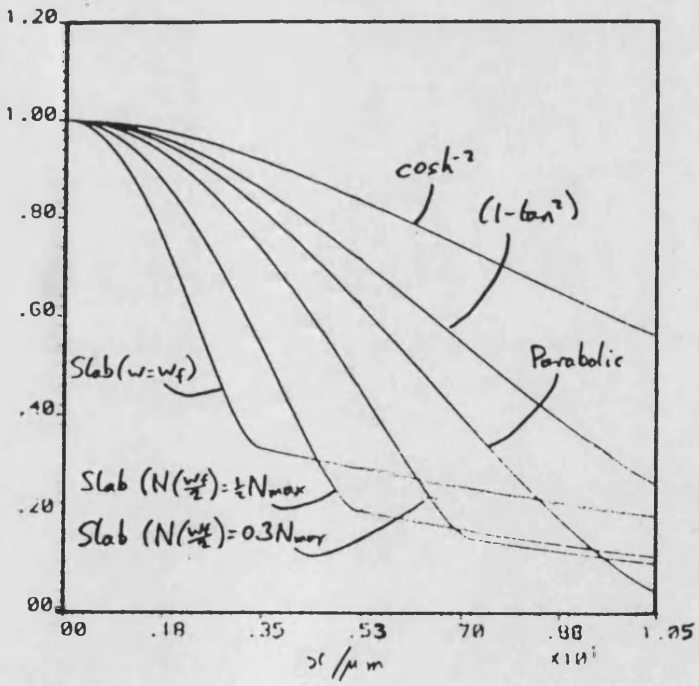

5-4 Two Dimensional solutions

The two dimensional cross-section functions are of the form $X(x)Y(y;x)$ where $Y(y;x)$ is the solution $Y(y)$ at a value of x. This varies with x since the refractive indices vary with x and so the y directed propagation constants do. This in turn implies that the normalisation coefficients for $Y(y)$ also vary with x. The general form of $X(x)$ and $Y(y)$ have already been presented. If both functions are normalised, it follows that their product is also normalised, i.e.

$$\int_{-\infty}^{\infty}\int_{-\infty}^{\infty}\left|X_m(x)Y_i(y;x)\right|^2 dx\, dy = 1 \qquad (5\text{-}4.1)$$

This is the normalisation implied in all calculations for a two dimensional cross-section. Orthogonality is given by equation

$$\int_{-\infty}^{\infty}\int_{-\infty}^{\infty}\left|X_m(x)Y_i(y;x)\right|\left|X_n(x)Y_j(y;x)\right| dx\, dy = 0 \qquad (5\text{-}4.2)$$

$$\text{for } p \neq q \text{ or } i \neq j$$

The change of refractive index with x is small so that in the limit of $\frac{\partial Y}{\partial x} << 1$ $Y(y;x)$ can be well represented by $Y(y)$. Generally only the zeroth order y directed mode is needed with $Y(y) = a_0\cos(\sigma_y y)$ but a number of x directed modes may required so that

$$X(x) = \sum_p \psi_p(x) \qquad (5\text{-}4.3)$$

The solutions are found by calculating the variation of electron density as a function of x, see Chapter 2, and using the results of Chapter 3 to calculate the corresponding imaginary part of the refractive index as a function of x. The variation of the real part of the refractive index is assumed to be

proportional to the carrier density. The average refractive indices required to calculate the two dimensional modes are calculated as being the average between the guide centre and $x = w_3$, which gives a value of about $0.71n(0) + 0.29n(\infty)$. The effective refractive index profile is calculated for TM modes from $n_f^2 k_0^2 = n_1^2 k_0^2 - \sigma_y^2$. Where n_1 is the refractive index of the active layer. A similar expression for n_e holds for TE modes. The inverse hyperbolic cosine profile is fitted to this by calculating the effective width from the expressions in table 2-2. This assumes that the effective refractive index profile approximates to $\cosh^{-2}$.

The local gain is directly related to the imaginary part of the refractive index and to η. A linear relationship between gain and inversion population is sought and this is found by taking two values of gain and inversion population and fitting a linear relationship to these. The two points chosen are the guide centre and the values of N and g at $x = \frac{w_3}{2}$.

The gain of the lowest order mode of the waveguide has been calculated for a spectrum of wavelengths or photon energies. Unlike previous analyses which have sought the peak gain these results show the gain for a range of photon energies. The properties of the zeroth order mode depend on the photon energy. This is a consequence of the slope of the gain curve and the actual value of the gain.

The results of Chapter 3 show that gain can be considered as being proportional to inversion population, that is $g = g_0(\alpha N - \beta)$, only if the coefficients are funtions of both photon energy and inversion population i.e. $\alpha = \alpha(h\nu, N)$ and $\beta = \beta(h\nu, N)$. It is important not to confuse this β with the z propagation constants β_e, β_m. Guiding is provided only by the differential gain at the stripe edge. That is by $\alpha(h\nu, N)$.

In this thesis an approximate expression has been obtained for the gain in terms of N and $h\nu$. This is equation (3-2.21). To obtain an approximation fo α this is now differentiated to give a result which is proportional to α.

$$\frac{dg}{dN} = C\left[\exp\left(\frac{N}{2\sqrt{2}N_0}\right)\left(1+\frac{N}{N_0}\right)+\exp\left(\frac{h\nu-E_g}{kT}\right)\frac{N_0P_0}{N^2}\right]\times \qquad (5\text{-}4.4)$$

$$\times\exp\left(-\frac{h\nu}{2kT}\right)\frac{(h\nu-E_g)^2}{h\nu}$$

This expression is only valid near the band edge but it should serve to give a good indication as to how α behaves. What this equation shows is that for energies near the band edge, $h\nu \approx E_g$, α increases with N for $N \geq N_0$. For energies further from the band edge the $\frac{N_0P_0}{N^2}\exp(h\nu - E_g/kT)$ term becomes significant and α decreases with N. The consequence of this is that increasing N improves the gain guiding for higher photon energies. The exponential and $(h\nu-E_g)^2/h\nu$ terms ensure that the guiding mechanism is always stronger at higher photon energies.

This increase in the strength of the guiding mechanism and hence improved field confinement is accompanied by an increase in $\beta(h\nu, N)$ and so the gain may actually be negative, i.e. the mode amplitude reduces.

As well as modal gain the properties of the parameter μ of equation (5-3.15b) can also be analysed. The behaviour of this parameter with wavelength and inversion population has not been previously reported either. The real part of μ is negative for a bound mode with modal cutoff for the zeroth order mode occuring for $\mu' = 0$ and for the p^{th} mode when $\mu' = -p$.

To approximate the parameter μ from equation (5-3.15b) the change in the refractive index η must be expressed as a complex number. If $\eta = -\rho + j\alpha$

then α is proportional to the slope of the gain curves and therefore to the α parameter described in the discussion of gain. ρ represents the change in the real part of the refractive index (not to be confused with ρ_y the y directed propagation constant.) Throughout this analysis it has been assumed that ρ is a constant although justification of this would require a Kramers-Kronig analysis using the calculated absorption coefficient of Chapter 3. This has not been attempted. A Kramers Kronig analysis has, however, been reported [9] which supports the idea of a constant value of ρ for a wide range of values of N. The same analysis shows only small variations of ρ with photon energy.

Now from (5-3.15b) it follows that

$$\mu = \tfrac{1}{2} \pm \left[1 + 2n_3(-\rho + j\alpha)k_0^2 w_3^2\right]^{\frac{1}{2}} \qquad (5\text{-}4.5a)$$

The quantity in the bracket can be obtained in the usual manner. If $(x+jy) = (a+jb)^2$ then $a+jb = \pm (x+jy)^{\frac{1}{2}}$. Equating real and imaginary parts leads to $2a^2 = x \pm (x^2+y^2)^{\frac{1}{2}}$. Since a is a real number the positive sign must be taken. Similarly b^2 can be obtained so that

$$(x+jy)^{\frac{1}{2}} = \pm \left[\tfrac{1}{2}((x^2+y^2)^{\frac{1}{2}}+x)^{\frac{1}{2}} + j\tfrac{1}{2}((x^2+y^2)^{\frac{1}{2}}-x)^{\frac{1}{2}}\right]$$

The negative sign must be taken for μ to represent a bound mode so that

$$\mu = \frac{1}{2} - \frac{1}{\sqrt{2}}\left[\left[(2n_3k_0^2w_3^2\rho - 1)^2 + (2n_3k_0^2w_3^2\alpha)^2\right]^{\frac{1}{2}} + 1 - 2n_3k_0^2w_3^2\rho\right]^{\frac{1}{2}} +$$

$$+ \frac{j}{\sqrt{2}}\left[\left[(2n_3k_0^2w_3^2\rho - 1)^2 + (2n_3k_0^2w_3^2\alpha)^2\right]^{\frac{1}{2}} - 1 + 2n_3k_0^2w_3^2\rho\right]^{\frac{1}{2}} \qquad (5\text{-}4.5)$$

Near the band edge, $h\nu \approx E_g$, $\frac{\partial g}{\partial N}$ is small and hence α is small so that, for $2n_3k_0^2w_3^2\rho > 1$

$$\mu = \tfrac{1}{2} - j\sqrt{2n_3}\, w_3 k_0 \rho^{\frac{1}{2}} \qquad (5\text{-}4.6)$$

This implies modes which are cut off as $\mu' > 0$ and is a consequence of α being small. When $h\nu - E_g$ becomes large, far from the band edge, then the term in α^2 dominates over that in ρ^2 and

$$\mu \approx -\sqrt{n_3}\, w_3 k_0 [(\alpha - \rho)^{\frac{1}{2}} + j(\alpha + \rho)^{\frac{1}{2}}] \qquad (5\text{-}4.7)$$

For photon energy increasing, α increases and so both real and imaginary parts of μ increase, but the imaginary part is always more negative than the real part. The increase in the real part implies an increasing number of guided modes. The real part of μ is analogous to the effective frequency v of the dielectric slab in that it is proportional to the guide width and wavenumber as well as $[n_3(\alpha - \rho)]^{\frac{1}{2}}$, a factor depending on the square root of a term involving the refractive indices. Some numerical examples are now presented to show, graphically, the behaviour of these curves. The curves presented represent the gain and the guiding parameter μ for a large range of photon energies. The guide thickness chosen for this is 0.3μm and the guide widths 5,7 and 10μm, shown in Figs.5-6, 5-7 and 5-8 respectively, have been used. The curves clearly demonstrate the behaviour described by the approximate analytic solutions.

The modal gain curves reflect the calculations of Chapter 3 but when the field is poorly confined, i.e. $E_g \approx h\nu$, then material gain is not sufficient to make up for the losses.

Fig. 5-4 Waveguide Optical Gain and Guiding Parameter vs. Photon Energy for a 5μm Width Stripe Contact, for different values of injection current density. The Photon energy is in eV, the gain in cm^{-1} and the injection current is in $(10^6 A/m)$

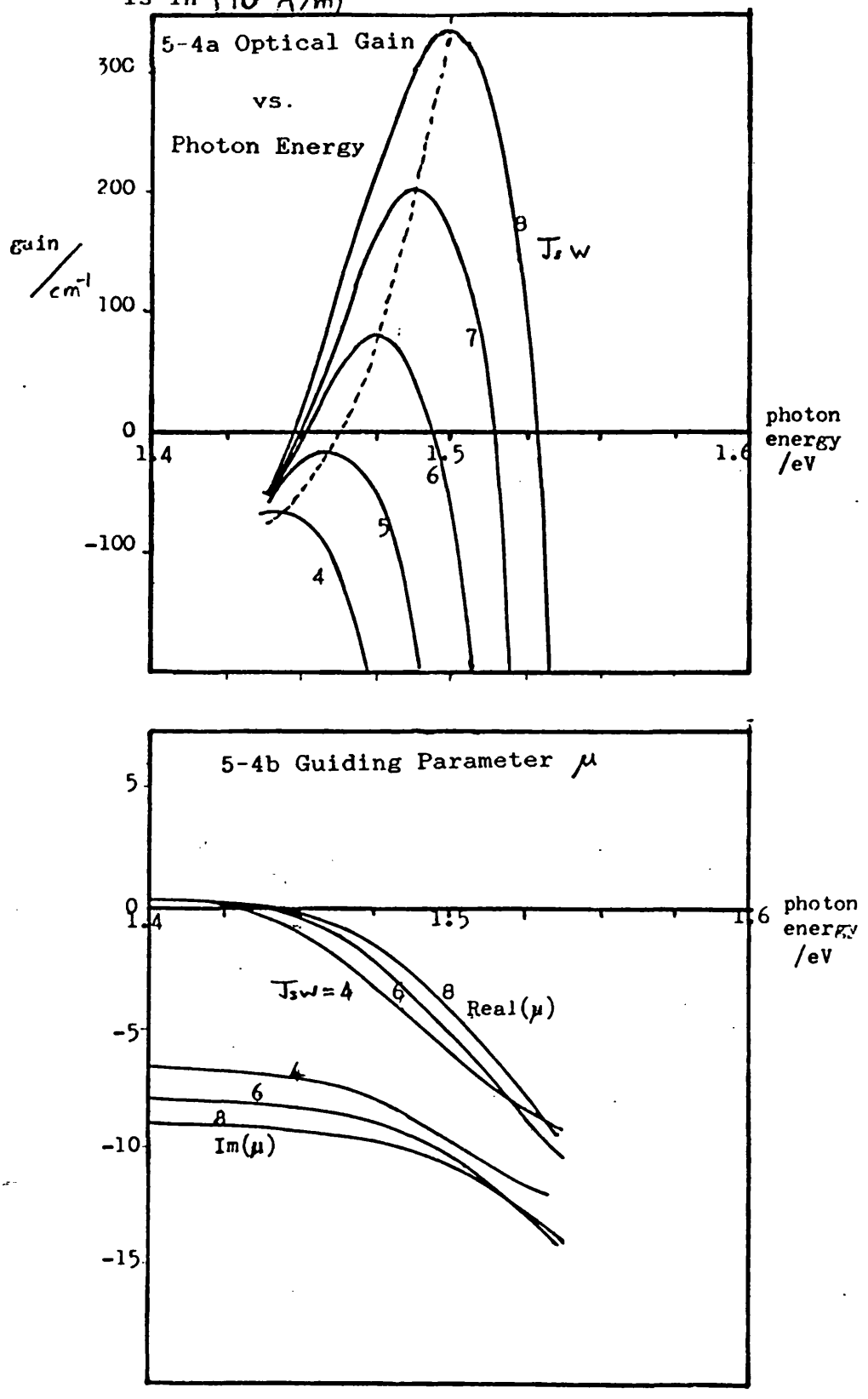

Fig. 5-5 Waveguide Optical Gain and Guiding Parameter vs. Photon Energy for a 7 m Width Stripe Contact, for different values of injection current density. The Photon energy is in eV, the gain in cm and the injection current is in $(10^3$ A/ m).

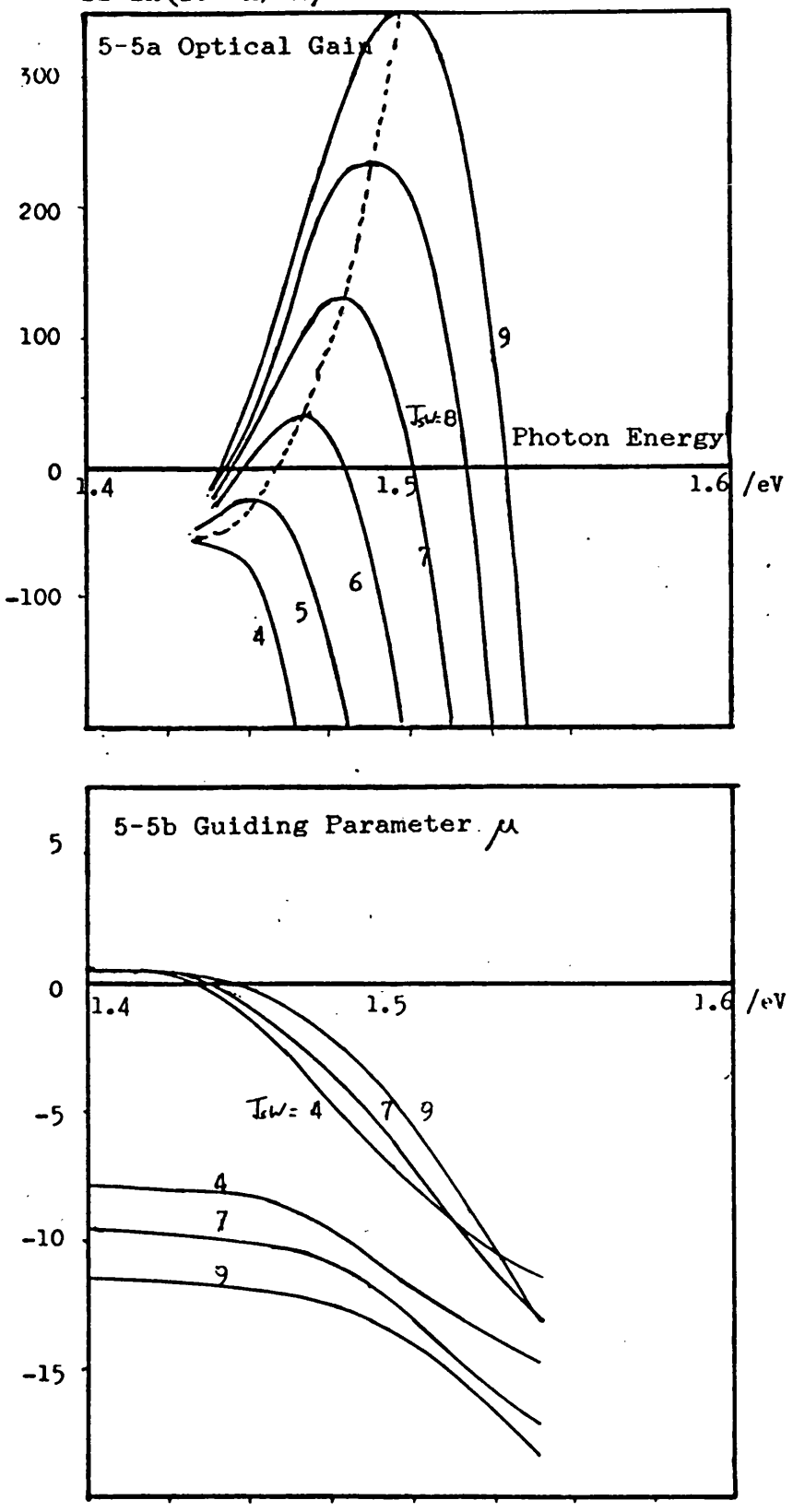

Fig. 5-6 Waveguide Optical Gain and Guiding Parameter vs. Photon Energy for a 10 m Width Stripe Contact, for different values of injection current density. The Photon energy is in eV, the gain in cm and the injection current is in $(10^3$ A/ m)

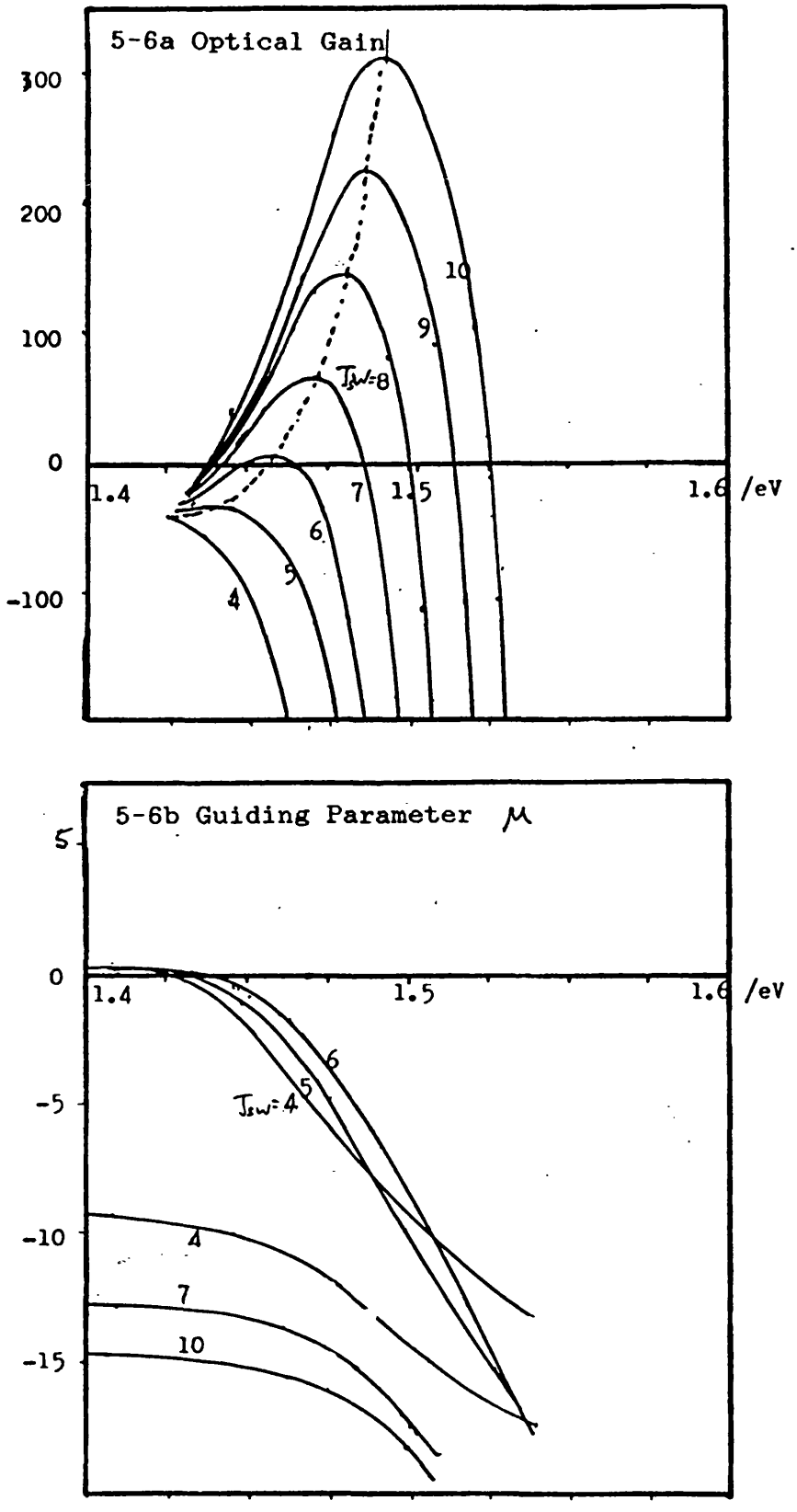

References for Chapter 5

1/ W.O.Schlosser, : Gain-induced modes in planar structues ", Bell Sys.Tech.J. 52 , (16), pp887-925, 1973.

2/ K.A.Shore, T.E.Rozzi, G.H.in't Veld, " Semiconductor laser analysis: general method for characterising devices of various cross-sectional geometries ", IEE.Proc., 127-1 , (5), pp221-229, 1980

3/ F.R.Nash, " mode guidance parallel to the junction plane of double-heterostructure GaAs lasers ", J.Appl.Phys., 44 , (10), pp4696-4707, 1973.

4/ W.Streifer, D.R.Scifres, R.D.Burnham, " Analysis of gain-induced waveguiding in stripe geometry diode lasers ", IEEE.J.Q.Electron., QE-14 , (6), pp418-427, 1978.

5/ W.Streifer, R.D.Burnham, D.R.Scifres, " Symmetrical and asymmetrical waveguiding in very narrow conducting stripe lasers ", IEEE.J.Q.Electron, QE-15 , (3), pp135-141, 1979.

6/ M.Abramowitz, I.A.Stegun, Handbook of mathematical functions, Dover International Inv., 9th printing. (22-6.20),(22-2.14).

7/ J.Buus, "A model for the static properties of DH lasers", IEEE J.Q.Electron, QE-15 , (8), pp734-739, 1979.

8/ M.Abramowitz, I.A.Stegun, Handbook of mathematical functions, Dover International Inv., 9th printing.

9/ G.Mendoza-Alvarez, F.D.Nunes, N.B.Patel, " Refractive index dependence on free carriers for GaAs ", 51 , (8), pp4365-4367, 1980.

CHAPTER 6

6-1 Spontaneous Emission in an Active Guide

In Chapter 3 spontaneous emission was considered as band to band transitions in a semiconductor. Only electric dipole transitions were considered because of the small size of the individual sources. In this chapter the dipole transitions are considered in an infinite medium and in a two dimensional waveguide structure, with only gain guiding in the x direction.

The edc method is used to calculate the electromagnetic fields in the guide. The formulation used here is the same as that used in preceding chapters, i.e. TE and TM to y. Although the dipole is considered as an infinitesimal source it is important to consider it as a vector source as well. It is assumed here that in any elementary volume there will be a random distribution of dipole directions and that these dipoles can be well represented by three orthogonal dipole sources of equal strengths.

The solution is to be found by using a Green's function to calculate the power coupled from a point source. The fact that this is a vector point source requires the Green's function to be a dyadic [1].

$$\bar{\mathbf{G}}(x,y,z;x_0,y_0,z_0)=\mathbf{G}_x\hat{\mathbf{x}}+\mathbf{G}_y\hat{\mathbf{y}}+\mathbf{G}_z\hat{\mathbf{z}} \qquad (6\text{-}1.1)$$

Where $\mathbf{G}_x=\hat{\mathbf{x}}G_{xx}+\hat{\mathbf{y}}G_{yx}+\hat{\mathbf{z}}G_{zx}$ etc. [2]. The dot product of a dyadic with a vector is another vector. There exists a special dyadic $\bar{\mathbf{I}}$ for which $\bar{\mathbf{I}}\mathbf{F}=\mathbf{F}\bar{\mathbf{I}}=\mathbf{F}$ for any arbitrary vectro $\mathbf{F}$, so that $\bar{\mathbf{I}}=\hat{\mathbf{x}}\hat{\mathbf{x}}+\hat{\mathbf{y}}\hat{\mathbf{y}}+\hat{\mathbf{z}}\hat{\mathbf{z}}$ and $\bar{\mathbf{I}}$ is the idemfactor.

In this chapter the dyadic Green's function for a dielectric waveguide is derived. This dyadic is a symmetric dyadic in that $\mathbf{F}\bar{\mathbf{G}}=\bar{\mathbf{G}}\mathbf{F}$ and $\bar{\mathbf{G}}(\mathbf{r};\mathbf{r}_0)=\bar{\mathbf{G}}(\mathbf{r}_0;\mathbf{r})$. This is used to calculate the increase in power per unit

length in the waveguide due to spontaneous emission. To do this the power emitted from a dipole in free space is calculated so that this can be compared to the calculations in Chapter 3.

Calculations of the effect of the variation of drive current and wavelength have been made. A number of graphs of results have been plotted for corresponding spontaneous and stimulated emission spectra. (Kane band tails [2], $\eta = 0.5kT, kT \approx 25$meV.) Some analytic expressions which explain these graphs have been obtained by using the approximate expressions for transitions between parabolic bands.

6-2 The Elementary Dipole in Infinite Media

This section outlines the calculation of the total radiated power from an infinitesimal dipole in infinite media.

For a dipole in an infinite homogeneous medium the fields can be described by only the electric vector potential, A_y, for a y oriented dipole with no loss of generality in the far field. [3] The electric and magnetic fields are then given by

$$\mathbf{E} = -\frac{\partial \mathbf{A}}{\partial t} = -j\omega \mathbf{A} \tag{6-2.1}$$

$$\mu \mathbf{H} = \nabla \times \mathbf{A} \tag{6-2.2a}$$

$$\nabla \times \nabla \times \mathbf{E} + n^2 k_0^2 \mathbf{E} = -\mathbf{J}(\mathbf{r})\, \delta(\mathbf{r} - \mathbf{r}_0) \tag{6-2.2b}$$

Where $\mathbf{J}$ is the source term $\mathbf{J} = I_0 l \hat{\mathbf{y}}$ and the magnetic vector potential $\mathbf{A}$ is given by

$$\mathbf{A} = \mu \int_v \mathbf{J}\, G\, dv \tag{6-2.3}$$

where G is the free space Green's function.

$$G = \frac{\exp(-jk(r - r'))}{4\pi(r - r')} \qquad r > r' \tag{6-2.4}$$

Since $\mathbf{J}$ is y directed and the dipole is in an infinite medium the magnetic vector potential has only a y component.

For an infinitesimal dipole

$$A_y = \frac{\mu I_0 l \exp(-jkr)}{4\pi r} \tag{6-2.5}$$

The magnetic potential in spherical co-ordinates is obtained by resolving A_y

into $\hat{r}$ and $\hat{\theta}$ components (see Fig 6-1)

$$A_r = A_y \cos(\theta) \tag{6-2.6a}$$

$$A_\theta = -A_y \sin(\theta) \tag{6-2.6b}$$

From the wave equation, in spherical co-ordinates it follows that

$$E_r = -j\omega A_r = \frac{-j\omega\mu I_0 l \exp(-jkr)\cos(\theta)}{4\pi r} \tag{6-2.7}$$

$$E_\theta = -j\omega A_\theta = \frac{j\omega\mu I_0 l \exp(-jkr)\sin(\theta)}{4\pi r} \tag{6-2.8}$$

$$H_\phi = \frac{1}{r}\left[\frac{\partial}{\partial r}(rA_\theta) - \frac{\partial A_r}{\partial \theta}\right] \tag{6-2.9}$$

$$= \frac{I_0 l \exp(-jkr)\sin(\theta)}{4\pi r}\left[jk + \frac{1}{r}\right]$$

The power flow from this dipole is given by the Poynting vector S. $\mathbf{S} = \mathbf{E}\times\mathbf{H}^*$ and the power flow is purely radial in the far field. The power flow across a spherical surface centred at the origin for $r \to \infty$ is then

$$P_0(h\nu) = \tfrac{1}{2}\int \mathrm{Re}(E_\theta H_\phi^*)\,\hat{r}.(ds) \tag{6-2.10a}$$

$$= \tfrac{1}{2}\int_0^{2\pi}\int_0^{\pi} \omega\mu k\left[\frac{I_0 l}{4\pi r}\right]^2 \sin^3(\theta) r^2\, d\theta\, d\phi \tag{6-2.10b}$$

$$P_0 = \frac{\omega\mu k I_0^2 l^2}{12\pi} \tag{6-2.10c}$$

This result will be useful in finding the relative power coupled into propagating modes by dipoles in a two dimensional waveguide.

Fig. 6-1 Dipole in Spherical Coordinates
The radiation from a dipole is most readily derived in spherical coordinates. The dipole is considered to be aligned along the vertical (y) , axis and a position in space is defined by the distace from the origin, (r) , and by two angles θ and ϕ .

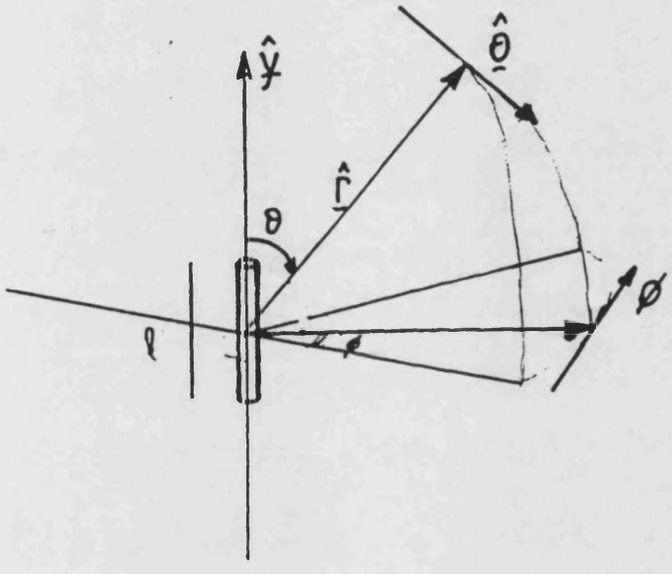

6-3 Vector Solution

This section derives a Green's function for a two dimensional waveguide cross-section. The Green's function must give te solution

$$\mathbf{E}(\mathbf{r}) = \iiint \bar{G}(\mathbf{r};\mathbf{r}_0) i\omega\mu \mathbf{J}(\mathbf{r}_0) dv_0 \tag{6-3.1}$$

Where $\mathbf{r}$ is used to denote a dependence on x, y and z and $\mathbf{r}_0$ denotes a dependency on x_0, y_0 and z_0. From Maxwell's equations the wave equation for the electric field including a source term for current density $\mathbf{J}$ is

$$\nabla \times \nabla \times \mathbf{E}(\mathbf{r}) - n^2 k_0^2 \mathbf{E}(\mathbf{r}) = -j\omega\mu \mathbf{J}(\mathbf{r}) \tag{6-3.2}$$

Substituting (6-3.1) into (6-3.2) and using the fact that

$$\mathbf{J}(\mathbf{r}) = \iiint \mathbf{J}(\mathbf{r}_0) \delta(\mathbf{r} - \mathbf{r}_0) dv_0 \tag{6-3.3}$$

leads to

$$\nabla \times \nabla \times \bar{G}(\mathbf{r};\mathbf{r}_0) - n^2 k_0^2 \bar{G}(\mathbf{r};\mathbf{r}_0) = -j\omega\mu \bar{I} \tag{6-3.4}$$

so that provided $\nabla \cdot \bar{G}(\mathbf{r};\mathbf{r}_0) = 0$ it follows that the wave equation for the dyadic is

$$\nabla^2 \bar{G}(\mathbf{r};\mathbf{r}_0) + n^2 k_0^2 \bar{G}(\mathbf{r};\mathbf{r}_0) = -\bar{I}\, \delta(\mathbf{r} - \mathbf{r}_0) \tag{6-3.5}$$

The form of the solution sought for $\mathbf{E}$ is that of LSE and LSM components so that $\bar{G}$ is also formed from LSE and LSM components. The dyadic must be of the form of a summation over x directed modes although only the fundamental y directed mode is considered.

$$\bar{G}(\mathbf{r};\mathbf{r}_0) = \sum_p \left| (\nabla \times \hat{\mathbf{y}} \psi_p(\mathbf{r})) \mathbf{B}_p(\mathbf{r}_0) \right| + \sum_p \left| (\nabla \times \nabla \times \hat{\mathbf{y}} \chi_p(\mathbf{r})) \mathbf{A}_p(\mathbf{r}_0) \right| \tag{6-3.6}$$

The two functions of x_0 must now be found. Substitution of this into (6-3.5), after noting that

$$(\nabla^2+n^2k_0^2)(\nabla\times\hat{\mathbf{y}}\psi)=\left[\frac{\partial^2}{\partial z^2}+\beta_e^2\right]\nabla\times\hat{\mathbf{y}}\psi$$

gives

$$\sum_p\left[\left[\frac{\partial^2}{\partial z^2}+\beta_{ep}^2\right]\nabla\times\hat{\mathbf{y}}\psi_p(x,y)e^{-j\beta_{ep}(z-z_0)}\mathrm{B}_p(x_0,y_0)\right] \qquad (6\text{-}3.7)$$

$$+\sum_p\left[\left[\frac{\partial^2}{\partial z^2}+\beta_{mp}^2\right]\nabla\nabla\times\hat{\mathbf{y}}\chi_p(x,y)e^{-j\beta_{mp}(z-z_0)}\mathrm{A}_p(x_0,y_0)\right]$$

$$=-\delta(x-x_0)\,\delta(y-y_0)\,\delta(z-z_0)\,\bar{\mathrm{I}} \qquad z>z_0$$

The restriction to $z>z_0$ applies so that the wave propagates away from the source. The expansions of the functions of x and y are

$$\nabla\times\hat{\mathbf{y}}\psi_p(x,y)e^{-j\beta_{ep}(z-z_0)} \qquad (6\text{-}3.8a)$$

$$=\left[\frac{\partial\psi_p(x,y)}{\partial x}\hat{\mathbf{z}}+j\beta_{ep}\psi_p(x,y)\hat{\mathbf{x}}\right]e^{-j\beta_{ep}(z-z_0)}$$

$$\nabla\nabla\times\hat{\mathbf{y}}\chi_p(x,y)e^{-j\beta_{mp}(z-z_0)} \qquad (6\text{-}3.8b)$$

$$=\left[\frac{\partial^2\chi(x,y)}{\partial x\partial y}\hat{\mathbf{x}}-n_f^2k_0^2\chi(x,y)\hat{\mathbf{y}}-j\beta_{mp}\frac{\partial\chi(x,y)}{\partial y}\hat{\mathbf{z}}\right]e^{-j\beta_{mp}(z-z_0)}$$

Dotting (6-3.7) on the left by $\nabla\times\hat{\mathbf{y}}\psi_n(x,y)e^{j\beta_{en}(z-z_0)}$ and integrating over x and y and omitting subscripts for simplicity gives

$$e^{j\beta(z-z_0)}\left[\frac{\partial^2}{\partial z^2}+\beta^2\right]e^{-j\beta(z-z_0)}\mathrm{B}\left[\iint\left[\frac{\partial\psi}{\partial x}\right]^2dxdy+\beta^2\iint\psi^2dxdy\right] \qquad (6\text{-}3.9)$$

$$= -\delta(z-z_0)\left[\nabla\times\hat{y}\psi(x_0,y_0)e^{j\beta(z-z_0)}\right]$$

Terms involving ψ and χ are omitted since, by restricting attention to the fundamental y directed mode it is possible to show that

$$\int_{-\infty}^{\infty}\frac{\partial\chi}{\partial y}\psi\,dy=0 \qquad (6\text{-}3.10)$$

because χ and ψ are both even functions.

The other terms in (6-3.9) are simplified if ψ is normalised and separable in x and y. Then $\int\psi^2dx=\int\psi^2dy=1$ and

$$\int_{-\infty}^{\infty}\left|\frac{\partial\psi}{\partial x}\right|^2dx=\left|\psi\frac{\partial\psi}{\partial x}\right|_{-\infty}^{\infty}-\int_{-\infty}^{\infty}\psi\frac{\partial^2\psi}{\partial x^2}dx=\sigma_x^2 \qquad (6\text{-}3.11a)$$

$$\sigma_x^2=n_1^2k_0^2-\sigma_{ya}^2-\beta^2 \qquad (6\text{-}3.11b)$$

It then follows that

$$e^{j\beta(z-z_0)}\left[\frac{\partial^2}{\partial z^2}+\beta^2\right]e^{-j\beta(z-z_0)}\mathrm{B}n_{ea}^2k_0^2 \qquad (6\text{-}3.12)$$

$$= -\delta(z-z_0)\left[\nabla\times\hat{y}\psi(x_0,y_0)e^{j\beta(z-z_0)}\right]$$

Now integrating over z between z_0-0 and z_0+0, remembering that z and z_0 are interchanged for $z<z_0$ gives

$$\int_{z_0-0}^{z_0+0}\left[e^{j\beta(z-z_0)}\frac{\partial^2}{\partial z^2}e^{-j\beta(z-z_0)}\right]dz\;\mathrm{B}\,n_{ea}^2k_0^2=-\left[\frac{\partial\psi(x_0,y_0)}{\partial x_0}\hat{z}-j\beta\psi(x_0,y_0)\hat{x}\right]$$

$$= -2j\beta\mathrm{B}\,n_{ea}^2k_0^2 \qquad (6\text{-}3.13)$$

The expression for B can now be written as

$$\mathbf{B}=\frac{1}{2j\beta n_{ea}^2 k_0^2}\left[\frac{\partial\psi(x_0,y_0)}{\partial x_0}\hat{\mathbf{z}}-j\beta\psi(x_0,y_0)\hat{\mathbf{x}}\right] \qquad (6\text{-}3.14)$$

The form of **A** can be similarly considered. Dotting (6-3.7) on the left by $\nabla\times\nabla\times\hat{\mathbf{y}}\chi e^{j\beta(z-z_0)}$ and integrating over x and y gives

$$e^{j\beta(z-z_0)}\left[\frac{\partial^2}{\partial z^2}+\beta^2\right]e^{-j\beta(z-z_0)}\mathbf{A}\left[\int\frac{\partial\chi}{\partial x^2}dx\int\frac{\partial\chi}{\partial y^2}dy+(n_f^2k_0^2)^2+\beta^2\int\left[\frac{\partial\chi}{\partial y}\right]^2dy\right]$$

$$=-\delta(z-z_0)\left[\nabla\times\nabla\times\hat{\mathbf{y}}\chi(x_0,y_0)e^{j\beta(z-z_0)}\right] \qquad (6\text{-}3.15)$$

So that

$$e^{j\beta(z-z_0)}\left[\frac{\partial^2}{\partial z^2}+\beta^2\right]e^{-j\beta(z-z_0)}\mathbf{A}[n_f^4k_0^4+n_{fa}^2k_0^2\sigma_{ya}^2] \qquad (6\text{-}3.16)$$

$$=-\delta(z-z_0)\left[\nabla\times\nabla\times\hat{\mathbf{y}}\chi(x_0,y_0)e^{j\beta(z-z_0)}\right]$$

Since $\sigma_y^2(\sigma y^2-\sigma_{ya}^2)<<n_f^4k_0^4$ it follows that

$$[n_f^4k_0^4+n_{fa}^2k_0^2\sigma_{ya}^2]\approx n_f^2k_0^2n_a^2k_0^2 \qquad (6\text{-}3.17)$$

and so integrating (6-3.16) between z_0-0 and z_0+0 gives

$$\mathbf{A}=\frac{1}{2j\beta n_f^2n_a^2k_0^4}\left[\frac{\partial^2\chi(x_0,y_0)}{\partial x_0\partial y_0}\hat{\mathbf{x}}-n_f^2k_0^2\chi(x_0,y_0)\hat{\mathbf{y}}+j\beta\frac{\partial\chi(x_0,y_0)}{\partial y_0}\right] \qquad (6\text{-}3.18)$$

The Green's function can now be written as

$$\bar{\mathbf{G}}(x,y,z;x_0,y_0,z_0)= \qquad z>z_0 \qquad (6\text{-}3.19)$$

$$\sum_p\frac{e^{-j\beta_{ep}(z-z_0)}}{2j\beta_{ep}n_{ea}^2k_0^2}\left[\frac{\partial\psi_p(x,y)}{\partial x}\hat{\mathbf{z}}+j\beta_{ep}\psi_p(x,y)\hat{\mathbf{x}}\right]\left[\frac{\partial\psi_p(x_0,y_0)}{\partial x_0}\hat{\mathbf{z}}-j\beta_{ep}\psi_p(x_0,y_0)\hat{\mathbf{x}}\right]+$$

$$+\sum_p \frac{e^{-j\beta_{mp}(z-z_0)}}{2j\beta_{mp} n_f^2 n_a^2 k_0^4}\left[\frac{\partial^2\chi_p(x,y)}{\partial x\partial y}\hat{x}-n_f^2k_0^2\chi_p(x,y)\hat{y}-j\beta_{mp}\frac{\partial\chi_p(x,y)}{\partial y}\right]\times$$

$$\times\left[\frac{\partial^2\chi_p(x_0,y_0)}{\partial x_0\partial y_0}\hat{x}-n_f^2k_0^2\chi(x_0,y_0)\hat{y}+j\beta_{mp}\frac{\partial\chi_p(x_0,y_0)}{\partial y_0}\right]$$

6-4 Dipole Power Coupled to Active Waveguide Modes

The power coupled from $\hat{x}, \hat{y}$ and $\hat{z}$ oriented dipoles in an active slab can now be calculated. The electric field is given by (6-3.1), the source function and the Green's function (6-3.19). The magnetic field follows from Maxwell's equations. The small fields involving $\frac{\partial \chi}{\partial x}$ and $\frac{\partial \psi}{\partial x}$ are not included in the following analysis. In this case the LSM and LSE fields reduce to TM and TE to z. However, since this section is interested in the z directed power flow, and these additional fields do not contribute any extra terms to z directed power flow.

In order to measure the spontaneous emission at the output of a real device it would be necessary to calculate the x directed power flow in order to calculate the far field pattern. The calculation of the x directed power flow follows directly from the Green's function in the same fashion as the z directed power flow but expressions are not given here.

For a $\hat{y}$-oriented elementary dipole with source function

$$\mathbf{J} = I_0 l \delta(x-x_0)\delta(y-y_0)\delta(z-z_0)\hat{y} \tag{6-4.1}$$

the electric field is given by

$$\mathbf{E} = \frac{-j\omega\mu I_0 l e^{-j\beta(z-z_0)}}{2\beta n_a^2 k_0^2} \chi_n(x_0, y_0) \left| -n_f^2 k_0^2 \chi_n \hat{y} - j\beta \frac{\partial \chi_n}{\partial y} \hat{z} \right| \tag{6-4.2}$$

$$\mathbf{H} = \frac{I_0 l\, e^{-j\beta(z-z_0)}}{2 n_a^2 k_0^2} \chi_n(x_0, y_0)\, n^2 k_0^2\, \chi_n \hat{x} \tag{6-4.3}$$

Then the power crossing an infinite plane at $z = z_0$ is given by

$$P_z = \frac{\omega\mu (I_0 l)^2}{8|\epsilon_a|^2} \mathrm{Re}\left| \frac{\epsilon_f \epsilon_1^*}{\beta} \right| |\chi_n(x_0, y_0)|^2 C_{nx}^m C_y^m \tag{6-4.4}$$

Where C_{nx}^{m} is a TM astigmatism factor defined by

$$C_{nx}^{m} = \frac{\int |\chi_n(x)|^2 \, dx}{\int \chi_n(x)^2 \, dx} = \int |\chi_n(x)|^2 \, dx \qquad (6\text{-}4.5)$$

since $\chi_n(x)$ can be normalised so that the denominator is unity. A similar astigmatism factor, C^e, can be defined for TE modes, C_{mx} and C_{ex} are both greater than unity.

The modes of a lossless dielectric slab are not astigmatic. The phase fronts of such a structure are flat (See Fig. 6-2a). In a gain guided structure, however, the phase fronts are curved, (See Fig.6-2b), as they are leaky wave type modes. This is most easily demonstrated for the fundamental mode of such a structure when it has a $ch^{\mu}(x/w)$ type profile. The phase front in the x-z plane can be shown to be curved by considering the solution for the modal profile. The profile is

$$\psi(x,z) = \mathrm{ch}^{\mu}(x/w)\, e^{-j\beta z} = \mathrm{ch}^{\mu'}(x/w)\, \mathrm{ch}^{\mu''}(x/w)\, e^{-j\beta z} \qquad (6\text{-}4.6)$$

$$\psi(x,z) = \mathrm{ch}^{\mu'}(x/w) \exp(-j\beta z + j\mu'' \ln(\mathrm{ch}(x/w))\ ) \qquad (6\text{-}4.7)$$

For small x/w $\mathrm{ch}(x/w) \simeq 1$ and the field profile can be approximated simply as

$$\psi(x \simeq 0, z) = e^{-j\beta z} \qquad (6\text{-}4.8)$$

and the phase fronts near the guide centre are parallel to x. For large x $\mathrm{ch}(x/w) \rightarrow \exp(x/w)$ and the mode profile becomes

$$\psi(x >> w, z) = e^{\mu' x/w} \quad \exp(-j\beta z + j\mu'' x/w) \qquad (6\text{-}4.9)$$

So, for large x, the field amplitude decays exponentially (since μ' is negative) and the phase fronts become increasingly x directed. It should be noted that μ'' is also negative and so the direction of propagation is away from the guide centre. The mode cuts off when $\mu' = 0$ but μ'' is still negative so the phase fronts do not change dramatically when the mode cuts off.

The x directed modes are not power orthogonal. Power orthogonality would require $\iint \psi_1 \psi_2^* dxdy = 0$, but this is not so. (See (5-4.1)) This means that the total power can not be calculated by summing the power in each of the modes. The total power propagating in the guide can only be found using all the orthogonal fields. For instance for LSM modes

$$P_x = \frac{\omega\mu(I_0 l)^2}{8} \mathrm{Re}\left[\int_{-\infty}^{\infty}\int_{-\infty}^{\infty} \left[\sum_n \frac{\epsilon_f e^{-j\beta(z-z_0)}}{\beta_n \epsilon_a} \chi_n(x,y)\, \chi_n(x_0,y_0) \right] \times \right.$$

$$\left. \times \left[\sum_m \frac{\epsilon_1^* e^{j\beta(z-z_0)}}{\epsilon_a^*} \chi_m^*(x,y)\, \chi_m^*(x_0,y_0) \right] dxdy \right] \qquad (6\text{-}4.10)$$

For a guide that supports only a few x directed modes, (6-4.4) is a useful result since the first odd and even mode may be power orthogonal. This is certainly true in the case of Gegenbauer polynomials as described in (5-3.15).

The $\hat{z}$-dipole will excite not only LSM, (TM), modes as might be expected but LSE, (TE), modes as well. For the n^{th} TE mode

$$\mathbf{E} = \frac{\omega\mu I_0 l}{2\beta n_{ea}^2 k_0^2} \frac{\partial\psi(x_0,y_0)}{\partial x_0} \left[\frac{\partial\psi}{\partial x}\hat{z} + j\beta\psi\hat{x} \right] e^{-j\beta(z-z_0)} \qquad (6\text{-}4.11)$$

and

$$\mathbf{H} = \frac{-j(I_0 l)}{2\beta n_{ea}^2 k_0^2} \frac{\partial\psi(x_0,y_0)}{\partial x_0} \psi e^{-j\beta(z-z_0)}\hat{y} \qquad (6\text{-}4.12)$$

So that

$$P_z = \frac{\omega\mu(I_0 l)^2}{8|\epsilon_{ea}|^2 k_0^2} \mathrm{Re}\left\{\frac{\epsilon_e}{\beta}\right\} \left|\frac{\partial\psi(x_0,y_0)}{\partial x_0}\right|^2 C_{nx}^e C_y^e \qquad (6\text{-}4.13)$$

Again , some power is y directed but $P_y << P_z$ and can be ignored. The TM mode is excited and the z directed power coupled to a mode can be calculated as

$$P_z = \frac{\omega\mu(I_0 l)^2|\beta|^2}{8|\epsilon_a|^2|\epsilon_f|^2 k_0^4} \mathrm{Re}\left\{\frac{\epsilon_f \epsilon_1^*}{\beta}\right\} |\chi(x_0)|^2 C_{nx}^m C_y^m \qquad (6\text{-}4.14)$$

The power coupled to propagating modes from the $\hat{x}$-dipole can also be calculated in a similar fashion. For the TE mode

$$P_z = \frac{\omega\mu(I_0 l)^2|\beta|^2}{8|\epsilon_{ea}|^2 k_0^2} \mathrm{Re}\left\{\frac{\epsilon_e}{\beta}\right\} |\psi(x_0)|^2 C_{nx}^e C_y^e \qquad (6\text{-}4.15)$$

$$P_z = \frac{\omega\mu(I_0 l)^2}{8|\epsilon_a|^2|\epsilon_f|^2 k_0^4} \mathrm{Re}\left\{\frac{\epsilon_f \epsilon_1^*}{\beta}\right\} \left|\frac{\partial\chi(x_0,y_0)}{\partial x_0}\right|^2 |\psi(x_0)|^2 C_{nx}^m C_y^m \qquad (6\text{-}4.16)$$

If the dyadic Green's function (6-3.14) had been reduced to contain components TE and TM to z then the only TE component would be from the $\hat{x}$-dipole. Similarly there would only be two TM components.

All these equations include astigmatism factors for both x and y field profiles. The x directed astigmatism is given by (6-4.5) and for the fundamental Gegenbauer polynomial and the hyperbolic cosine carrier distribution this becomes [4,5]

$$C_x = \frac{\Gamma(-\mu')\Gamma(-\mu+\tfrac{1}{2})}{\Gamma(-\mu)\Gamma(-\mu'+\tfrac{1}{2})} \qquad (6\text{-}4.17)$$

Where Γ is the complex gamma function. This astigmatism factor is related to Peterman's factor, K, in that $K=C^2$. This does not disagree with Peterman's analysis, see Ref 6 equation (13), it is simply more convenient to express astigmatism in terms of C and not K.

The y directed astigmatism factor is given by

$$C_y = |a_0|^2 \left[\frac{\sin(\sigma' d)}{2\sigma'} + \frac{\sinh(\sigma'' d)}{2\sigma''} - \frac{\cos(2\sigma' d)}{2\rho'} - \frac{\cosh(2\sigma'' d)}{2\rho''} \right] \quad (6\text{-}4.18)$$

In an active medium σ_y is no longer real but is perturbed so little that $C_y^e \approx C_y^m \approx 1$. The x astigmatism factor is now expressed in product form as it was by Streifer [4] but using a quite different relationship [5] to expand the complex gamma function in (6-4.13).

$$C_0 = \frac{\left| \frac{(-\mu' + \frac{1}{2}) e^{q\mu''}}{\frac{1}{2} - \mu} \right| \prod_{n=1}^{\infty} \left| \frac{e^{-j\mu''/n}}{1 + \frac{-j\mu''}{\frac{1}{2} - \mu' + n}} \right|}{\left| \frac{\mu' e^{q\mu''}}{\mu} \right| \prod_{n=1}^{\infty} \left| \frac{e^{-j\mu''/n}}{1 + \frac{-j\mu''}{-\mu' + n}} \right|} \quad (6\text{-}4.19)$$

Now from its definition, (6-4.5), C_0 is a positive real number, so that $C_0 = (|C_0|^2)^{1/2} = (C_0 C_0^*)^{1/2}$ so taking the square root of the modulus sqared of (6-4.19) gives

$$C_0 = \frac{(-\mu' + \frac{1}{2})|\mu|}{-\mu' |-\mu + \frac{1}{2}|} \prod_{n=1}^{\infty} \left[1 + \frac{|\mu''|^2}{(n-\mu')|n + \frac{1}{2} - \mu|^2} \left[1 + \frac{1}{4(n-\mu')} \right] \right] \quad (6\text{-}4.20)$$

This will be useful relationship in later discussions and holds for all wavelengths if the correct value of μ is used. For astigmatic modes $|\mu''| > |\mu'|$ and both are negative for guided modes. For modes near cut off μ' tends to zero, and for such modes the astigmatism factor is dominated by the $-\mu'$ term in the denominator.

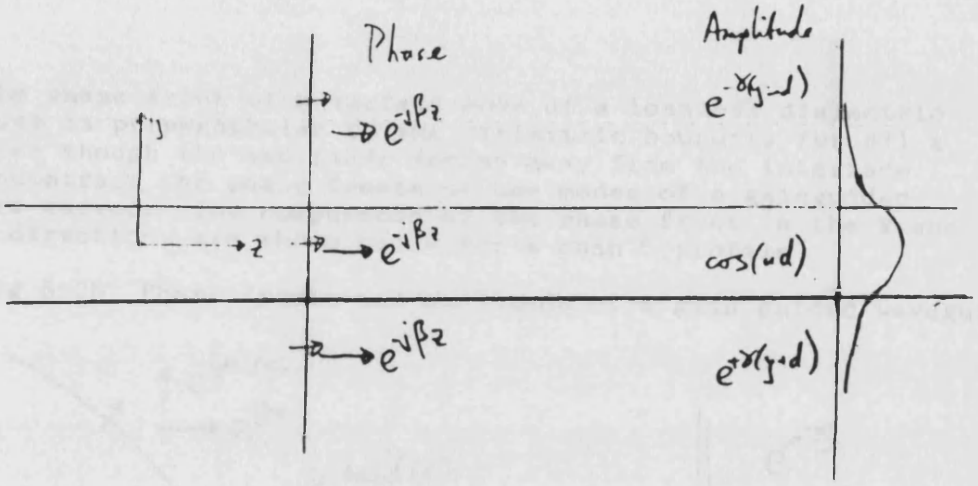

Fig.6-2a Phase fronts and amplitude of a lossless slab.

The phase front of a surface mode of a lossless dielectric slab is perpendicular to the dielectric boundary for all x even though the amplitude decays away from the interface. Incontrast the phase fronts of the modes of a gainguided are curved. The components of the phase front in the x and z directions are shown below for a $\cosh^{-2}$ profile.

The phase front of a surface mode of a lossless dielectric slab is perpendicular to the dielectric boundary for all x even though the amplitude decays away from the interface. Incontrast the phase fronts of the modes of a gainguided are curved. The components of the phase front in the x and z directions are shown below for a $\cosh^{-2}$ profile.

Fig.6-2b Phase fronts and amplitude of a gain guided waveguide.

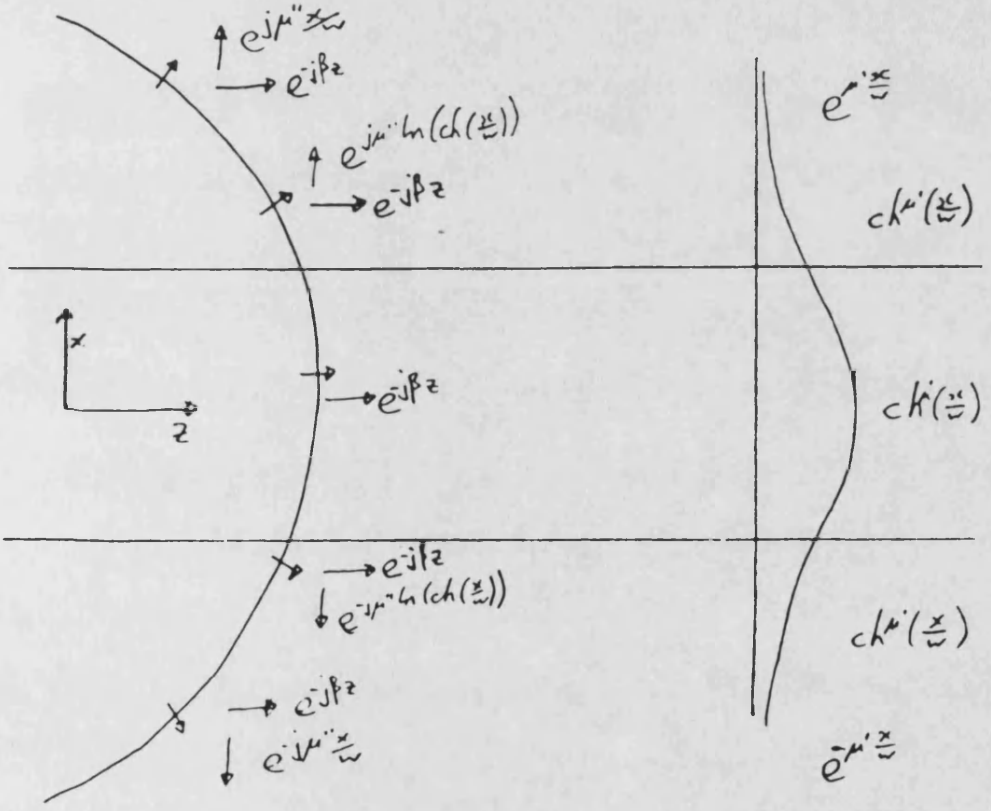

6-5 Lateral Distribution of Sources

The sources considered in the previous sections are distributed in x_0 and y_0 and so an integral over all possible values of these variables is needed. Sources only occur in the active region so that the integral over y is only between $y = \pm d$. The y directed field function is $a_0 \cos(\sigma y_0)$ so that

$$f_y = \int_{-d}^{d} |\chi(y_0)|^2 \, dy_0 = |a_0|^2 \left| \frac{\sin(2\sigma' d)}{2\sigma'} + \frac{\sinh(2\sigma'' d)}{2\sigma''} \right| \qquad (6\text{-}5.1)$$

For $\sigma_y'' \to 0$ this result is equivalent to the confinement factor for y directed modes. The integral of the derivative is

$$g_y = \int_{-d}^{d} \left| \frac{\partial \chi(y_0)}{\partial y_0} \right|^2 dy_0 = |\sigma_y|^2 |a_0|^2 \left| \frac{\sinh(2\sigma'' d)}{2\sigma''} - \frac{\sin(2\sigma' d)}{2\sigma'} \right| \qquad (6\text{-}5.2)$$

The integrals of interest for the x direction involve $(I_0 l)^2$ since it is a function of N, the inversion population. If $\frac{w_{spon}}{3}$ is equivalent to the power from a dipole in a refractive index n then

$$\frac{4\pi}{n k_0} w_{spon} \, d\nu = \omega \mu (I_0 l)^2 = q_{spon} \, d\nu = \frac{2\lambda_0}{n} w_{spon} \, d\nu \qquad (6\text{-}5.3)$$

The integral over x and y then gives the incremental power due to spontaneous emission coupled to a given mode with increasing z. Using the notation introduced in Chapter 1 this is δ where $\frac{dP}{dz} = gP + \delta$. For the y dipole the power couples to the TM mode and

$$TM_y: \qquad \delta = \frac{1}{8|\epsilon_a|^2} \mathrm{Re}\left(\frac{\epsilon_f \epsilon_1^*}{\beta} \right) C_{nx}^m C_y^m \int_{-\infty}^{\infty} |\chi(x_0)|^2 q_{spon} f_y \, dx_0 \qquad (6\text{-}5.4)$$

Where q_{spon} is a function of $N(x_0)$ and σ_y and hence f_y are also functions of

x_0. The $\hat{z}$-dipole excites both TE and TM modes, giving

$$TE_z: \qquad \delta = \frac{1}{8|\epsilon_{ea}|^2 k_0^2} \frac{|\epsilon_{ea}|^2}{|s_x^2|^2} C_{nx}^e C_y^e \int_{-\infty}^{\infty} \left| \frac{\partial \psi(x_0)}{\partial x_0} \right|^2 q_{spon} f_y \mathrm{Re}\left| \frac{\epsilon_e}{\beta} \right| dx_0 \quad (6\text{-}5.5)$$

$$TM_z: \qquad \delta = \frac{|\beta|^2}{8|\epsilon_f|^2 |\epsilon_a|^2 k_0^4} \mathrm{Re}\left| \frac{\epsilon_f \epsilon_1^*}{\beta} \right| C_{nx}^m C_y^m \int_{-\infty}^{\infty} |\chi(x_0)|^2 q_{spon} g_y \, dx_0 \quad (6\text{-}5.6)$$

Similarly for the $\hat{x}$-dipole both TE and TM are excited giving

$$TE_x: \qquad \delta = \frac{\beta|^2}{8|\epsilon_{ea}|^2 k_0^2} C_{nx}^e C_y^e \int_{-\infty}^{\infty} |\psi(x_0)|^2 q_{spon} f_y \mathrm{Re}\left| \frac{\epsilon_e}{\beta} \right| dx_0 \quad (6\text{-}5.7)$$

$$TM_x: \qquad \delta = \frac{1}{8|\epsilon_a|^2 |\epsilon_f|^2 k_0^4} \mathrm{Re}\left| \frac{\epsilon_f \epsilon_1^*}{\beta} \right| C_{nx}^m C_y^m \int_{-\infty}^{\infty} \left| \frac{\partial \chi(x_0)}{\partial x_0} \right|^2 q_{spon} g_y \, dx_0 \quad (6\text{-}5.8)$$

These integrals can be evaluated numerically or some approximations can be considered. The functions f_y and g_y depend only on the y directed propagation constants and to a first approximation σ_y is constant in x_0. The integrals of interest for TE are then,

$$I_1 = \int_{-\infty}^{\infty} |\psi(x_0)|^2 w_{spon}\left[N(x_0)\right] dx_0 \quad (6\text{-}5.9)$$

and

$$I_2 = \int_{-\infty}^{\infty} \left| \frac{\partial \psi(x_0)}{\partial x_0} \right|^2 w_{spon}(N(x_0)) \, dx_0 \quad (6\text{-}5.10)$$

and similar expressions involving $\chi(x_0)$ apply for TM modes. As a first approximation the formula (3-4.19) can be used to represent w_{spon}.

$$w_{spon} \;\alpha\; \frac{N_{\max}}{N_0} \cosh^{-2}\left(\frac{x_0}{w}\right) \left| 1 + \frac{N_{\max}}{2\sqrt{2} N_0} \cosh^{-2}\left(\frac{x_0}{w}\right) \right| \quad (6\text{-}5.11)$$

The integral (6-5.9) then becomes

$$I_1 \alpha |b_p|^2 \int_{-\infty}^{\infty} \cosh^{2\mu'}\left(\frac{x_0}{w}\right) \left| C_p^{(\mu)}\left(j\sinh\left(\frac{x_0}{w}\right)\right)\right|^2 \times$$

$$\times \frac{N_{max}}{N_0}\cosh^{-2}\left(\frac{x_0}{w}\right)\left|1+\frac{N_{max}}{2\sqrt{2}N_0}\cosh^{-2}\left(\frac{x_0}{w}\right)\right| dx_0 \qquad (6\text{-}5.13)$$

For the fundamental mode function, $\psi(x_0)$, since the zeroth order Gegenbauer polynomial, $C_0^{(\mu)}$, is unity, this becomes

$$\frac{N_{max}}{N_0}\int_{-\infty}^{\infty} |b_0|^2\cosh^{2(\mu'-1)}\left(\frac{x_0}{w}\right) dx_0 \times$$

$$\times \frac{N_{max}^2}{2\sqrt{2}N_0}\int_{-\infty}^{\infty} |b_0|^2\cosh^{2(\mu'-2)}\left(\frac{x_0}{w}\right) dx_0 \qquad (6\text{-}5.14)$$

This can be solved using the substitution $t = \cosh^{-2}(x_0/w)$ [7] so that the integral (6-5.9) is proportional to

$$C_0\frac{N_{max}}{N_0}\frac{(-\mu')}{(-\mu'+\frac{1}{2})}\left|1+\frac{N_{max}}{2\sqrt{2}N_0}\frac{(-\mu')}{(-\mu'+1\frac{1}{2})}\right| = F_0(N) \qquad (6\text{-}5.15)$$

In equations (6-5.5) and (6-5.8) it is the $\frac{\partial\psi(x_0)}{\partial x_0}$ which appears and not $\psi(x_0)$. Using the same approximations a similar integral to (6-5.1) can be formed from (6-5.10) which must also be solved. The integral for the fundamental mode function, ψ_0, gives

$$G_0(N) = C_0\frac{1}{(-2\mu'+1)}\frac{|\mu|^2}{w^2}\frac{N_{max}}{N_0}\frac{(-\mu')}{(-\mu'+1\frac{1}{2})}\times \qquad (6\text{-}5.1)$$

$$\times\left|1+\frac{N_{max}}{2\sqrt{2}N_0}\frac{(-\mu'+1)}{(-\mu'+2\frac{1}{2})}\right|$$

More complicated formulas for higher order modes could be found by the same method. However, the gain in such modes is always far less than that in the fundamental modes and so this has has not been done.

6-6 Results

Several graphs have been plotted to illustrate the behaviour of the dominant spontaneous emission terms. The graphs are arranged in sets of four for different waveguide thicknesses and stripe widths. The current spreading calculated in Chapter 2 is used to find the injection current density into the active layer. The effects of carrier diffusion are calculated by the numerical method described in Chapter 2. The carrier profile is then approximated by a $\cosh^{-2}$ profile by matching the carrier density at the stripe centre and stripe edge. The real part of the refractive index has been assumed to be linearly dependent on the carrier density [8] but the gain is obtained from the gain curves calculated in Chapter 4. These gain curves do not show a linear variation with inversion population and so at each wavelength, and for each injection current density, the slope of the gain curves is approximated using the values at the stripe centre and stripe edge. All the parameters in the expressions for δ in section 6-5 can then be calculated.

The first graph in each series of four shows the integral over the cross section of the spontaneous emission parameter q_{spon}. This is included to give a reference and to show that the wavelength dependence of the total spontaneous emission, calculated in this way, is simply a blurred copy of the calculated curves in Chapter 4. The blurring occurs because peak spontaneous emission is dependent on inversion population and hence position, in x.

The second graph shows the frequency dependence of the total TE coupled spontaneous emission. This is mainly power coupled from the x oriented dipole but about 2% is from the z oriented dipole. The TM coupled power is less than the TE and the ratio between TM and TE is dealt with separately. The z oriented dipole also couples about 0.02% of the TM power. The contribution of the x oriented dipole to the TE power is about 3×10^{-4} of

the y oriented dipole.

The third graph in each series shows C_0, the square root of the astigmatism factor. This parameter tends to infinity as the real part of μ goes to zero. This happens when the mode is cut off and can be qualitively explained as a very large number of power orthogonal modes being required to express the astigmatic gain-guided mode. As the field spreads out this number increases and so C_0, (and K), becomes infinite.

The fourth graph in each sequence shows the TE coupled power divided by the integral of the spontaneous emission over the cross section and divided by K ($=C_0^2$). This graph is proportional to the y confinement factor divided by Peterman's effective width. The position of the peak gain is also plotted on this graph to show the variation of this parameter for laser diodes.

The graphs show that for well guided modes far from cut off the spontaneous emission is proportional to K. However, for this case K tends to unity. For the peak gain the effective width is nearly constant provided the gain is positive. In other words, for laser diodes, the spontaneous emission seems to be proportional to K. Near cut off the effective width becomes large and so the analysis breaks down. This point is discussed further in the conclusion.

Two other graphs are also presented. These show the variation of the ratio of total TM coupled power to total TE coupled power for different waveguide widths and thicknesses and the individual contributions from each of the dipoles for one of the examples above.

Fig 6-3 The following four graphs illustrate the variation of parameters discussed in the text for a 5 μm stripe width and 0.3 μm active layer thickness. The parameters are shown for a range of photon energies and drive currents.

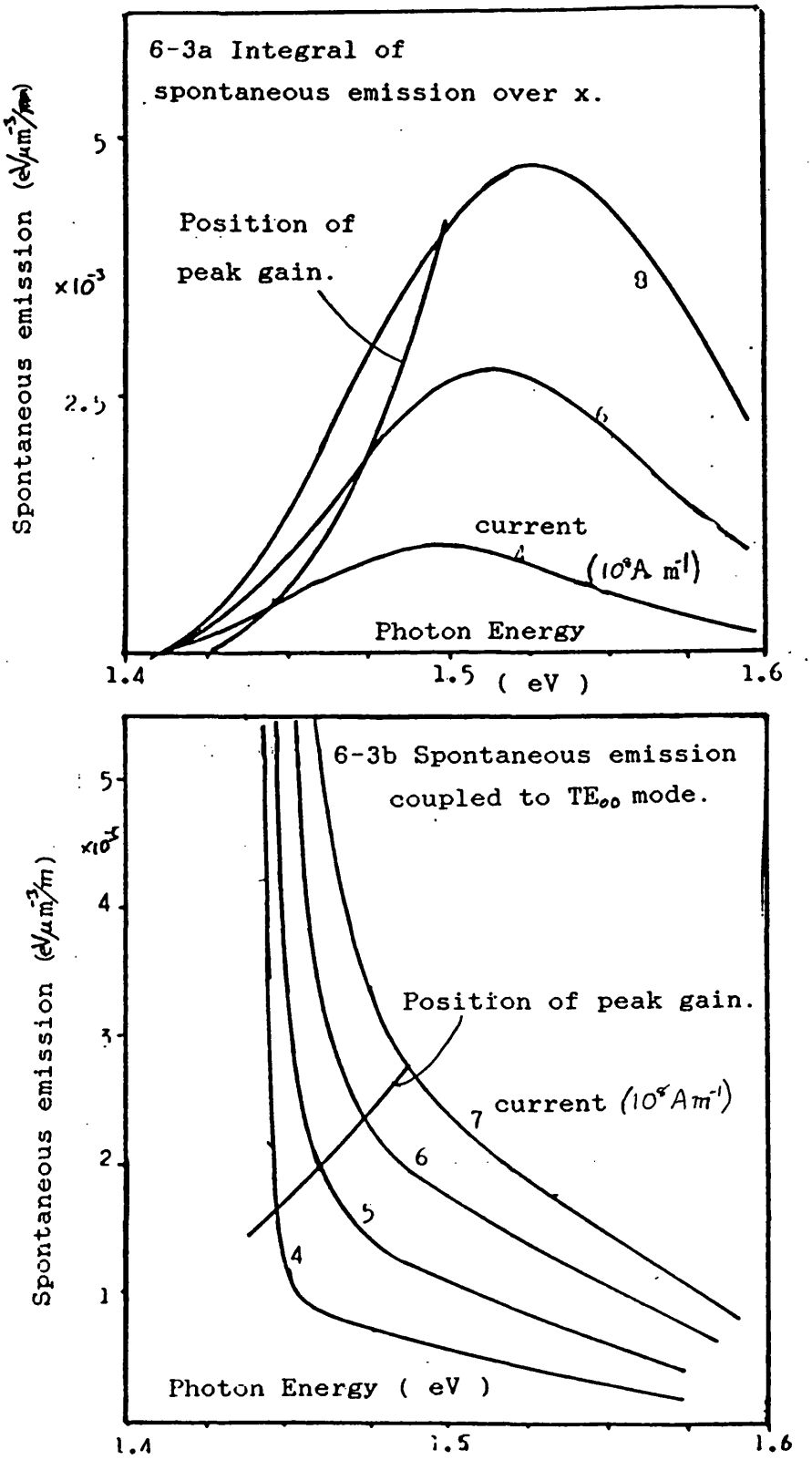

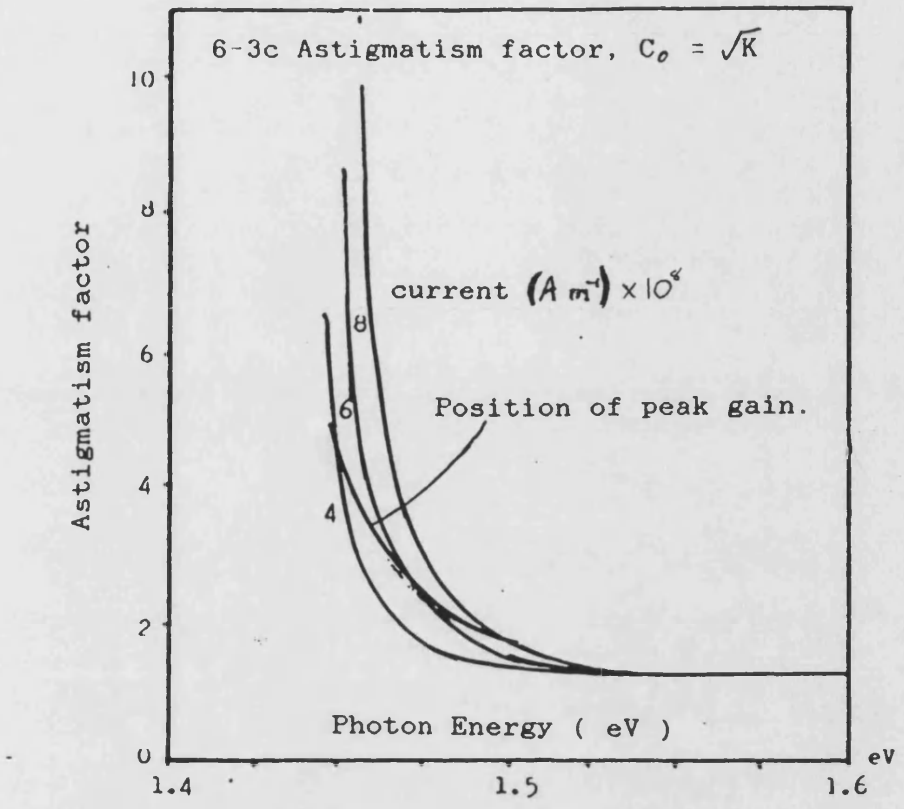

6-3d Spontaneous emission coupled to the TE mode divided by the integral of spontaneous emission over x and the astigmatism factor $K = C_o^2$.

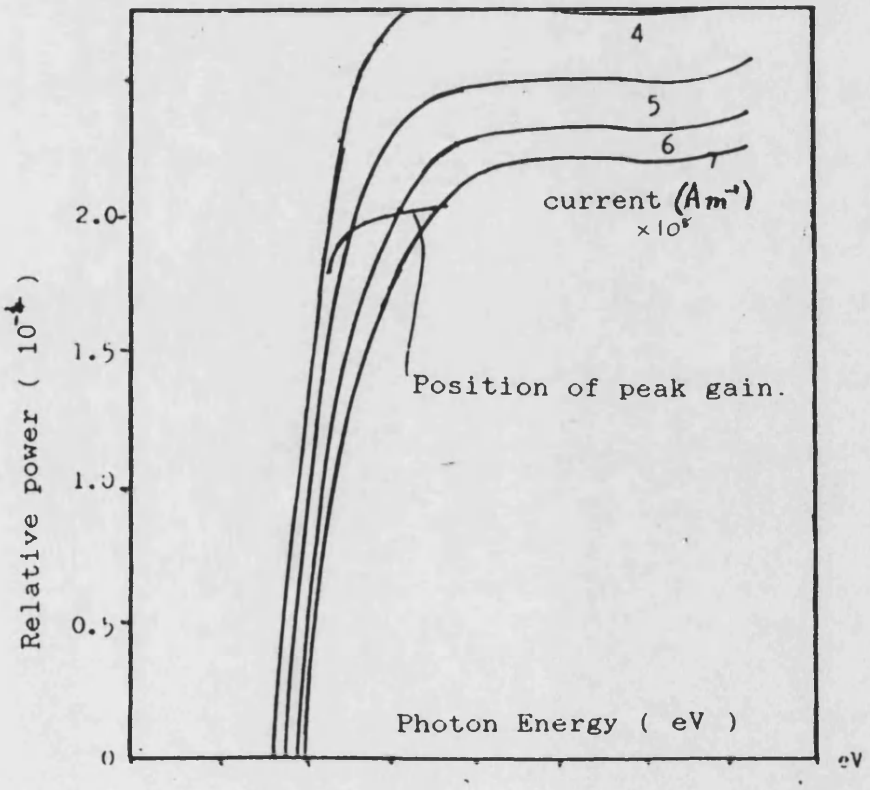

Fig 6-4 The following four graphs illustrate the variation of parameters discussed in the text for a 7 μm stripe width and 0.3 μm active layer thickness. The parameters are shown for a range of photon energies and drive currents.

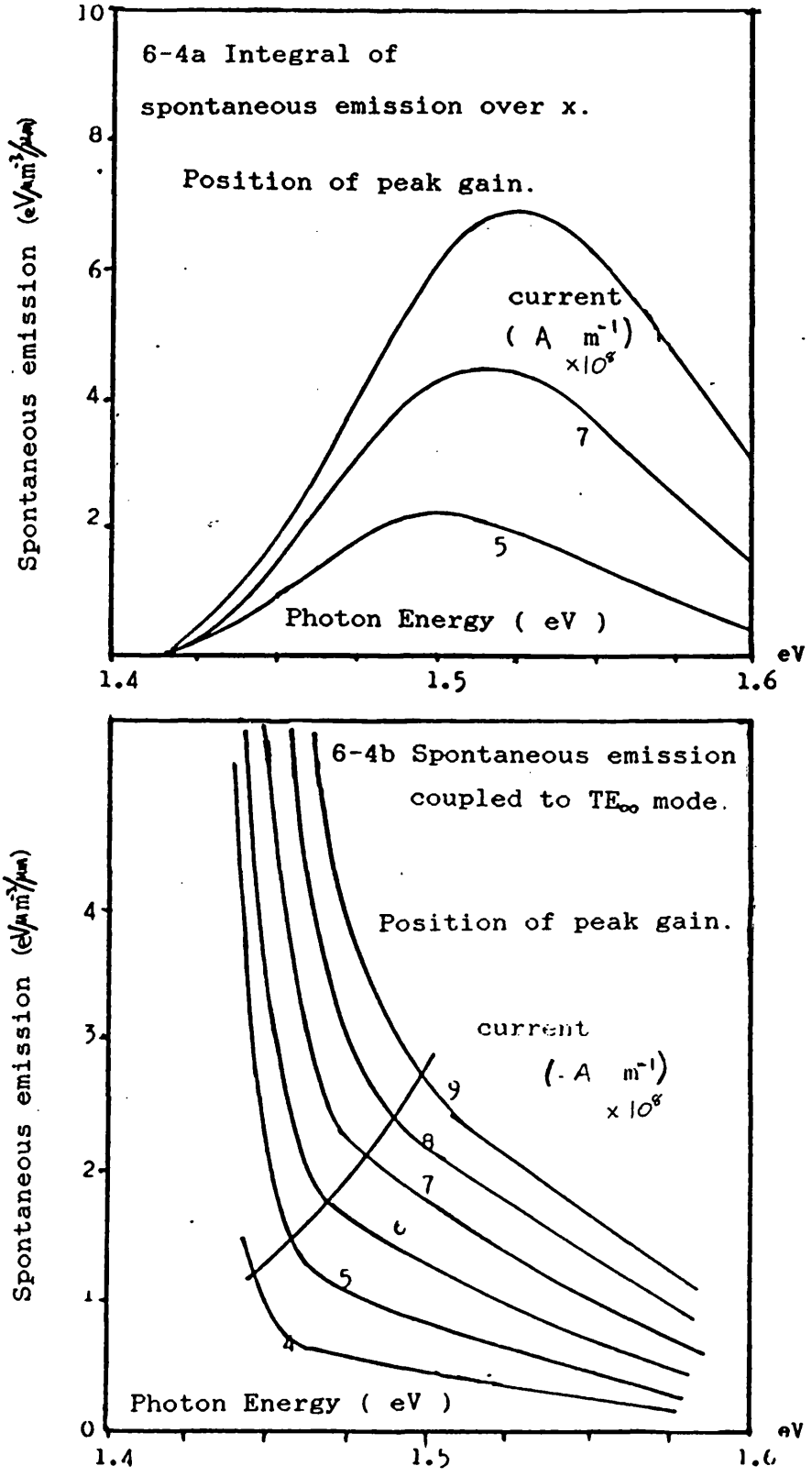

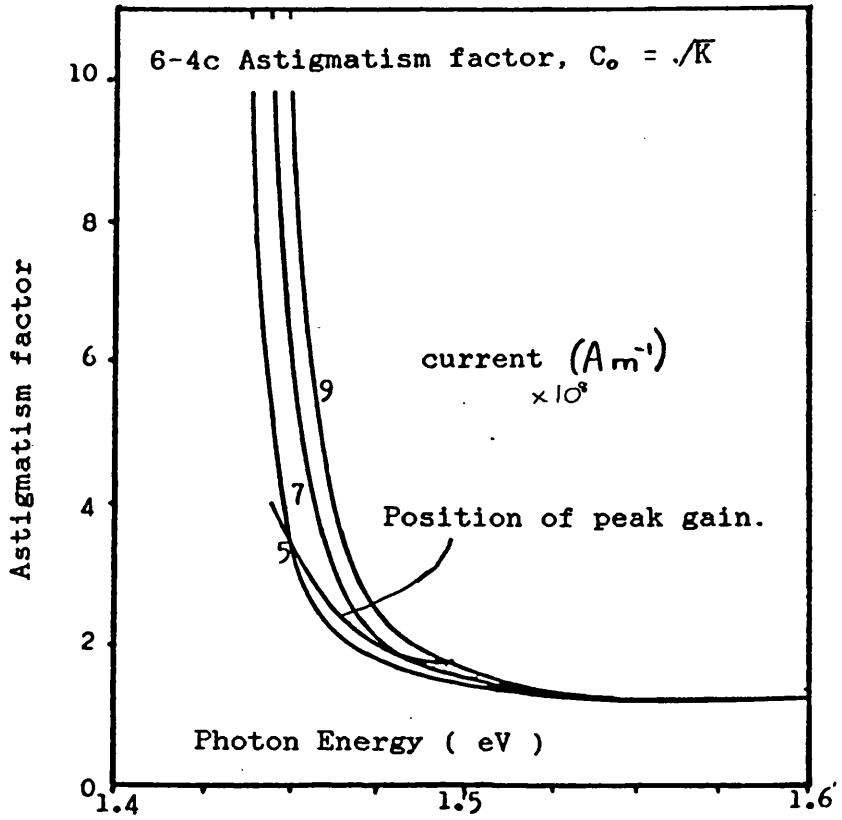

6-4d Spontaneous emission coupled to the TE mode divided by the integral of spontaneous emission over x and the astigmatism factor $K = C_o^2$.

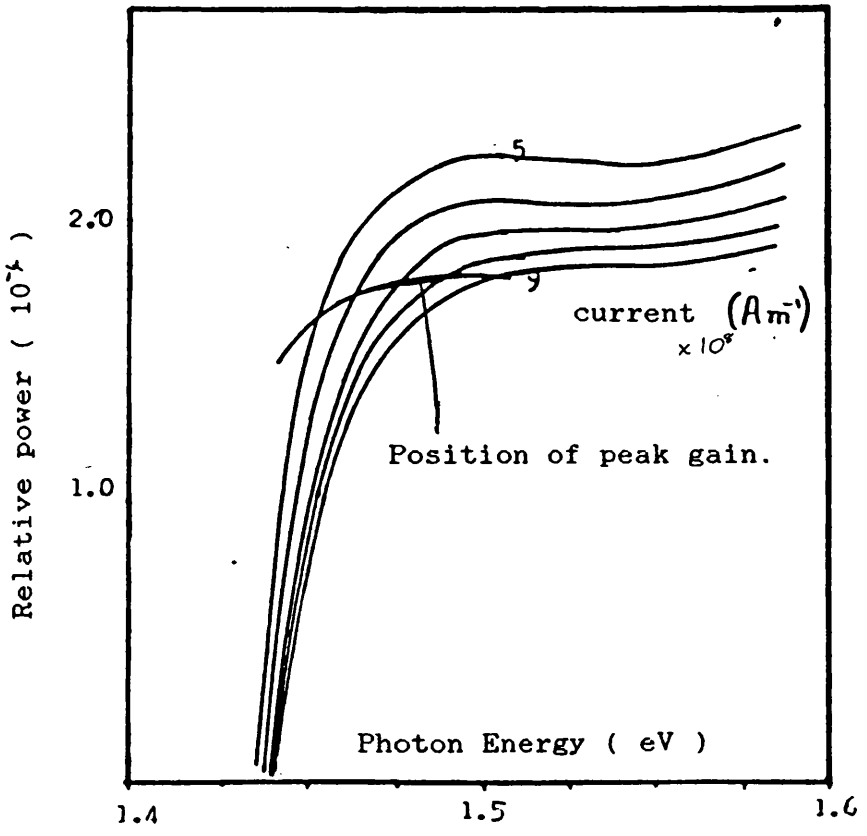

Fig 6-5 The following four graphs illustrate the variation of parameters discussed in the text for a 10 μm stripe width and 0.3 μm active layer thickness. The parameters are shown for a range of photon energies and drive currents.

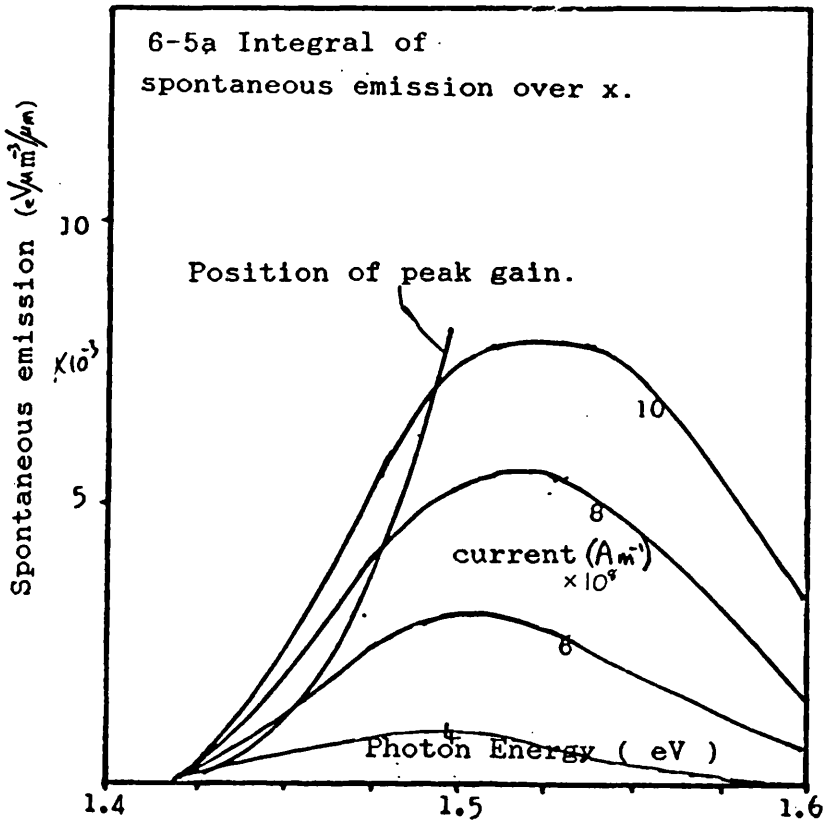

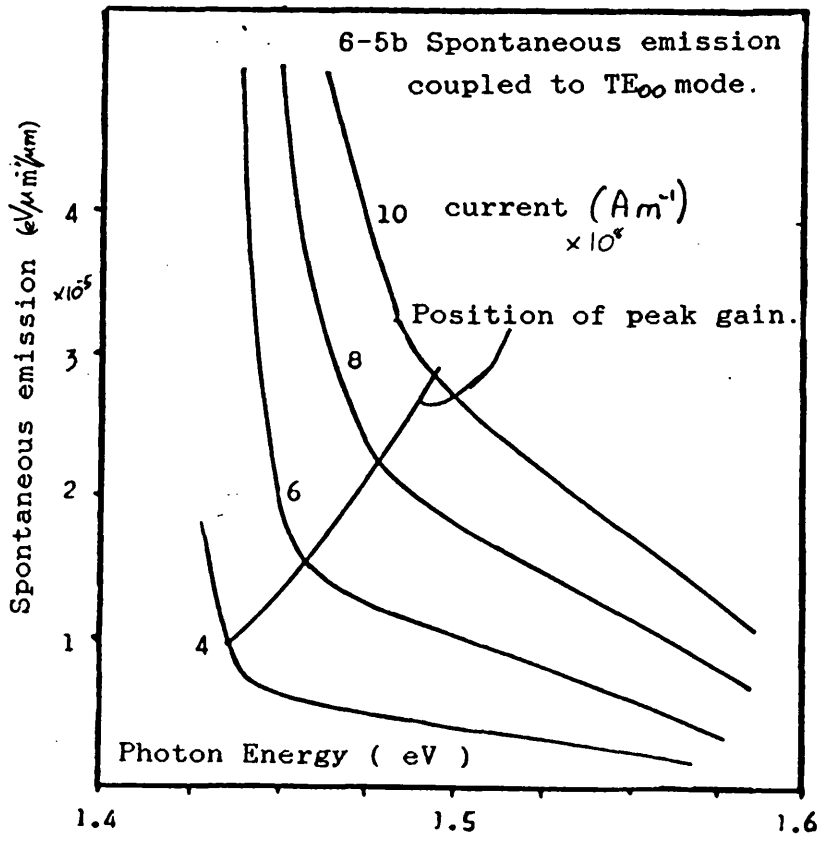

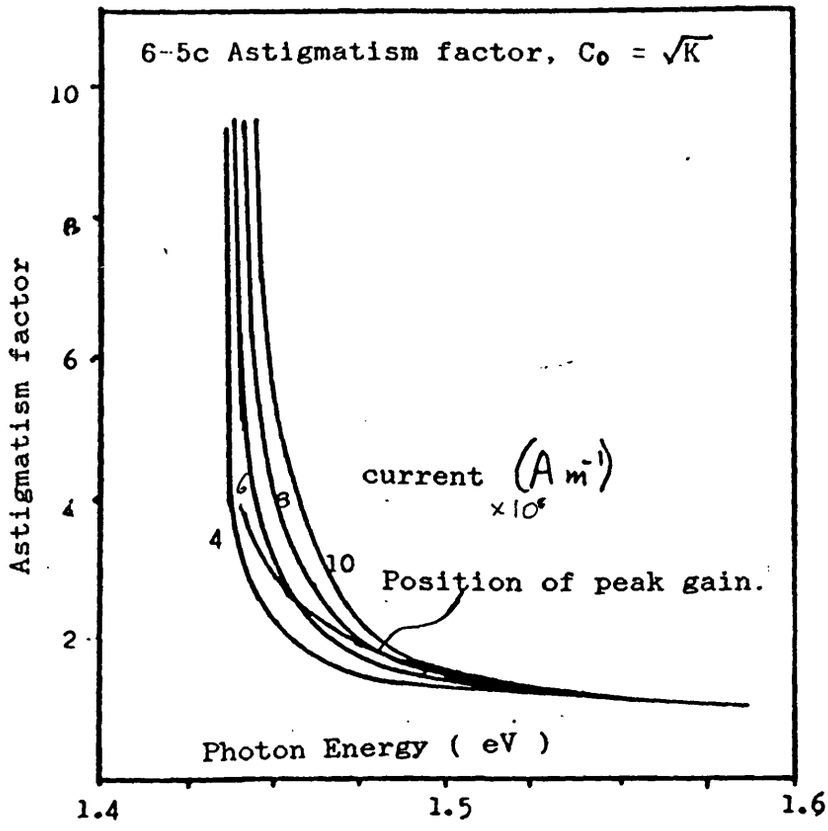

6-5d Spontaneous emission coupled to the TE_{∞} mode divided by the integral of spontaneous emission over x and the astigmatism factor $K = C_0^2$.

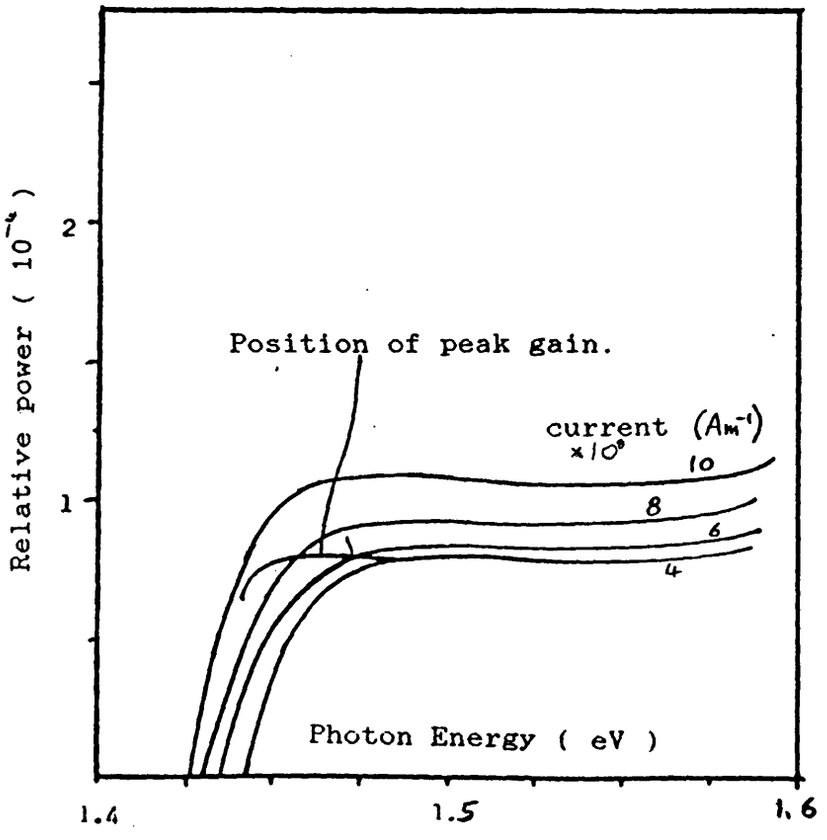

Fig 6-6 The following four graphs illustrate the variation of parameters discussed in the text for a 7μm stripe width and 0.25μm active layer thickness. The parameters are shown for a range of photon energies and drive currents.

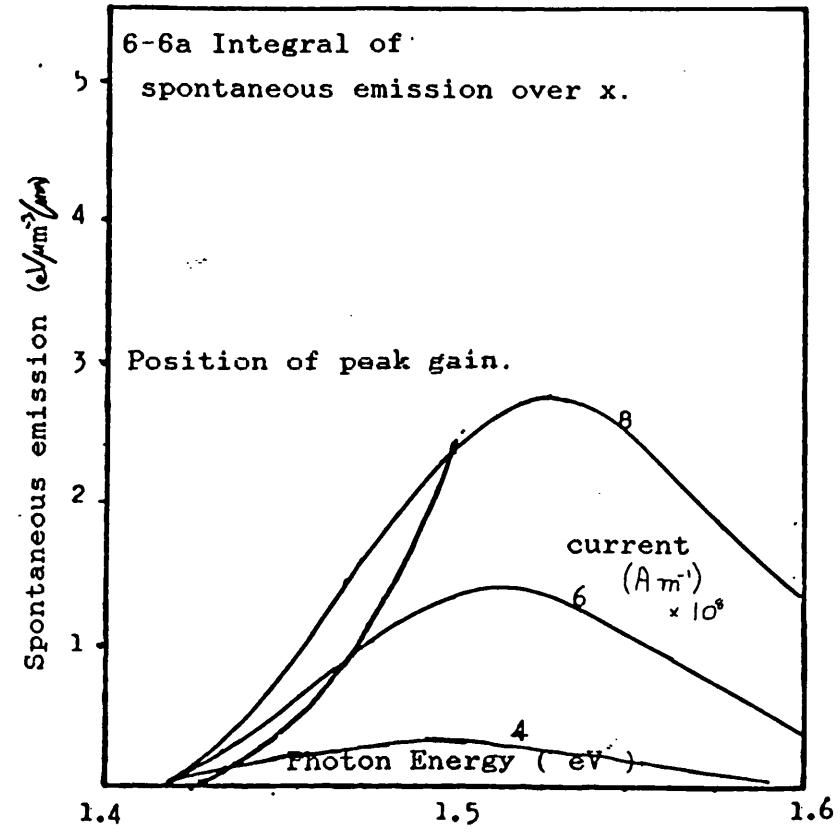

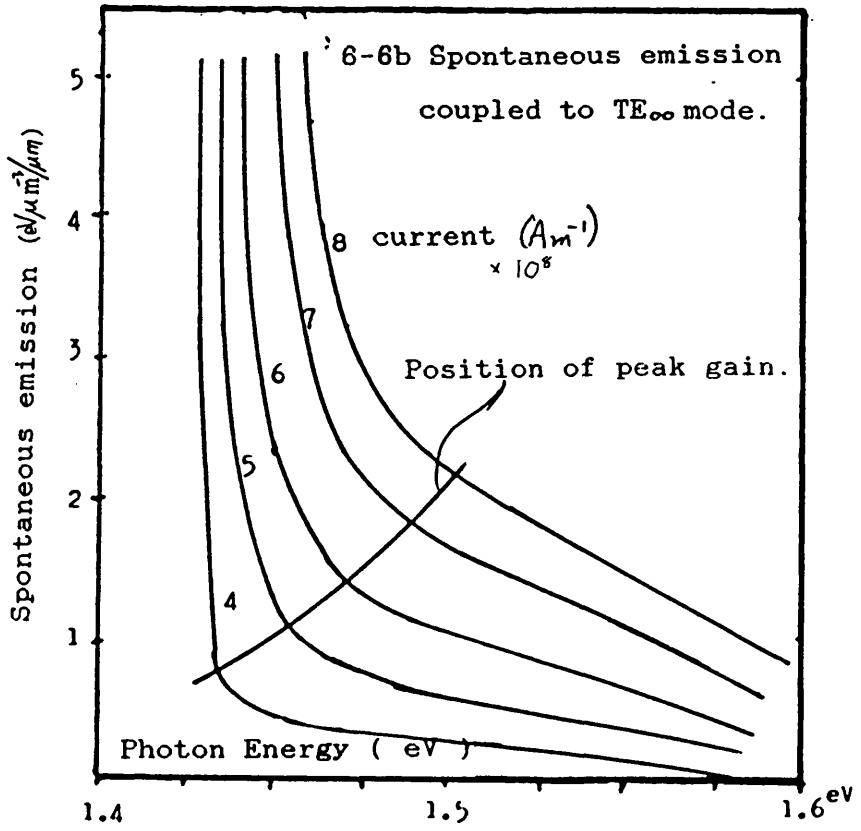

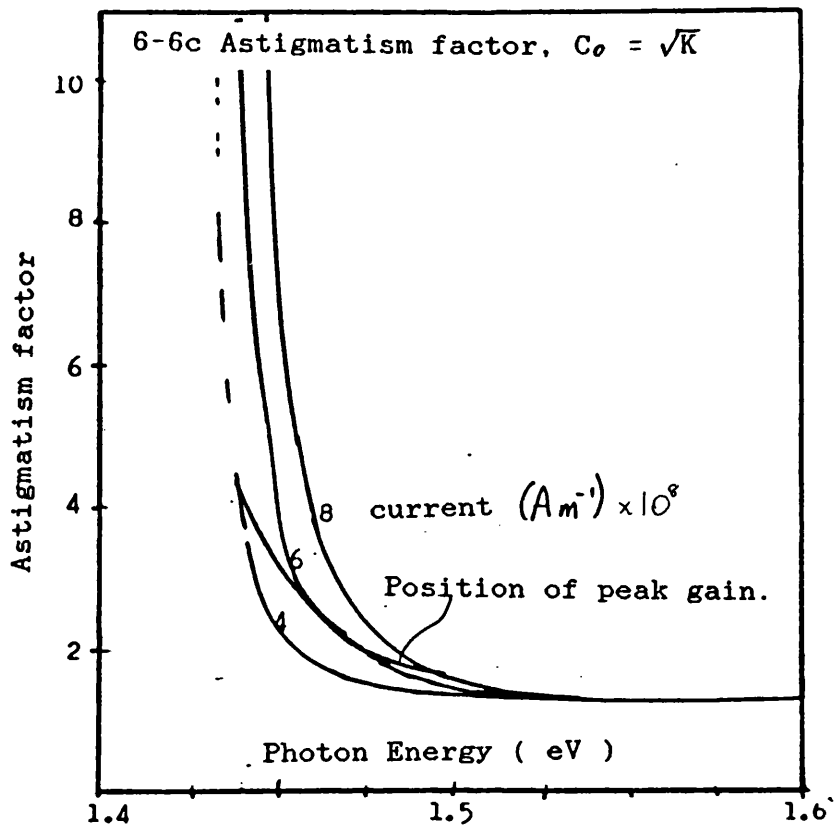

6-6d Spontaneous emission coupled to the TE_{oo} mode divided by the integral of spontaneous emission over x and the astigmatism factor $K = C_o^2$.

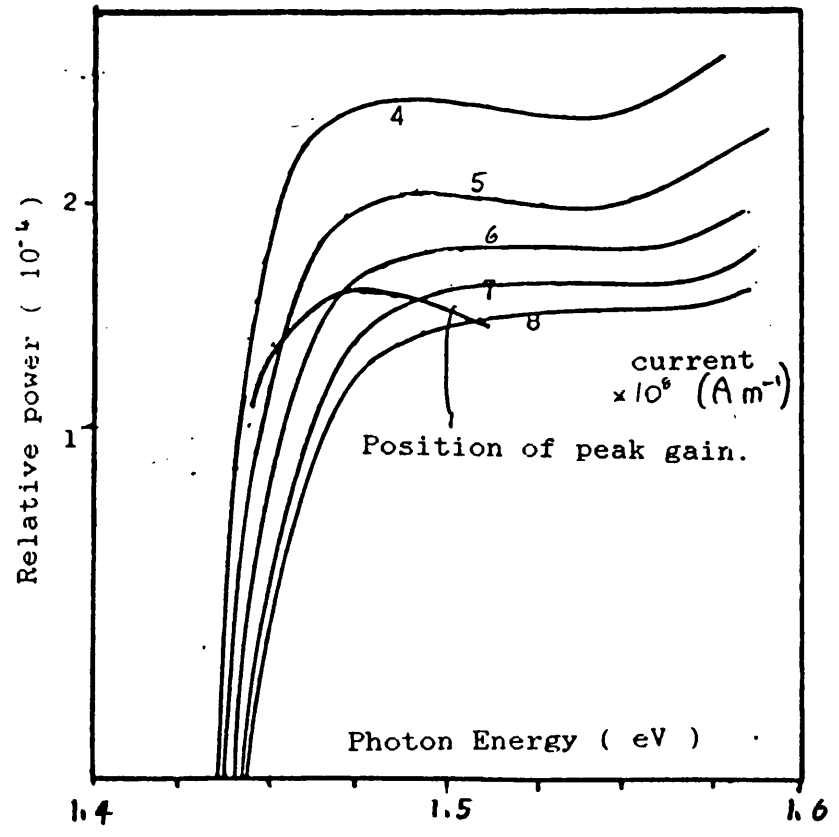

Fig 6-7 The following four graphs illustrate the variation of parameters discussed in the text for a 7 μm stripe width and 0.2 μm active layer thickness. The parameters are shown for a range of photon energies and drive currents.

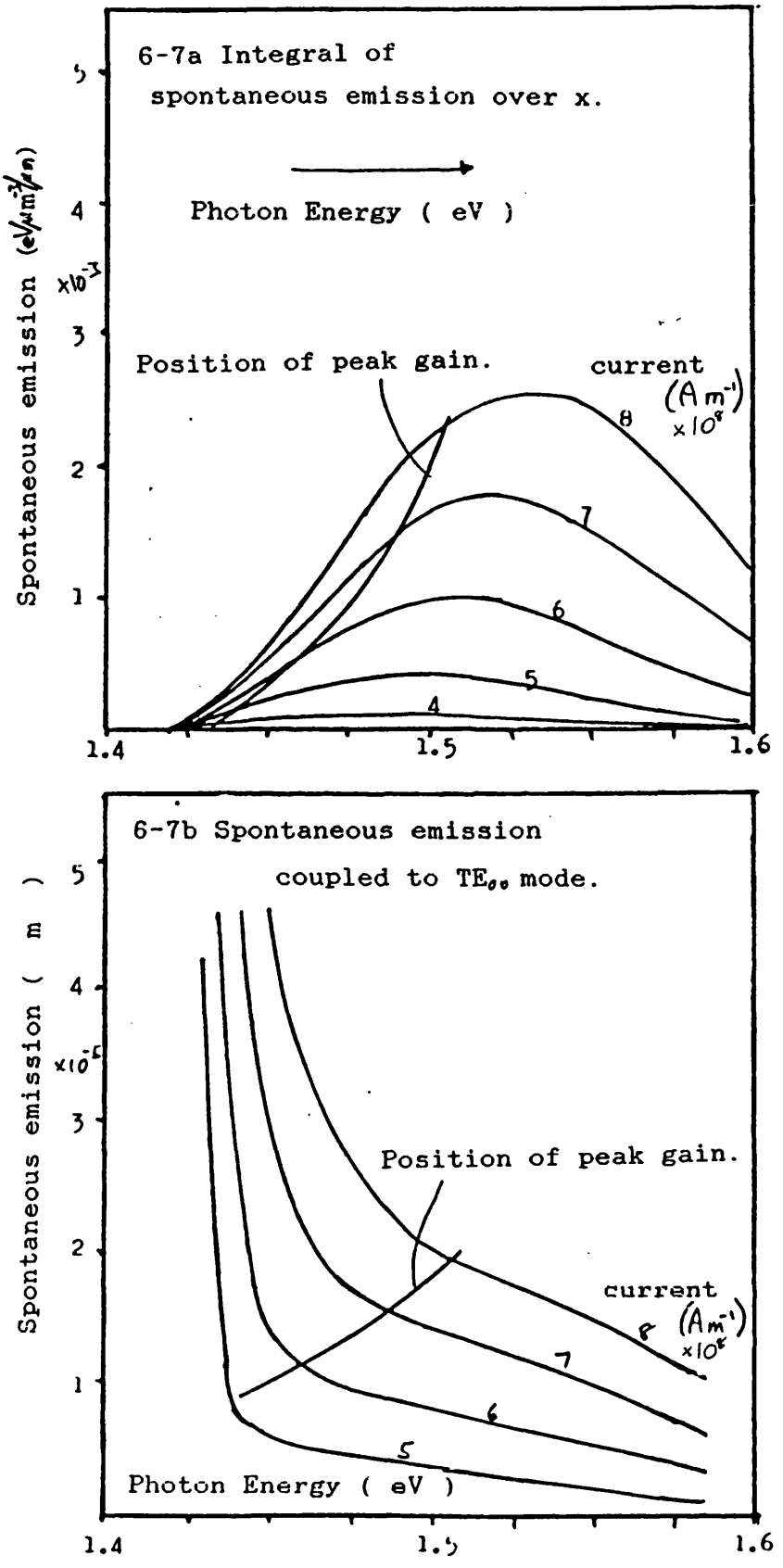

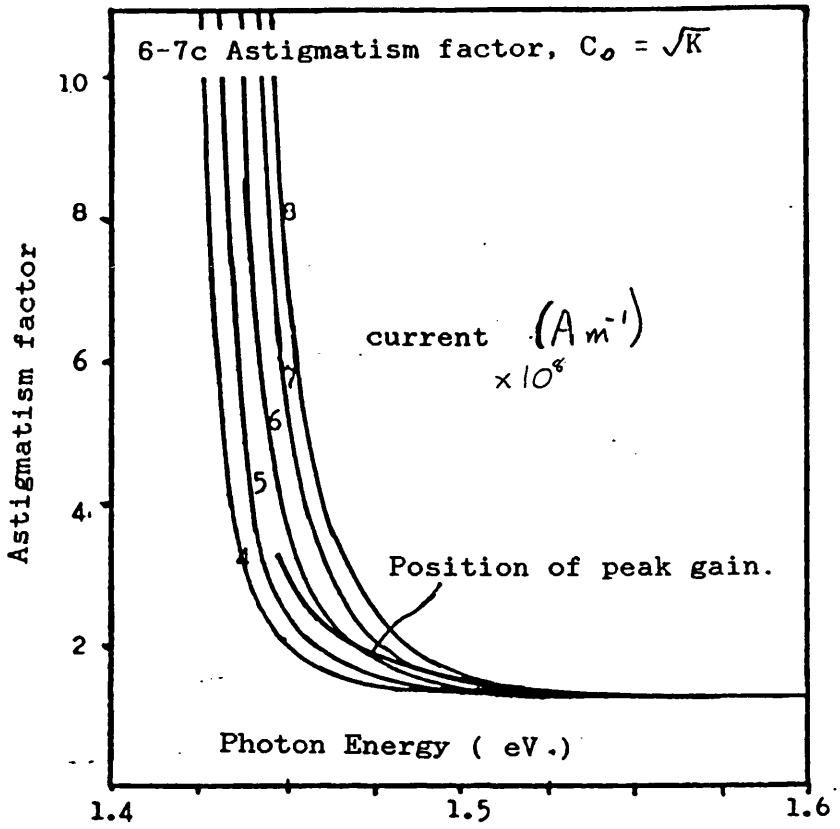

6-7d Spontaneous emission coupled to the TE_{oo} mode divided by the integral of spontaneous emission over x and the astigmatism factor $K = C_o^2$.

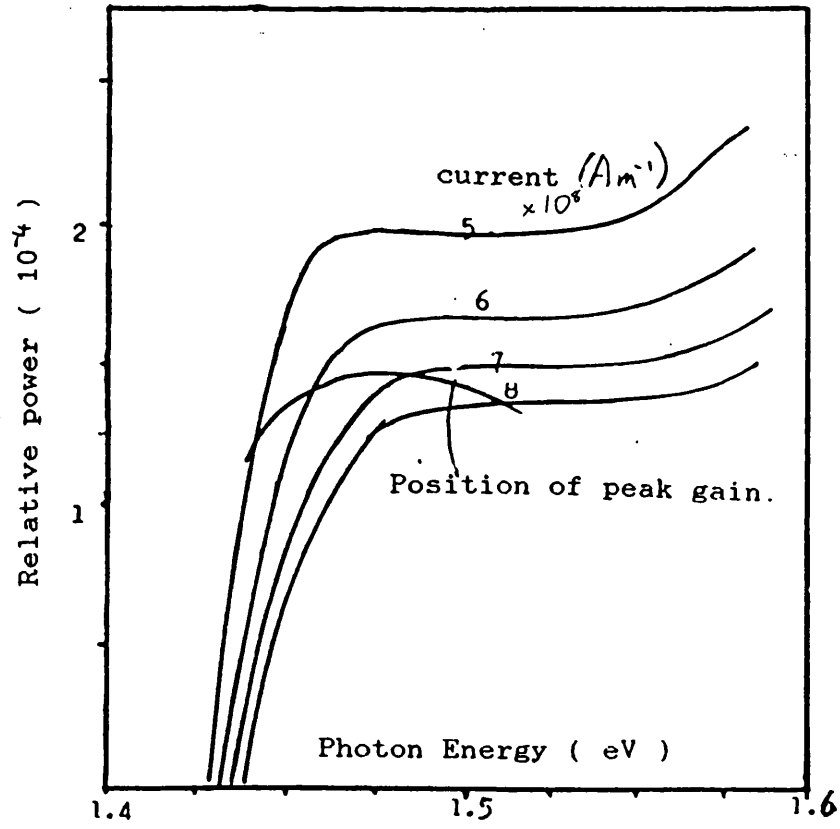

Fig. 6-8 This graph illustrates the variation of the ratio of TM to TE coupled power for different active layer thicknesses for a 7μm stripe width. The ratios are almost independent of drive current and for the results presented the TE coupled power is greater than the TM coupled power.

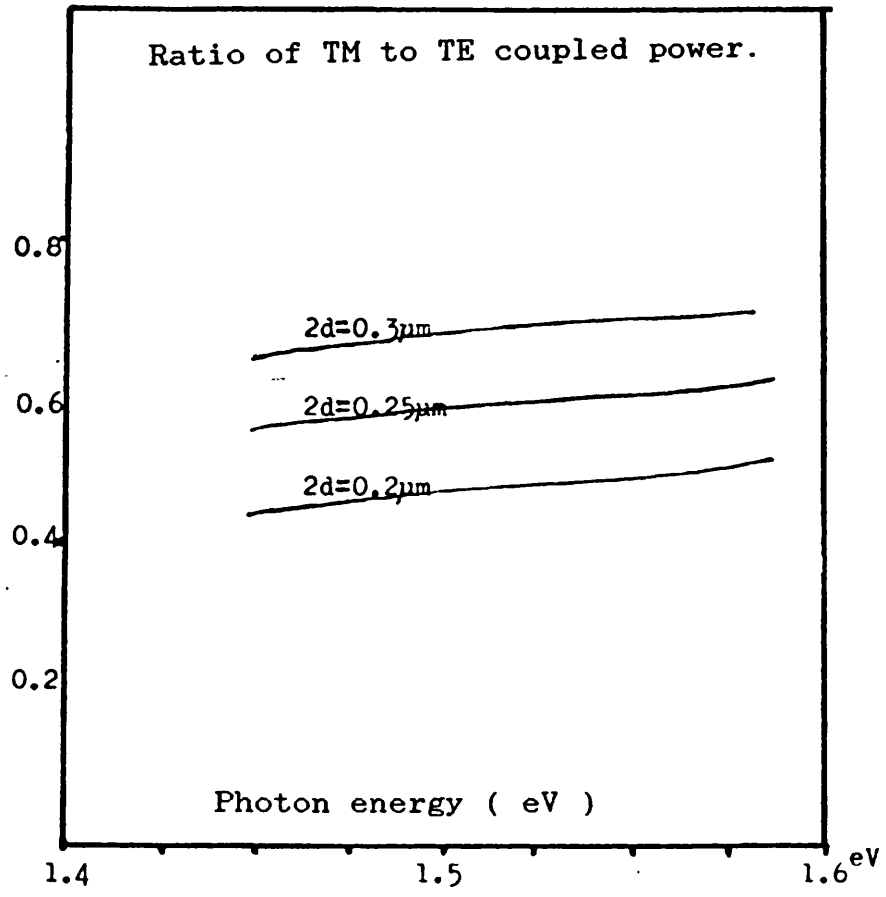

Fig. 6-9 The power coupled to the guided modes from the different dipoles for a 7 μm stripe width and 0.3 μm active layer thickness is shown here on a log (- log) scale because of the wide rage of coupling strengths.

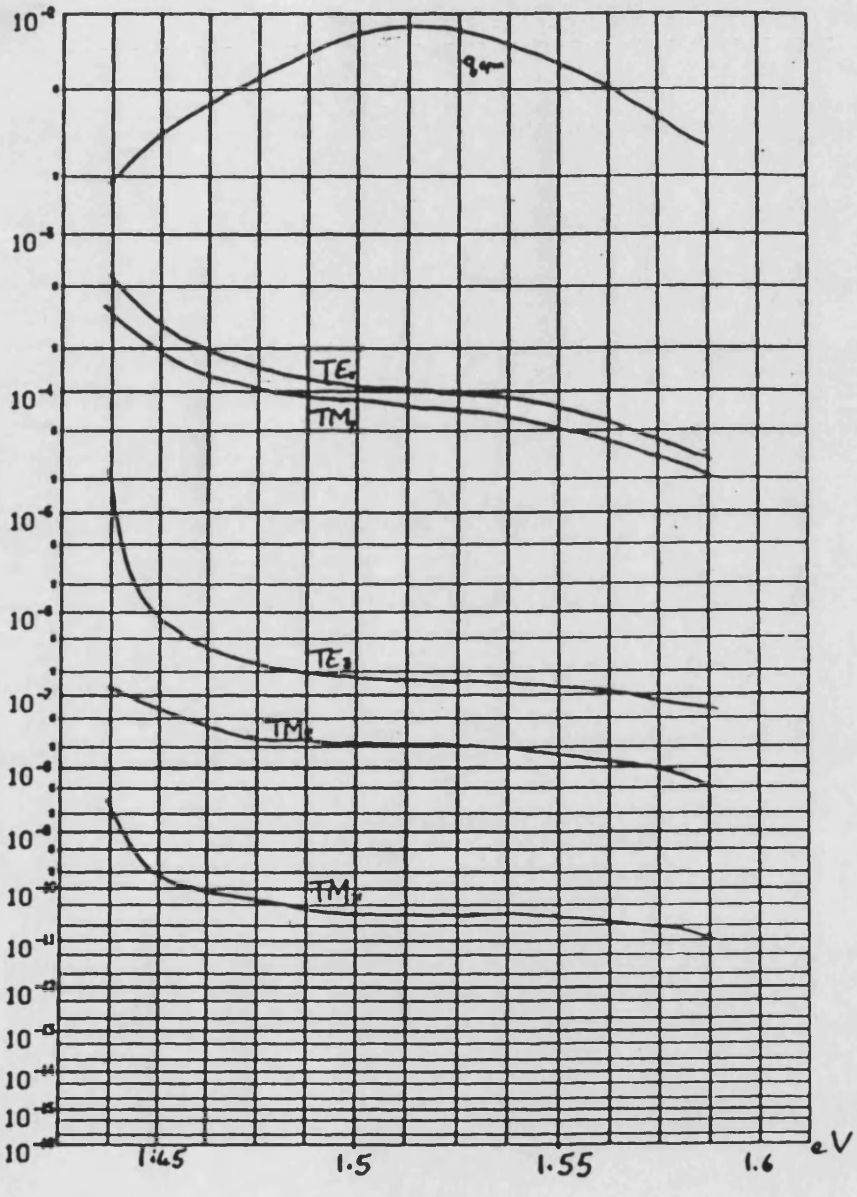

References for Chapter 6

1/ P.M.Morse, H.Feshbach, Methods of theoretical phsiics, part II, McGraw Hill, 1953. (See Chapt 13).

2/ E.O.Kane, "Thomas-Fermi approach to impure semiconductor band structure", Phys.Rev., 131 , (1), pp79-88, 1963.

3/ Kraus, Carver, McGraw Hill.

4/ W.Streifer, D.R.Scrifes, R.D.Burnham, "Spontaneous emission factor of narrow-stripe gain-guided diode lasers", Electron.Lett., 17 , (24), pp933-934, 1981.

5/ M.Abramowitz, I.A.Stegun, Handbook of mathematical functions, Dover International Inv., 9th printing.

6/ K.Peterman, "Calculated spontaneous emission factor for double-heterostructure injection lasers with gain-induced waveguiding", IEEE J.Q.Electron, QE-15 , (7), pp566-569, 1979.

7/ M.Abramowitz, I.A.Stegun, Handbook of mathematical functions, Dover International Inv., 9th printing. Eqn. (8-326.2).

8/ G.Mendoza-Alvarez, F.D.Nunes, N.B.Patel, "Refractive index dependence on free carriers for GaAs", 51 , (8), pp4365-4367, 1980.

CHAPTER 7

7-1 Conclusions

The spontaneous emission in an active optical waveguide has been analysed as the emissions from elementary dipoles in the active layer. The dominant terms are for TE type modes from the x directed dipole and for TM type modes from the y directed dipole. The contributions from these and the other possible dipole orientations have been evaluated. The TE modes do not couple power from the y dipole and the TM coupling from the x dipole is very much less than from the y dipole. The contributions from the z dipole is about 0.2% of the total for TE and 0.02% of the total for TM modes in the examples shown. (See Table 7-1).

It is possible to get the result that the TE_x and TM_y contributions to the spontaneous emission, expressed as a fraction of the spontaneous emission, are proportional to Peterman's astigmatism factor [1], K. If the y guidance is dominated by the real refractive index difference so that σ_y is real then $C_y = 1$ and if it is independent of x then f_y is the y confinement factor. If ϵ_e is also independent of x then from (6-4.5) the TE_x contribution divided by the total spontaneous emission over the cross section is

$$\delta = \frac{dP}{dz} = \frac{\beta f_y}{8\epsilon_e k_0^2}(C_{nx}^e)^2 \frac{\int_{-\infty}^{\infty} |\psi(x_0)|^2 \, q_{spon} \, dx_0}{\int_{-\infty}^{\infty} q_{spon}(x_0) \, dx_0} \qquad (7\text{-}1.1)$$

If w_{eff} is defined as

$$w_{eff} = \frac{\int_{-\infty}^{\infty} |\psi(x_0)|^2 \, dx_0 \int_{-\infty}^{\infty} q_{spon} \, dx_0}{\int_{-\infty}^{\infty} |\psi(x_0)|^2 \, q_{spon} \, dx_0} \qquad (7\text{-}1.2)$$

then the fraction of the total power coupled to the mode is

$$\frac{\beta f_y}{8 w_{eff} n_{ea}^2 k_0^2} K \tag{7-1.3}$$

This applies equally to the TM_y contribution.

This cannot be applied directly to the TE_z coupling unless the structure is an index guided structure in the x direction. For an index guided structure

$$\int_{-\infty}^{\infty} \left| \frac{\partial \psi}{\partial x_0} \right|^2 dx_0 = -|\sigma_x|^2 \int_{-\infty}^{\infty} |\psi|^2 dx_0 \tag{7-1.4}$$

For a gain guided structure $|\sigma_x|^2$ must be found by direct integration. In this case for the limits previously described for TE_z coupling

$$\delta = \frac{f_y}{8} \frac{|\sigma_x|^2}{n_{ea}^2 k_0^2} \frac{K}{w_{eff}} \tag{7-1.5}$$

Since $|\sigma_x|^2/n^2 k_0^2 << 1$ this term is small.

The TM_z coupling involves g_y and not f_y and so is smaller than the TM_y term by a factor of about $|\sigma_y|^2/n^2 k_0^2$ The TM_x coupling involves differentials with respect to both x and y so that the power coupled is smaller by a factor $|\sigma_y|^2 |\sigma_x|^2/n^4 k_0^4$ to make this a very small term.

Attention is drawn at this point to the approximate expressions for $F(N)$ and $G(N)$, equations (6-5.15), (6-5.16), for the integrals I_1 and I_2, equations (6-5.9) and (6-5.10). Each of these involves a C_0 term which implies that δ in all cases is proportional to $C_0^2 = K$. However, if the expression for C_0 is substituted into (6-5.15), (6-5.16) then the dominant term in C_0, the $-\mu'$ in the denominator, is no longer present. The functions $F(N)$ and $G(N)$ should not be considered as being proportional to C_0. This implies that δ is not proportional

to K but to C_0. This is simply explained by considering the expression for the effective width (7-1.2). For a gain guided mode with TE_x or TM_y excitation

$$w_{eff} = C_0 \frac{\int_{-\infty}^{\infty} q_{spon}\, dx_0}{F(N)} \qquad (7\text{-}1.6)$$

and so w_{eff} is proportional to C_0.

The remaining terms in the expression for C_0 (6-4.1), also involve μ' in the denominator, but only in the form $(n-\mu')$. This has a minimum value of one when μ' is zero and for $-\mu'$ large is approximately $-\mu'$. This has the result that when $C_0 \rightarrow 1$ this product is also one and as $-\mu'$ reduces this product increases, but not as fast as $1/(-\mu')$ and it still has a finite value when $\mu' = 0$. It is not suprising then that the graphs of the last section show that the fractional spontaneous emission coupled to waveguide modes is not proportional to K when the mode is near cut off.

Table 7-1
This table shows the approximate relative coupling strengths from the different dipoles to the TE_{oo} and TM_{oo} modes. These results are for a 7 μm stripe width and a 0.3 μm active layer thickness.

Mode		TE	TM
	x	1	$4 \quad 10^{-7}$
Dipole	y	=0	0.5
	z	$2 \quad 10^{-3}$	$2 \quad 10^{-4}$

7-2 Review of results

The analysis of this thesis has not concentrated on the peak gain in the the waveguide which is used when the aim is to study laser diodes. Rather the aim has been to investigate the dependence of the effects of spontaneous emission in waveguides with gain. The numerical examples must use corresponding gain and spontaneous emission profiles from the same calculation of band to band transitions if this aim is to be acheived. For this reason a computer program to calculate simplified emission spectra has been developed. To produce realistic results some band tailing effects have been included so that, unlike models which rely on parabolic bands, the emission spectra do not cut off sharply at the band edge.

In order to calculate the carrier density profile for a realistic device, current spreading and carrier out-diffusion have been considered. This results in a numerical profile for the carrier distribution in the active layer. This carrier distribution has been approximated to a $\cosh^{-2}$ profile in order to analyse the electromagnetic fields in the waveguide. Several other approximate profiles have been considered both for the carrier profile and the electromagnetic field profile. These have been shown to be unsatisfactory for describing modes near cut-off in gain guided waveguides.

The spontaneous emission coupled to gain guided waveguide modes has been calculated and numerically generated results for the $\cosh^{-2}$ carrier profile have been presented.

These results show that the astigmatism factor of Peterman [1] only holds for the peak wavelength when the waveguide has gain. For the peak wavelength the astigmatism is dependent on carrier density but Peterman's effective volume is almost constant. The gain guided modes cut off at energies near the band edge. This causes the astigmatism to increase to infinity. The

effective width in Peterman's analysis becomes zero. For waveguides with built in waveguiding, through the real part of the refractive index, the modes may not cut off at low photon energies. However, the astigmatism factor for such waveguides is not identically unity unless the waveguide is passive. It can be close to unity when the guiding mechanism is predominantly due to the real refractive index differences.

7-3 Suggestions for Further Work

As with any thesis it is not possible to cover the entire topic in three years. There will always be some calculations which have not been performed or short cuts which could be avoided given more time. Some gaps left by this thesis are worthy of further study and these deficiencies are noted.

The model used for gain and spontaneous emission is extremely simple and contains all the necessary features required of it. However, it would be possible to extend this analysis to include variation of parameters such as temperature and see how the model behaves. The analysis could also be expanded to include other III-V semiconductors, particularly InP-InAsP which has taken over from GaAs as the major material for lasers for communications systems. This would simply mean exchanging the effective masses, band gap, refractive index etc. of GaAs for those of InP. The calculations would be identical. This simple change is quite important if the results are to have practical importance.

The properties of gain guided waveguide modes have been outlined using a $\cosh^{-2}(x/w)$ formulation for the inversion population density. Several other possible approximations have been outlined but were rejected as being unsuitable. It would be useful to continue with these approximations to calculate the spontaneous emission as before.

This thesis only considers gain guided modes. Most guiding structures now include some passive, real refractive index, guiding as well. This should be included in the analysis. The simplest method would be to use a slab approximation since there would then be a suitable place to put the slab boundaries. The solutions for the electric and magnetic fields would then show a field profile confined to this slab for low injection currents, as expected. The spontaneous emission could be calculated relatively easily through a slight

modification of the results for the gain guided case.

The calculation of spontaneous emission in a gain guided waveguide calculates only the emission coupled into the fundamental transverse mode. The total power coupled into the other transverse modes is not calculated, nor is any attention paid to the continuous spectrum of radiation for the y directed modes, although this is certainly of importance if the results obtained here are to be applied to semiconductor lasers.

No treatment of the near and far field patterns produced at the output of the kind of travelling wave amplifier described here has been undertaken. Before the results of this thesis can have any practical importance the near and far field patterns must be analysed and compared to measured results. [2]

The main feature of this thesis has been the calculation of the wavelength dependence of the effects of gain and spontaneous emission. In many practical instances, particularly calculations about laser diodes, the gain spectrum may be considered very broad and the spontaneous emission spectrum even broader. However, for any non resonant device the wavelength dependent effects become important. Serious consideration is currently being given in various research centres woldwode to the use of single pass optical amplifiers in optical communications systems. Whether they are used as laser power amplifiers, optical repeaters or signal boosters in an optical receiver the importance of the wavelength variation of gain and spontaneous noise and spontaneous emission is certain to be of importance.

References for Chapter 7

1/ K.Peterman, "Calculated spontaneous emission factor for double-heterostructure injection lasers with gain-induced waveguiding", IEEE J.Q.Electron, QE-15 , (7), pp566-569, 1979.

2/ P.M.Asbeck, D.A.Cammack, J.J.Daniele, V.Klebanoff, "Lateral mode behaviour in narrow stripe lasers", IEEE J.Q.Electron, QE-15 , (8), pp727-733, 1979.

APPLICATION FOR THESIS/PERIODICAL RETRIEVAL FROM STORE

NAME (please print in large letters)

PEK SIM LOW

Date 29-9-97 School Electrical

You may apply for a maximum of 3 items a day. Please use a separate form for each volume

THESIS

Author	*Title*	*Date of Publication*
W.J. Liddell	Polarisation and spectral characteristics of spontaneous emission in active optical waveguides.	1986

Please leave this form at the Issue Desk - it will be dealt with as soon as possible
Items may be collected from the Issue Desk - you should allow 24 hours for retrieval

DAVIES, TONY AN P/BACK AUG 87

When the Moon Rises

Sphere Books 0 7221 2850 9 Pub. Pr £2.75
176 pages

The extraordinary true story of a daring escape through wartime Italy.

First paperback edition. 940.547245
MORLEY BOOKS List 10/08/87 87/33 Ref 000697